



The Standard Submarine Model: A Survey of Static Hydrodynamic Experiments and Semiempirical Predictions

M. Mackay

Defence R&D Canada

Technical Report

DRDC Atlantic TR 2003-079

June 2003

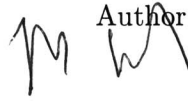
Copy No. _____

The Standard Submarine Model: A Survey of Static Hydrodynamic Experiments and Semiempirical Predictions

M. Mackay

Defence R&D Canada – Atlantic

Technical Report
DRDC Atlantic TR 2003-079
June 2003

Author


M. Mackay

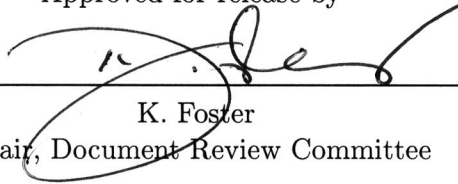
Approved by



N. Pegg

Head, Warship Signatures and Safety

Approved for release by



K. Foster

Chair, Document Review Committee

Abstract

This report describes comparison between measurements of static hydrodynamic loads on the Standard Submarine Model in a number of different test facilities, and comparison between selected experimental data and predictions from the DSSP20 manoeuvring simulation code. The experiments constitute a substantial database for code development and validation. Differences between data from various facilities are in general not very great. Agreement with the predictions is generally satisfactory within a modest range of incidence, i.e., angles below 20 to 30 degrees, although some significant deviations are observed outside this range.

Résumé

Le présent rapport établit une comparaison entre des mesures de charges hydrodynamiques statiques exercées sur le modèle standard de sous-marin dans un certain nombre d'installations d'essai différentes et une comparaison entre des prédictions et des données expérimentales choisies dans le code de simulation de manœuvres DSSP20. Les expériences constituent une base de données substantielle pour le développement et la validation du code. Les différences entre les données provenant de diverses installations ne sont pas très importantes en général. La concordance avec les prédictions est généralement satisfaisante à l'intérieur d'une gamme étroite d'incidences, c.-à-d. les angles entre 20 et 30 degrés, bien que certaines déviations significatives soient observées à l'extérieur de cette gamme.

This page intentionally left blank.

Executive Summary

Introduction

The Standard Submarine Model was devised for a series of systematic hydrodynamic experiments jointly funded by DRDC and the RNLN. Since the original experiments in the MARIN towing tanks, the model and variations of it have been tested at a number of different facilities including NAE, IAR, DERA, and IMD. This report is in two parts: the first documents comparisons between the results of static load measurements in the different facilities, and the second compares a subset of these results with predictions from the DRDC semiempirical simulation code DSSP20.

Significance

DSSP20 is a manoeuvring simulation code developed at DRDC to support safe operation of the Victoria class, to evaluate other submarines, and to develop and evaluate small underwater vehicles. The experimental data discussed here constitute both a database for further code development and a resource for validating future versions of the code. Testing the same model in different facilities and at different scales gives a much improved perspective on the strengths and weaknesses of the experimental data.

Principal Results

Agreement between results from the different facilities is generally quite good within the limits of stall inception. However, the spread of data is sufficient to obscure the effects of Reynolds number on force derivatives obtained from the different data sets. The comparisons with DSSP20 suggest a number of areas for improvement in the code; nevertheless, within a modest range of incidence — angles below 20 to 30 degrees, depending on the measurement — the agreement is satisfactory for simulation purposes. Outside this range, some significant deviations are observed.

Further Investigations

There are no immediate plans to extend the Standard Model database. Development of DSSP20 is ongoing.

M. Mackay, 2003, The Standard Submarine Model: A Survey of Static Hydrodynamic Experiments and Semiempirical Predictions, DRDC Atlantic TR 2003-079.

Defence R&D Canada – Atlantic.

Sommaire

Introduction

Le modèle standard de sous-marin a été conçu pour une série d'expériences hydrodynamiques systématiques qui ont été mises au point en commun par RDDC et la RNLN. Depuis les premières expériences effectuées dans les bassins d'essais des carènes MARIN, le modèle et ses variantes ont été mises à l'essai à un certain nombre d'installations, y compris la NAE, l'IRA, DERA et l'IDM. Le présent rapport est divisé en deux parties: la première compare les résultats de mesures de charges statiques dans les différentes installations et le deuxième compare un sous-ensemble de ces résultats avec des prédictions du code de simulation semi-empirique DSSP20.

Signification

DSSP20 est un code de simulation de manœuvres qui a été développé par RDDC pour contribuer à sécuriser l'utilisation des sous-marins de la classe Victoria, pour évaluer d'autres sous-marins et pour développer et évaluer de petits véhicules sous-marins. Les données expérimentales dont il est question ici constituent une base de données pour le développement ultérieur des codes et une ressource pour la validation des futures versions du code. Le fait de mettre à l'essai le même modèle dans différentes installations et à différentes échelles donne une bien meilleure perspective sur les forces et les faiblesses des données expérimentales.

Résultats principaux

La concordance entre les résultats des différentes installations est généralement très bonne dans les limites de la plage de décrochage. Cependant, l'écart entre les données est suffisant pour brouiller les effets du nombre de Reynolds sur les dérivées de force obtenues à partir des différents ensembles de données. Les comparaisons avec DSSP20 semblent indiquer qu'il existe un nombre de zones à améliorer dans le code; néanmoins, à l'intérieur d'une plage d'incidence plus restreinte (les angles inférieurs à 20 à 30 degrés, dépendant de la mesure), la concordance est satisfaisante pour les besoins de la simulation. À l'extérieur de cette plage, quelques déviations importantes sont observées.

Suite des investigations

On ne prévoit pas étendre la base de données du modèle standard dans un avenir rapproché. Le développement de DSSP20 est en cours.

M. Mackay, 2003, The Standard Submarine Model: A Survey of Static Hydrodynamic Experiments and Semiempirical Predictions, DRDC Atlantic TR 2003-079.

R & D pour la défense Canada – Atlantique.

Table of Contents

Abstract	i
Résumé	i
Executive Summary	iii
Sommaire	iv
Table of Contents	v
List of Tables	vi
List of Figures	vii
Acknowledgments	xi
1 Introduction	1
2 The Standard Submarine Model	1
3 Principal Static Experiments with the Standard Model	2
3.1 NAE	3
3.2 MARIN	3
3.3 STR	4
3.4 DERA	5
3.5 MDTF	5
4 Overall Comparisons by Facility	6
4.1 Hull Alone (H)	6
4.2 Hull and Sail (HS) in Pitch	7
4.3 Hull and Sail (HS) in Yaw	8
4.4 Hull and Tail (HT)	8
4.5 Hull, Sail, and Tail (HST) in Pitch	9
4.6 Hull, Sail, and Tail (HST) in Yaw	9
4.7 Review	10
5 Specific Comparisons	10
5.1 Hull Force and Moment	10
5.2 Sail Forces	13
5.3 Tailplane Efficiency	15
5.4 Comparison of HST Loads at Moderate Incidence	16
5.5 Very High Incidence	16
5.6 Review	17
6 Concluding Remarks	18

Continued over.

References	19
Tables	25
Figures	30
Annex A. Standard Submarine Series Experiments	87
Annex B. Symmetry Error Estimate	91
Nomenclature	93

List of Tables

Table 1.	Estimates of nondimensionalized symmetry error S'_x , in percent, for the HS configuration in yaw.	25
Table 2.	Estimates of nondimensionalized symmetry error S'_x , in percent, for the HST configuration in yaw.	25
Table 3.	Estimates of neutral point x'_n for hull alone.	26
Table 4.	Estimates of vertical plane neutral point x'_{vn} for hull and sail. ..	26
Table 5.	Estimates of horizontal plane neutral point x'_{hn} for hull and sail.	26
Table 6.	Estimates of neutral point x'_n for hull and tail.	27
Table 7.	Estimates of vertical plane neutral point x'_{vn} for hull, sail, and tail.	27
Table 8.	Estimates of horizontal plane neutral point x'_{hn} for hull, sail, and tail.	27
Table 9.	Hull alone: ratios of slopes $Z'_{w'}$ and $M'_{w'}$ to predicted values. ...	28
Table 10.	Sail: ratios of apparent sail factor k_s to the predicted value.	29
Table 11.	Sail: ratios of the roll moment arm as $\beta \rightarrow 0$ to the predicted value.	29
Table 12.	Sail: apparent chordwise center of pressure, C_{Pc} , as $\beta \rightarrow 0$	29

List of Figures

Figure 1.	The Standard Model: parent (HST) definition.	30
Figure 2.	NAE 2×3 m wind tunnel: (a) general arrangement for sting-supported models; (b) oil flow visualization with a Hull + Sail + Deck Casing configuration.	31
Figure 3.	MARIN PMM: (a) conventional twin-sword model support; (b) modified support arrangement.	32
Figure 4.	STR (IAR 9×9 m wind tunnel): (a) sting model support arrangement; (b) standard twin strut support arrangement. ...	33
Figure 5.	DERA (Haslar) Ship Tank: model DSJ Hull + Tail configuration on PMM twin-sword mounting.	34
Figure 6.	MDTF (IMD 200 m towing tank): (a) general arrangement; (b) model internal balance arrangement.	35
Figure 7.	Hull alone axial force: all data sets.	36
Figure 8.	Hull alone normal force: all data sets.	36
Figure 9.	Hull alone pitching moment: all data sets.	37
Figure 10.	NAE normal force and pitching moment for hull alone at $-6 < \alpha < +6$ degrees.	37
Figure 11.	MARIN normal force and pitching moment at for hull alone $-6 < \alpha < +6$ degrees.	38
Figure 12.	STR normal force and pitching moment for hull alone at $-6 < \alpha < +6$ degrees.	38
Figure 13.	DERA normal force and pitching moment for hull alone at $-6 < \alpha < +6$ degrees.	39
Figure 14.	MDTF normal force and pitching moment for hull alone at $-6 < \alpha < +6$ degrees.	39
Figure 15.	Hull alone $Z'_{w'}$ and $M'_{w'}$: all data sets.	40
Figure 16.	Hull alone pitching moment vs normal force: all data sets.	40
Figure 17.	Hull alone hydrodynamic center: all data sets.	41
Figure 18.	Hull and sail in pitch, axial force: all data sets.	41
Figure 19.	Hull and sail in pitch, normal force: all data sets.	42
Figure 20.	Hull and sail in pitch, pitching moment: all data sets.	42
Figure 21.	MARIN normal force and pitching moment for hull and sail at $-6 < \alpha < +6$ degrees.	43
Figure 22.	STR normal force and pitching moment for hull and sail at $-6 < \alpha < +6$ degrees.	43
Figure 23.	DERA normal force and pitching moment for hull and sail at $-6 < \alpha < +6$ degrees.	44

Figure 24.	MDTF normal force and pitching moment for hull and sail at $-6 < \alpha < +6$ degrees.	44
Figure 25.	Hull and sail, $Z'_{w'}$ and $M'_{w'}$: all data sets.	45
Figure 26.	Hull and sail, pitching moment <i>vs</i> normal force: all data sets.	45
Figure 27.	Hull and sail, vertical plane hydrodynamic center: all data sets.	46
Figure 28.	Hull and sail in yaw, axial force: all data sets.	46
Figure 29.	Hull and sail in yaw, side force: all data sets.	47
Figure 30.	Hull and sail in yaw, normal force: all data sets.	47
Figure 31.	Hull and sail in yaw, rolling moment: all data sets.	48
Figure 32.	Hull and sail in yaw, pitching moment: all data sets.	48
Figure 33.	Hull and sail in yaw, yawing moment: all data sets.	49
Figure 34.	NAE in-plane force and moments for hull and sail at $-6 < \beta < +6$ degrees.	49
Figure 35.	MARIN in-plane force and moments for hull and sail at $-6 < \beta < +6$ degrees.	50
Figure 36.	STR in-plane force and moments for hull and sail at $-6 < \beta < +6$ degrees.	50
Figure 37.	DERA in-plane force and moments for hull and sail at $-6 < \beta < +6$ degrees.	51
Figure 38.	MDTF in-plane force and moments for hull and sail at $-6 < \beta < +6$ degrees.	51
Figure 39.	Hull and sail, Y'_v , K'_v , and N'_v : all data sets.	52
Figure 40.	Hull and sail, yawing moment <i>vs</i> side force: all data sets.	52
Figure 41.	Hull and sail, horizontal plane hydrodynamic center: all data sets.	53
Figure 42.	Hull and tail axial force: all data sets.	53
Figure 43.	Hull and tail normal force: all data sets.	54
Figure 44.	Hull and tail pitching moment: all data sets.	54
Figure 45.	STR normal force and pitching moment for hull and tail at $-6 < \alpha < +6$ degrees.	55
Figure 46.	DERA normal force and pitching moment for hull and tail at $-6 < \alpha < +6$ degrees.	55
Figure 47.	MDTF normal force and pitching moment for hull and tail at $-6 < \alpha < +6$ degrees.	56
Figure 48.	Hull and tail, $Z'_{w'}$ and $M'_{w'}$: all data sets.	56
Figure 49.	Hull and tail, pitching moment <i>vs</i> normal force: all data sets. .	57
Figure 50.	Hull and tail, hydrodynamic center: all data sets.	57
Figure 51.	Hull, sail, and tail in pitch, axial force: all data sets.	58
Figure 52.	Hull, sail, and tail in pitch, normal force: all data sets.	58

Figure 53.	Hull, sail, and tail in pitch, pitching moment: all data sets.	59
Figure 54.	STR normal force and pitching moment for hull, sail, and tail at $-6 < \alpha < +6$ degrees.	59
Figure 55.	DERA normal force and pitching moment for hull, sail, and tail at $-6 < \alpha < +6$ degrees.	60
Figure 56.	MDTF normal force and pitching moment for hull, sail, and tail at $-6 < \alpha < +6$ degrees.	60
Figure 57.	Hull, sail, and tail, Z'_w , and M'_w : all data sets.	61
Figure 58.	Hull, sail, and tail, pitching moment <i>vs</i> normal force: all data sets.	61
Figure 59.	Hull, sail, and tail, vertical plane hydrodynamic center: all data sets.	62
Figure 60.	Hull, sail, and tail in yaw, axial force: all data sets.	62
Figure 61.	Hull, sail, and tail in yaw, side force: all data sets.	63
Figure 62.	Hull, sail, and tail in yaw, normal force: all data sets.	63
Figure 63.	Hull, sail, and tail in yaw, rolling moment: all data sets.	64
Figure 64.	Hull, sail, and tail in yaw, pitching moment: all data sets.	64
Figure 65.	Hull, sail, and tail in yaw, yawing moment: all data sets.	65
Figure 66.	STR in-plane force and moments for hull, sail, and tail at $-6 < \beta < +6$ degrees.	65
Figure 67.	DERA in-plane force and moments for hull, sail, and tail at $-6 < \beta < +6$ degrees.	66
Figure 68.	MDTF in-plane force and moments for hull, sail, and tail at $-6 < \beta < +6$ degrees.	66
Figure 69.	Hull, sail, and tail, Y'_v , K'_v , and N'_v : all data sets.	67
Figure 70.	Hull, sail, and tail, yawing moment <i>vs</i> side force: all data sets.	67
Figure 71.	Hull, sail, and tail, horizontal plane hydrodynamic center: all data sets.	68
Figure 72.	Hull normal force.	68
Figure 73.	Hull pitching moment.	69
Figure 74.	Hull normal force for $-6 < \alpha < +6$ degrees.	69
Figure 75.	Hull pitching moment for $-6 < \alpha < +6$ degrees.	70
Figure 76.	Hull axial force.	70
Figure 77.	Sail incremental axial force (HS-H).	71
Figure 78.	Sail incremental sideforce (sail lift, HS-H).	71
Figure 79.	Rolling moment arm of sail incremental sideforce (HS-H).	72
Figure 80.	Sail rolling moment.	72
Figure 81.	Yawing moment arm of sail incremental sideforce (HS-H).	73
Figure 82.	Sail incremental yawing moment (HS-H).	73

Figure 83.	Sail incremental axial force; (HST-HT) and (HS-H).	74
Figure 84.	Sail incremental sideforce; (HST-HT) and (HS-H).	74
Figure 85.	Sail incremental yawing moment; (HST-HT) and (HS-H).	75
Figure 86.	Tail incremental axial force (HT-H).	75
Figure 87.	Tail incremental normal force (tail lift, HT-H).	76
Figure 88.	Pitching moment arm of tail incremental normal force (HT-H).	76
Figure 89.	Tail incremental pitching moment (HT-H).	77
Figure 90.	Tail incremental axial force; (HST-HS (yaw and pitch)) and (HT-H).	77
Figure 91.	Tail incremental normal force; (HST-HS (yaw and pitch)) and (HT-H).	78
Figure 92.	Tail incremental pitching moment (HST-HS (yaw and pitch)) and (HT-H).	78
Figure 93.	HST load comparison: X' (pitch).	79
Figure 94.	HST load comparison: Z' (pitch).	79
Figure 95.	HST load comparison: M' (pitch).	80
Figure 96.	HST load comparison: X' (yaw).	80
Figure 97.	HST load comparison: Y' (yaw).	81
Figure 98.	HST load comparison: K' (yaw).	81
Figure 99.	HST load comparison: N' (yaw).	82
Figure 100.	HST high incidence load comparison: Z' (pitch).	82
Figure 101.	HST high incidence load comparison: M' (pitch).	83
Figure 102.	HSsT high incidence load comparison: X' (pitch).	83
Figure 103.	HSsT high incidence load comparison: Z' (pitch).	84
Figure 104.	HSsT high incidence load comparison: M' (pitch).	84
Figure 105.	HST/HSsT high incidence load comparison: X' (yaw).	85
Figure 106.	HST/HSsT high incidence load comparison: Y' (yaw).	85
Figure 107.	HST/HSsT high incidence load comparison: K' (yaw).	86
Figure 108.	HST/HSsT high incidence load comparison: N' (yaw).	86

Acknowledgments

The author would like to thank the numerous investigators who have worked with the Standard Model and thereby contributed in some way to this report. Particular acknowledgments for discussions and background on the principal test series documented here are due to Jan Hooft, MARIN; George Watt, DRDC; David Atkins, QinetiQ; and Christopher Williams and Caroline Muselet, IMD.

This page intentionally left blank.

1 Introduction

Since 1984, hydrodynamic model tests with the Standard Submarine Series have been done in a number of different facilities for a wide range of different configurations. The test programs are summarized in annex A and, where data or analysis have been formally reported, are documented in references [1–41]. The primary purpose of static measurements in these experiments was to obtain manoeuvring forces and moments for developing and validating semiempirical or coefficient-based simulation methods and for validating CFD codes. In most cases accurate determination of the drag or axial force was a secondary consideration.

This report has two objectives. The first is to make a general examination of static data for the Standard Model in order to highlight areas of agreement, disagreement, and overall uncertainty between results from different test facilities. However, differences in the procedures and test conditions, and differing degrees of thoroughness in the error analysis provided, preclude picking a “best” set of data. In these circumstances, favourable agreement with a trend or consensus in other data is not necessarily a reliable indicator of correctness.

The second objective is to document comparisons between selected static data and predictions from the DSSP20 code (DRDC Submarine Simulation Program, version 2.0) [42,43]. The semiempirical methods incorporated in DSSP20 are still under development, and these comparisons were made in the course of refining some of the hydrodynamic calculations in recent revisions of the code.

These objectives are related to each other in that development of semiempirical prediction methods invariably uses data from different sources. It is important to gauge whether apparent inconsistencies arise from differences between facilities and procedures, or represent physical phenomena that should be modeled.

Since much of the Standard Model database is proprietary to the various sponsors, this report omits ordinate scales (apart from the zero) on data plots and gives only relative values in numerical comparisons. However, ordinate axes are scaled identically on corresponding figures wherever possible.

2 The Standard Submarine Model

The geometry of this submarine was originally developed as the basis for systematic experiments at MARIN that were jointly funded by DRDC and the RNLN, and is hence called in a number of the older references the “Canada-Netherlands Systematic Series”. The designation “Standard Submarine Model”, or simply “Standard Model”, was subsequently adopted for brevity.

The series parent consists of a hull, sail, and four cruciform tail appendages; it is defined in figure 1. Variations on this configuration that have been tested include

modified nose and tail sections, modified sail chord, span, and location, X-rudders, sailplanes, bowplanes, and deck casings. The most significant geometric parameter that has not been investigated to any extent is L/D . Many of the aforementioned variations have been tested in only one or two facilities, so for the comparative survey in the first part of this report only the series parent is considered. Almost all of the experiments involved strip tests (in US jargon: build-up tests), and four configurations of the submarine are discussed: the hull alone (H), the hull and sail (HS), the hull and tail (HT), and the hull, sail and tail (HST).

It is standard practice at DRDC to use the CB of the parent hull alone as the coordinate origin for moments. Where necessary, data discussed in this report have been transformed to this location, $0.4448L$ aft of the FP.

3 Principal Static Experiments with the Standard Model

This section summarizes the five principal test series used in the present comparisons. In discussing the results, they are identified by facility as follows:

- NAE: 1988–89 tests in the IAR (formerly NAE) 2×3 m wind tunnel.
- MARIN: 1985–91 tests in the MARIN high speed and depressurized towing tanks.
- STR: 1988 tests in the IAR 9×9 m wind tunnel, with additional 1991 corrections.
- DERA: 1996 tests in the DERA (Haslar) Ship Tank.
- MDTF: 1998–99 tests in the IMD towing tank.

Other static test programs outlined in annex A were conducted for specialized investigations and the scope or nature of their data does not permit a general comparison.

Error analysis was done for most of the data to different degrees. Stochastic or random error estimates were generally available, and are noted for each facility in the subsections below. However, random errors typically constitute only a small component of the total (the larger component being systematic errors [44,45]). For example, measurement (population) standard deviations for the DERA and MDTF data result in standard random errors that are no more than one percent of the maximum forces and moments, and it is reasonable to expect that they exceed no more than a few percent for all the data.

Some discussion of the systematic errors was available for the MARIN [14] and STR [20] results, but not the others. In all cases standard tank or tunnel corrections were applied so far as was possible, but there are residual systematic errors which are typically difficult to identify and estimate. More extensive correction procedures such as suggested in reference [46] for the STR tests are not generally attempted because of the large amount of consequent testing that may be required. To simplify comparison

of the systematic errors, a significant component of them, the errors in data symmetry, was estimated by the method outlined in annex B. It constitutes a lower bound to uncertainty in the measurements with respect to an idealized perfect test.

Analysis of residual symmetry errors was limited to pre-stall data in order to simplify the polynomial fitting procedure for the idealized force or moment (annex B). Table 1 lists the nondimensional symmetry error S'_x as a percentage of axial force at zero incidence, and as a percentage of the other forces and moments at 10 degrees incidence, for the HS configuration in yaw. Table 2 lists S'_x for the HST configuration in yaw.

3.1 NAE

The 1988–89 NAE 2×3 metre wind tunnel tests were done with a 1.8 m model mounted on a sting attached to the main balance located below the tunnel floor. The general arrangement is illustrated in figure 2. The tunnel as it was at the time of these experiments is documented in reference [47]. Today, the working section and main balance are unchanged, but data acquisition systems and instrumentation have been extensively upgraded.

Tunnel blockage and some other corrections were applied by the data acquisition software. The strut connecting the tunnel balance and sting is shielded by a fairing that maintains alignment with the tunnel axis to minimize tare correction. Tares for the exposed part of the sting were derived from a combination of model-off tests and empirical corrections.

The following tunnel and systems specifications relate to the accuracy of these tests:

- flow speed uniformity in the working section, 0.7%,
- turbulence level, 0.14%,
- main balance force and moment accuracy, $\pm 0.1\%$ of full scale.

The NAE tests have fewer data than the other results, comprising only the H and HS configurations, but are included because they formed the empirical basis for DRDC numerical models of out-of-plane force and moment [48–50], and these comparisons demonstrate consistency with the other data. Test Reynolds number was about 7 million. Incidence, produced by rotation of the tunnel turntable and rolling the model, was within a range of about ± 20 degrees, limited by model vibration at the highest values.

3.2 MARIN

Between 1985 and 1991 a comprehensive set of static and dynamic tests in the MARIN towing tanks was jointly funded by RNLN and DRDC [4–18]. The 5.3025 m long model was initially tested in the 220 × 4 × 4 m high speed tank, where it was

supported from the MARIN hydraulic PMM [51] by conventional twin sword mounting, figure 3(a). Concerns with tank blockage, support interference, and surface wave reflections in proposed near-surface experiments resulted in later tests being done in the larger $240 \times 18 \times 8$ m depressurized towing tank using the modified PMM support sketched in figure 3(b). In both cases, the hydrodynamic forces and moments were measured by an arrangement of strain-gauge links inside the model.

There were no model support corrections applied. Although the MARIN error analysis [14] reports differences in measured in-plane forces of up to four percent, there is no consistent distinction between comparable results from each of the tanks or methods of model support, so they are not distinguished in this report. Nominal Reynolds number was between 6.5 and 13 million; a range in water temperature of some 5 degrees Celsius between different data sets results in an uncertainty of about 15 percent in Reynolds number at a given carriage speed. Model incidence was limited by surface proximity to ± 16 degrees.

Reference [14] describes numerous potential sources of error in model manufacture, test set-up, instrumentation, and data reduction. It illustrates the consequences on overall uncertainty for some key examples. From errors in, principally, the last three sources, an estimated uncertainty of about five percent in the in-plane results is reasonable for measurements not limited by resolution. Uncertainty in the out-of-plane results may be two or three times as much, which is fairly typical.

3.3 STR

A series of tests was done in the fall of 1988 to benchmark the Static Test Rig [52] at the IMD 9×9 m wind tunnel. Results are reported in reference [20], and post-test support interference corrections, based on further experiments done in 1991, are reported in reference [24]. Subsequent test programs with the STR have been more specialized, and are not included in the present comparisons.

The principal force and moment measurements were done using the tunnel underfloor main balance with the model supported on two struts entering on the keel line, figure 4(a). Variations in the model mounting were used for the tare and post-test correction procedures [24,52]. A sting mount was required to minimize support interference for wake survey measurements, figure 4(b).

The Static Test Rig is capable of very high incidence. Data shown in the facility comparisons were obtained within an incidence range of ± 30 degrees, and additional tests over a greater range are discussed in section 5.5. However, it is noted in reference [24] that the tare and interference correction procedures may have lost reliability once the sail stalled — for the STR at about ± 20 degrees or so. While all the data discussed here should be considered in light of the secondary effects of sail stall, that problem should not affect sting-mounted models (NAE, MDTF), and may not have been significant in the other results (MARIN, DERA), which incorporated

less rigorous corrections. (Of course, the latter approach presents different, perhaps more serious, problems!)

Data were obtained at Reynolds numbers between 13 and 23 million. Most are for 23 million, where appendage flows should be in the supercritical regime (i.e., local $Re > 1$ million, based on appendage chord). The effect of Reynolds number on derived hydrodynamic coefficients is discussed in section 4.

3.4 DERA

In 1996, DERA (whose marine hydrodynamics and experimental units are now part of QinetiQ) performed static towing tank tests with a 4.606 m model, designated DSJ, in the $270 \times 12 \times 5.5$ m Ship Tank at Haslar. Some results from these experiments are reported in reference [41]. The model was supported by a conventional PMM twin-sword mounting, see figure 5, and forces and moments were measured with an arrangement of internal strain-gauge links. In addition, pressure coefficients were measured round the hull at four stations aft of the sail to provide validation for CFD support interference predictions.

Statistical data from tares and from the gauge signals individually, as well as for overall forces and moments, were used to reject a few questionable results from the present comparisons. However, this did not entirely exclude systematic error; asymmetry in some of the results suggests surface or tank bottom interference as noted in reference [41].

Reynolds number for these experiments was between about 7.5 and 15 million, with transition tripping pins applied on the hull and appendage leading surfaces. Model incidence was in the range of ± 16 degrees, with relatively few high Reynolds number data obtained at the maximum incidence angles. There were no support interference corrections — one purpose of the tests was to measure and compare with CFD predictions what this contribution to uncertainty might be.

3.5 MDTF

A series of static and dynamic experiments were done in 1998–99 with a 4.445 m model sting-mounted on the MDTF in the IMD $200 \times 12 \times 7$ m towing tank. The program, which included acceptance and commissioning tests for the MDTF itself, provided a fairly comprehensive set of static data with a Reynolds number of 11.5 million and incidence in the range ± 30 degrees.

Figure 6 shows the MDTF sting mounting arrangement and the model internal strain-gauge balance. No support corrections were made, so the axial force data are expected to have a relatively large systematic error. The sting used in these tests was an interim design for commissioning; it was an untapered tube with a diameter 30 percent of model hull diameter.

Compared with the other test rigs, the MDTF is relatively compliant under load. (However, sting mounts, e.g., the NAE rig, are inevitably somewhat compliant, and the strut and PMM supports used in the other tests in this comparison are susceptible to lateral flexing, which typically occurs due to out-of-plane loads.) There was therefore some uncertainty in model incidence, notably in yaw relative to the tank; an inclinometer provided independent pitch data. At the time of writing, a detailed error analysis had not been done for the MDTF results.

4 Overall Comparisons by Facility

Note that angles of incidence, which relate the submarine axes to motion or oncoming flow, are referred to here by the designations pitch, α , and yaw β ; in model experiments the corresponding terms angle of attack and angle of drift may be used.

4.1 Hull Alone (H)

Hull alone results were available for all five selected data sets. In general there is little variation with Reynolds number, but some aspects of the results differ considerably by facility. An overall comparison of the data is presented in figures 7 to 9. They are all reported *vs.* pitch, no matter how incidence was defined.

For axial force, figure 7, the MDTF results are compromised, at least at incidence angles within ± 10 degrees, by the sting support, because the data were not corrected for support effects. Tare corrections for the other sting-supported measurements, NAE, appear to have been adequate. Overall agreement in normal force and pitching moment, figures 8 and 9, is fair within at least ± 10 degrees; outside this region differences in the nonlinear contributions become apparent. The NAE results lie somewhat outside the trend of the other data sets.

Figures 10 to 14 illustrate linearity and uncertainty in normal force and pitching moment from the different facilities in the limited range $-6 < \alpha < +6$ degrees; only datasets with enough points to allow curve fitting within this range are included. The figures are all to the same scale. The abscissa in the graphs, $w' = \sin \alpha$, is used as the independent parameter in a third-order curve fit to each set of data. In these figures, random errors, seen as scatter, and systematic errors, seen as, amongst other things, offsets from zero at $w' = 0$, are of similar magnitude. Two of the figures, 11 (MARIN) and 13 (DERA), have data at more than one Reynolds number (additional MARIN data at $R_e = 9.75 \times 10^6$ have been omitted because there were too few for regression), but any effect of this is masked by offset errors. The STR data for Z' , figure 12, have a small even-order component that results in a non-negligible coefficient for w'^2 in the curve fit.

Reynolds number appears to have a weak influence on the force derivative $Z'_{w'} = dZ'/dw'$, and a negligible one on the moment derivative $M'_{w'} = dM'/dw'$,

figure 15 . These derivatives are the linear component of the data fits shown in the previous set of figures; note that they are defined slightly differently from the hydrodynamic coefficients Z'_w, M'_w , etc., conventionally used in the submarine equations of motion. The values for NAE were considered to be outliers and were not included in calculating the linear-fit lines shown on figure 15. It is unfortunate that STR is the only data set with Reynolds number greater than 14 million, because the lines therefore reflect differences between facilities at least as much as in Reynolds number. For example, both MARIN and DERA results suggest that $M'_{w'}$ should increase slightly with Reynolds number, but the trend is obscured in the linear fit.

Normal force effectively acts at the hydrodynamic center x'_h , which is equal to $-M'/Z'$ relative to the model reference point. A plot of M' vs. Z' , figure 16, shows that the data, apart from NAE, are reasonably consistent except in the small pitch angle region where $Z' \rightarrow 0$. As well as the near-singularity, data falling in the bottom-left and top-right quadrants of this figure result in incorrect sign-reversal for x'_h . Since these are quite localized errors, standard statistical error analysis does not give much insight into the uncertainty in this region.

The estimated hydrodynamic center, which will be the same in both vertical and horizontal planes, is plotted against pitch angle in figure 17. Values for $-5 < \alpha < +5$ degrees are generally useless, and those further out in the ranges $-10 < \alpha < -5$ and $+5 < \alpha < +10$ degrees have a fair degree of scatter. At zero pitch, the hydrodynamic center should converge on the neutral point, $x'_n = -M'_{w'}/Z'_{w'}$ ($= N'_{v'}/Y'_{v'}$). Table 3 lists estimates of the neutral point for each data set. The notably lower values for NAE and STR are consistent with the derivative data in figure 15.

4.2 Hull and Sail (HS) in Pitch

Data for the hull and sail in pitch were available for MARIN, STR, DERA, and MDTF. Comparisons presented in figures 18 to 20 are similar to those for the hull alone. Scales for all figures in this section are the same as for corresponding figures in the previous section, although the vertical origin has been shifted for axial force.

Normal force and pitch moment in the range $-6 < \alpha < +6$ degrees are again similar, see figures 21 to 24, with a couple of exceptions. The slope of Z' is noticeably greater for the MARIN data (figure 21) than for the others. This is also evident in figure 25, where including the MARIN results eliminates a possible Reynolds number effect in $Z'_{w'}$. The STR data for Z' , figure 22, have a significantly larger even-order component than was observed for the hull alone.

In the plot of M' vs. Z' , figure 26, there is somewhat more scatter around the origin than for the hull alone. The estimated vertical plane hydrodynamic center, $x'_{vh} = -M'/Z'$, figure 27, is a little further aft than for the hull alone at around ± 10 degrees, where the results from different facilities are reasonably consistent. The vertical plane neutral points, $x'_{vn} = -M'_{w'}/Z'_{w'}$, table 4, are also further aft —

considerably so in the MARIN estimates, which are driven by the relatively high values for $Z'_{w'}$.

4.3 Hull and Sail (HS) in Yaw

An overall comparison of data for the hull and sail in yaw is presented in figures 28 to 33. There is a fair amount of variation in the axial force and out-of-plane force and moment (Z' and M'), but little in the in-plane force and moments (Y' , K' , and N'). STR out-of-plane data are shown both with and without the later corrections described in reference [24]. NAE data generally agree reasonably well with the rest at modest angles of yaw out to ± 12 or ± 15 degrees, at which point there is sail stall; both STR and MDTF data show evidence of sail stall at about ± 25 degrees. Stall angles for NAE and STR data are consistent with flow visualization observations [2,19].

In-plane data fall within ± 2 degrees of yaw at the zero force or moment. This uncertainty represents a combination of alignment errors, model inaccuracy or deformations, and yaw measurement errors. Out-of-plane measurements, particularly M' , show much greater scatter and variability. For example, in figure 32 the STR data are notably asymmetrical around zero yaw (this may have been exacerbated by the 1994 correction; see figure 13 of reference [24]), and the DERA data are negative at zero yaw when sail drag should result in a small positive value.

The in-plane force and moments are shown for the range $-6 < \beta < +6$ degrees in figures 34 to 38. (The ordinate axes are detached in these figures to emphasize that different ordinate scales and origins are used for Y' , K' , and N' .) In all these figures, linearity over this limited range of incidence is greater than for the hull alone. The influence of Reynolds number on the slopes $Y'_{v'}$, $K'_{v'}$, and $N'_{v'}$ is shown on figure 39. As previously, the NAE data were omitted in fitting the trend and, also as previously, the MARIN and DERA data suggest small increases in the slope of moment *vs.* Reynolds number that are not reflected in the STR results.

Plots of N' *vs.* Y' and the horizontal plane hydrodynamic center $x'_{hh} = N'/Y'$ are presented in figures 40 and 41 respectively. There is still some difficulty near zero yaw, although the hydrodynamic centers are converging to a neutral point less far forward than for the hull alone. Horizontal plane neutral point estimates, $x'_{hn} = N'_{v'}/Y'_{v'}$ are given in table 5.

4.4 Hull and Tail (HT)

Data for the hull and tail were available for STR, DERA, and MDTF; they are all reported here *vs.* pitch, no matter how incidence was defined. The overall comparisons are presented in figures 42 to 44; vertical scales are different from those in previous figures. Trends for the axial and normal forces are generally in line with previous observations. For the MDTF data, tailplane stall at about ± 20 degrees might be

inferred from figure 42. Pitching moment, which is quite small, shows a great deal of variation, figure 44. The STR results have an offset that is about equal to the peak value of M' . The reflex trend in all these data suggests neutral or positive directional stability at large incidence. However, even shifting the STR results to remove their offset does not resolve differences between data sets outside the range $-10 < \alpha < +10$ degrees, i.e., on the reflexed part of the trend.

Normal force and pitching moment in the range $-6 < \alpha < +6$ degrees are plotted in figures 45 to 47. The STR data shows the unexpectedly large even-order component noted in section 4.2, and has a larger-than-usual degree of scatter. Derived slopes $Z'_{w'}$ and $M'_{w'}$ are plotted in figure 48. As before, the variation with Reynolds number may well be an artifact of facility differences.

Uncertainties and errors in pitching moment contribute to a poor definition of the hydrodynamic center, figures 49 and 50. It can be seen that it is small, and tending to a value of zero, i.e., neutral directional stability, at large incidence. The neutral point estimates, table 6, are reasonably consistent.

4.5 Hull, Sail, and Tail (HST) in Pitch

Data for the fully appended model in pitch were available for STR, DERA, and MDTF, and are generally similar to the results for the hull and tail, section 4.4 (vertical scales are the same on corresponding figures). Overall comparisons are presented in figures 51 to 53. In this case, all the data have relatively large offsets and scatter in pitching moment; the STR data again show a marked asymmetry.

Results in the limited range $-6 < \alpha < +6$ degrees, figures 54 to 56, are also generally similar to those for HT; however, DERA normal force has an unexpectedly large offset at the highest Reynolds number. Variation of the slope $Z'_{w'}$ with Reynolds number, figure 57, is more consistent than before.

The vertical plane hydrodynamic center, figures 58 and 59, and neutral point, table 7, locations are a little further aft than for HT. This configuration also approaches neutral directional stability in the vertical plane at large angles of incidence.

4.6 Hull, Sail, and Tail (HST) in Yaw

An overall comparison of data for the hull, sail, and tail in yaw is presented in figures 60 to 65. These data are for STR (three Reynolds numbers), DERA (three Reynolds numbers), and MDTF. The STR data are the uncorrected (1988) versions — see section 3.3 — except for Z' , K' , and M' , for which corrected versions (1994) are also available at $R_e = 23 \times 10^6$. The corrected data are denoted STR⁺. Results for this configuration are generally more consistent, and have less scatter, than in some of the previous comparisons. Out-of-plane force and moment, especially the latter, are more symmetrical than for HS in yaw.

The in-plane force and moments are shown for the range $-6 < \beta < +6$ degrees in figures 66 to 68. The DERA high Reynolds number data are significantly offset (by an amount equivalent to about one degree of yaw) from the others in figure 67. There is a small apparent increase in magnitude of Y'_v with Reynolds number, figure 69.

Ignoring the usual uncertainty at small yaw angles, the horizontal plane hydrodynamic centers, figures 70 and 71, and neutral point estimates, table 8, are reasonably close for all these data.

4.7 Review

In general, in-plane results agree quite well in these comparisons, at least to incidence angles at which separation or stall becomes evident, the most prominent example being sail stall in yaw. The out-of-plane force and moment, and axial force, data have considerable scatter, individually and collectively, so reliance on any one set of these measurements for semiempirical model development should be done with caution.

With a few exceptions, residual symmetry errors in these results are modest. The STR data tended to have a larger even-symmetrical component in the hull related in-plane force than the others when a zero or negligible one was expected, i.e., in figures 22, 45, and 54. This was reflected in a significant coefficient for w'^2 in the corresponding curve fits.

Even for results from one facility alone, there were few cases in which Reynolds number effects were at all discernable, and those data have not been presented here. Where there may be some effect on the different force derivatives for some configurations, they cannot be separated in these comparisons from facility or procedural differences. We can, however, see the expected Reynolds number trend for sail stall (combined with separation characteristics of the hull and other appendages); it routinely occurs at higher incidence for the STR results at 23 million than for lower- R_e data. Differences between data in the mid- R_e range may be attributable in part to differences in transition tripping effectiveness.

5 Specific Comparisons

This section discusses comparisons between selected data and predictions made with the underwater vehicle simulation code DSSP20 [42,43]. In general, the DSSP20 nomenclature is used.

5.1 Hull Force and Moment

The current version of DSSP20 uses HULFOR, Hooft's version of the method of potential flow with viscous corrections [53,54], to calculate hull loads. Comparison of HULFOR

predictions with submarine-like hull and body data has raised questions concerning the accuracy and range of applicability of the method, and alternative methods for calculating the hull force and moment are under review.

The basis of the DSSP20 approach is exemplified by Allen and Perkins' derivation of lift, drag, and pitching moment coefficients for slender blunt-based bodies [55,56]. In incompressible flow the simplified expressions are

$$\begin{aligned} L' &= 2 \frac{A_B}{L^2} \alpha + C_{dc} \frac{A_P}{L^2} \alpha |\alpha| \\ D' &= D'_0 + \frac{A_B}{L^2} \alpha^2 + C_{dc} \frac{A_P}{L^2} |\alpha|^3 \\ M' &= 2 \frac{\nabla - A_B(x_o - x_t)}{L^3} \alpha + C_{dc} \frac{A_P(x_{cp} - x_o)}{L^3} \alpha |\alpha| \end{aligned} \quad (1)$$

where A_B is base area, A_P is planform area, ∇ is volume, and x_o , x_t , and x_{cp} are the vehicle x -coordinates of the reference point, the tail, and the planform area centroid respectively. D'_0 is the zero-lift drag coefficient. C_{dc} is a net crossflow drag coefficient based on planform area. Allen and Perkins discuss its estimation from equivalent infinite cylinder data [57]; the following approximation to these data by the present author gives $C_{dc} = 0.846$ for the standard model:

$$C_{dc} = 1.2 \left[1 - 0.45 \left[2 \frac{A_P}{L^2} - \left(\frac{A_P}{L^2} \right)^2 \right]^{\frac{1}{4}} \right] \quad (2)$$

The force coefficients in equation (1) transform to body axes in the usual manner.

$$\begin{aligned} Z' &= -L' \cos \alpha - D' \sin \alpha \\ X' &= -D' \cos \alpha + L' \sin \alpha \end{aligned} \quad (3)$$

Given the differences between missile bodies, for which these expression were derived, and submarine hulls, close agreement with the standard model data is not expected, although Allen and Perkins show reasonable agreement of some results with airship hull data. Of more interest than the general results are the derivatives

$$\begin{aligned} Z'_{w'} &\approx -2 \frac{A_B}{L^2} - D'_0 \\ M'_{w'} &\approx 2 \frac{\nabla - A_B(x_o - x_t)}{L^3} \end{aligned} \quad (4)$$

In the case of the standard model, $Z'_{w'} = -D'_0 \approx 0$, since $A_B = 0$.

Because $(x_{cp} - x_o) \approx 0$, the nonlinear component of M' is quite small. It is also evident that the parabolic nonlinear component of X' is $(A_B/L^2) w'^2$, or equivalently, $-\frac{1}{2}(Z'_{w'} + D'_0) w'^2$; this approximation is employed in the current release of DSSP20, but using the HULFOR formulation of $Z'_{w'}$.

Hooft's HULFOR algorithms are analogous to equation (1), with additional empiricism incorporated into both the linear and nonlinear components of Z' and M' . Thus, the calculated linear coefficient of Z' has A_B replaced by A_{BM} , the cross-sectional area at location x_{BM} , which Hooft calls the "stalling point" (i.e., a quasi-separation point); x_{BM} is the location where there is a maximum in $dA(x)/dx$. Reference [53] also gives expressions for purely empirical linear coefficients. The nonlinear component of Z' is the integral over the hull of an empirical expression for crossflow drag. Algorithms for the transverse forces and moments in both translation and rotation are all similar. The method is claimed to be applicable for incidence up to 24 degrees and for hull length/diameter ratios between 4.5 and 15.

DSSP20 uses the HULFOR calculated linear coefficients in estimating Y' , Z' , M' , and N' for a hull. It also outputs the HULFOR empirical linear coefficients [53]. Comparison of both with empirical translational coefficients derived for a version of the UK SUBSIM code [58], and with experimental measurements, yielded mixed results.

Nevertheless, HULFOR force and moment estimates are reasonably good for the Standard Model at incidence angles between -15 and $+15$ degrees. Figures 72 and 73 show the hull alone data for normal force and pitching moment, corrected to zero the offsets found in the small-incidence regressions, in comparison with values from Allen and Perkins and from HULFOR. The nonlinear component of Z' is overestimated in both cases. The HULFOR estimate for M' shows a high order nonlinear component resulting in a reflex in the curve at incidence beyond 15 degrees; this behavior has been observed for some other hulls. The Allen and Perkins estimate has too great a linear slope and, as previously noted, a negligible nonlinear component.

These comparisons are shown for the limited range of incidence $-6 < \alpha < +6$ degrees in figures 74 and 75, which are to the same scales as figures 10 to 12. For further comparison, DSSP20 estimates for $-6 < \alpha < +6$ degrees were regressed to obtain slopes $Z'_{w'}$ and $M'_{w'}$; ratios of all the regressed and nominal slopes with these values are given in table 9. For the experimental data, agreement is good in almost all cases for $M'_{w'}$, i.e., the ratio is very nearly one. Variation in the ratio for $Z'_{w'}$ is greater, with the experimental slopes generally less than predicted, notably so for the DERA data, but for two sets, NAE and STR, it is considerably larger. The HULFOR empirical slopes are in quite good agreement with most of the data.

The requirement for accuracy in estimating axial force for a DSSP20 simulation is less stringent than for the other forces and moments since uncertainties in drag can be compensated for in the propulsion model. Nevertheless, zero-lift drag is generally well predicted using the conventional summation of friction, form, roughness allowance, and base drag components. The friction drag calculation in DSSP20 uses Schoenherr's method; form drag is estimated from Hoerner [59], or from torpedo data if more appropriate. Variation with incidence is also reasonably well predicted. Hull axial force predictions and data are plotted in figure 76.

5.2 Sail Forces

Standard semiempirical methods can predict the lift or normal force of an isolated appendage quite well, but accounting for its interaction with other vehicle components is less straightforward. A similar situation exists for predicting the spanwise and chordwise centers of pressure, from which roll and pitching moments, respectively, are derived. Reference [60] reviews methods suitable for appendages (including sails) on submarines and other fully-submerged underwater vehicles, and outlines the procedure used in DSSP20. Submarine sails are specifically discussed in reference [61].

Interaction with the hull can be represented as having two components: the influence of the hull on the appendage, in this instance the sail, and the influence of the appendage on the hull. Thus the total normal force (i.e., normal to the appendage planform) on a simple hull/appendage configuration can be expressed as

$$Z = Z_h + Z_{h(a)} + Z_a + Z_{a(h)} \quad (5)$$

where Z_h is the contribution of the hull alone, $Z_{h(a)}$ is the influence of the appendage on the hull, Z_a is the contribution of the isolated appendage, and $Z_{a(h)}$ is the influence of the hull on the appendage. In model experiments, appendage incremental force is typically obtained in a strip test, e.g., for the sail, by subtracting hull measurements from corresponding hull and sail measurements, or (HS–H). In the notation of equation (5) this is equal to $Z_a + Z_{a(h)} + Z_{h(a)}$. Note that (HST–HT) will not give precisely the same result as (HS–H) because there are additional interactions between sail and tail in the former case.

In DSSP20, interaction contributions are embedded as modifications to the calculation for an isolated appendage; the calculated incremental force is equivalent to the result of a strip test. In the current edition of the code, normal and axial force coefficients on a sail at angle of attack α in local coordinates (see nomenclature and reference [42]) are

$$\begin{aligned} C_Z &= C_{Z\alpha} k_s \alpha + C_{Z\alpha\alpha\alpha} \alpha^3 \\ C_X &= C_{X0} + C_{X\alpha\alpha} \alpha^2 + C_{XJ} \end{aligned} \quad (6)$$

where $C_{Z\alpha}$, $C_{Z\alpha\alpha\alpha}$, C_{X0} , and $C_{X\alpha\alpha}$ are coefficients corresponding to normal force slope, crossflow drag, zero-lift axial force, and induced drag, respectively; these coefficients are obtained from Aucher [62]. C_{XJ} represents junction drag. k_s is the sail factor derived from slender-body and slender-wing theory [63,64].

$$k_s = \left(1 + \frac{r}{b}\right)^2 \quad (7)$$

For an axisymmetric submarine hull with no deck casing, r is local hull radius and b is sail span measured from the hull centerline. In equation (6), k_s does not influence crossflow drag or, unlike earlier DSSP20 models [61], induced drag.

DSSP20 estimates for the spanwise and chordwise centers of pressure are

$$\begin{aligned} C_{Pb} &= \frac{4}{3\pi} b \\ C_{Pc} &= 0.05 + 0.1\sqrt{a_e} \end{aligned} \quad (8)$$

C_{Pb} is the spanwise center of pressure derived from elliptic loading between the sail tip and hull centerline, and C_{Pc} is the chordwise center of pressure in mean chordlengths aft of the mid exposed semispan; a_e is the effective aspect ratio. For low aspect-ratio appendages such as sails, C_{Pc} is predicted to be in the vicinity of the leading edge.

Comparisons between (HS–H) experimental values and DSSP20 predictions — which are independent of Reynolds number — are shown in figures 77 to 82. In plotting these figures, the offsets at zero incidence have been removed and the H data interpolated in yaw to correspond to HS data points.

The increase of axial force with yaw angle is a little underpredicted by DSSP20, figure 77. Sideforce (i.e., sail normal force, in local axes), figure 78, is predicted very well for $-25 < \beta < 25$ degrees, but at greater yaw angles there is evidence of sail stall in the data. For the spanwise center of pressure, there is good agreement between equation (8) and the experimental data, so roll moment is similarly well-predicted, figures 79 and 80. On the other hand, the experimental chordwise center of pressure is considerably further aft (at about 70 percent of chord) than predicted, and the incremental yawing moment is consequently overpredicted, figures 81 and 82. C_{Pc} is only approximated by equation (8), even for an isolated appendage [61], but the disagreement with measurement shown in these figures, likely arising from unaccounted-for hull-sail interactions, merits further investigation.

Incremental sail axial force, sideforce, and yawing moment for (HST–HT) and (HS–H) experimental values are compared in figures 83 to 85. There is little visible difference between the two sets of data for the axial force and sideforce, but a noticeably larger yawing moment slope for (HST–HT). However, regression over $-25 < \beta < 25$ degrees indicates that there is also a reduction in sideforce slope of between 10 and 15 degrees for (HST–HT).

Some numerical comparisons between the (HST–HT) and (HS–H) results are given in tables 10 to 12. Equation (7) gives a value $k_s = 1.873$ for the Standard Model. The experimental (HS–H) results are on average about 93% of this, with only the MARIN data giving a value below 90%, table 10. For (HST–HT), the average drops to 80% of the predicted value, indicating residual interaction with the tail. The sail roll moment arm is essentially equal to $(4/3\pi)b$ in all data sets; there is some scatter, but the differences appear to be correlated with facilities, table 11. On the other hand, location of the chordwise center of pressure, given in table 12, appears to be moved forward a considerable amount for the (HST–HT) data. There is a fair degree of scatter in the (HS–H) results, but in general they are consistent with asymptotic $\beta = 0$ values that would be obtained from figure 81. Overall, C_{Pc} appears to be much more susceptible to differences between experimental facilities, and to interference effects,

than the other quantities discussed here, and the validation, or lack thereof, of the current method of predicting this quantity must be viewed with some scepticism.

5.3 Tailplane Efficiency

Tail appendages — whether cruciform rudders and sternplanes, X-rudders, or in some other arrangement — are handled in DSSP20 like other lifting appendages, with interference effects accounted for as in equation (5). Experimentally, strip tests will give the incremental force. For a cruciform tail, this incremental force is for opposing pairs of appendages, and may be obtained from measurements of (HT–H (pitch)) or (HST–HS (pitch)) for the sternplanes, and from (HT–H (yaw)) or (HST–HS (yaw)) for the rudders. Residual interference effects from the sail will be present in (HST–HS) in each case, but to a greater extent in yaw. The Standard Model has identical cruciform sternplanes and rudders, so (HT–H) is reported here as if for pitch, regardless of the actual incidence direction.

In DSSP20, the normal and axial load coefficients for a tail appendage at an angle of attack α in local coordinates (see nomenclature and reference [42]) are

$$\begin{aligned} C_Z &= C_{Z\alpha} K_{WB} \alpha + C_{Z\alpha\alpha\alpha} (K_{WB} \alpha)^3 \\ C_X &= C_{X0} + C_{X\alpha\alpha} (K_{WB} \alpha)^2 + C_{XJ} \end{aligned} \quad (9)$$

where the coefficient notation is the same as for equation (6), and K_{WB} is tailplane efficiency, generally < 1.0 . There will be additional terms in both C_Z and C_X if flap or all-moving appendage deflections are present. C_{XJ} is generally negligible for a tail appendage.

In the above equation, tail efficiency is effectively a modification of the local incidence angle; this model, like that for the sail factor, is justified primarily on empirical evidence. The basis for assigning a value to K_{WB} has at present a large degree of uncertainty [60,65]. By default, estimation of K_{WB} in DSSP20 is dependent on chord Reynolds number R_c . If $R_c \leq 1 \times 10^6$, K_{WB} is calculated by Dempsey’s method [66] (a function of b/r_M , where r_M is the maximum hull radius); if $R_c \leq 2 \times 10^6$, it is set equal to 1.0; and it is varied linearly for R_c in between. This estimate may be overridden by an input value.

Comparisons between (HT–H) experimental values and DSSP20 predictions are shown in figures 86–89; as in the previous section, zero incidence offsets have been removed and the H data interpolated. In figures 86, 87, and 89, DSSP20 curves are given for three regimes in the default calculation: for K_{WB} calculated by Dempsey’s method; at $R_c = 1.5 \times 10^6$, the mid-point of the interpolation region; and for $K_{WB} = 1.0$. These curves correspond to model Reynolds numbers $R_e \leq 14.28 \times 10^6$, $R_e = 21.43 \times 10^6$, and $R_e \geq 28.57 \times 10^6$, respectively, and we would expect the experimental data to lie between the first two curves. This is essentially the case, but at higher Reynolds number the STR normal force and pitching moment data tend to be lower in

magnitude than the others, rather than greater as the DSSP20 model requires. As previously discussed, this likely reflects facility differences.

Predicted chordwise center of pressure is independent of Reynolds number. As for the sail, the experimental data indicates that C_{Pc} is further aft than predicted, figure 88, although there is a large degree of scatter, especially at low incidence.

Incremental tail axial force, normal force, and pitching moment for (HST–HS) and (HT–H) experimental values are compared in figures 90 to 92. Differences in the normal force and pitching moment data are not large, suggesting that the sail wake interaction was not great with respect to incremental tail loads.

It will be noted in figure 87, and also in figure 91, that the normal force data are reflexed, resulting in a lower normal force slope at small incidence, and hence lower conventional tail efficiency, than even Dempsey’s method predicts. This phenomenon is corroborated in the recent systematic study of hull–tail configurations reported in reference [67]. It has the consequence that K_{WB} derived from the normal force slope at zero incidence is valid for stability determination, i.e., small incidence angles, but not for estimating tailplane loads at higher incidence. Conversely, K_{WB} derived from regressing the full range of force data is not valid for determining stability.

5.4 Comparison of HST Loads at Moderate Incidence

This section compares overall HST loads estimated by DSSP20 against data from the facility comparisons. Out-of-plane force and moment for the model in yaw are not included as these calculations are not yet fully implemented in the program. Dempsey’s method was used for calculating tailplane efficiency. Figures 93 to 99 show the experimental data with DSSP20 predictions superimposed.

The axial force in both pitch and yaw, in-plane forces Y' (yaw) and Z' (pitch), and roll moment in yaw are all predicted reasonably well within the range of the data, approximately -30 to $+30$ degrees, although at the extreme ends of the range the X' and K' data show some evidence of stall, which is not modeled in DSSP20. On the other hand, prediction of both in-plane moments, M' (pitch) and N' (yaw), diverges rapidly at angles greater than ± 20 degrees, especially yaw. Reviewing load comparisons for the individual components of the configuration in sections 5.1 to 5.3, it is likely that divergence of the hull moment estimate starting at these incidence angles, see figure 73, is the major contributor to this discrepancy.

5.5 Very High Incidence

The tests discussed so far have been conducted with the model at angles of incidence up to about 30 degrees. (It should be recalled that incidence comprises the submarine-axis angles with respect to oncoming flow or net velocity, not the earth-axis angles of pitch, etc., that are familiar to the operator.) An incidence of 30 degrees is

large for normal submarine operations and is infrequently exceeded even in emergency recovery — the notable exception being the large negative angle of attack that would occur when rising in level trim with low forward speed, i.e., by blowing ballast. Combined with the practical difficulties of testing at very high incidence, this means that such tests are rarely done, and semiempirical and other numerical models are even more rarely validated for this region.

Most algorithms in DSSP20 are inherently restricted to modest incidence angles of no more than about 30 degrees. For this reason, predictions within and outside this range are differentiated in the remaining figures.

Support interference experiments done with the STR in 1991 included some high incidence tests with the HST configuration mounted on a sting. Pitch angle ranged to about -70 degrees, and yaw angle to about -50 degrees; the tests were done at a Reynolds number of 20 million or more. Results from the pitch tests are added to the data previously shown (figures 94 and 95) in the extended comparisons of figures 100 and 101. They are consistent with the other data and DSSP20 prediction of Z' is in good agreement out to the highest pitch angle. On the other hand, the high incidence data for pitching moment M' is less consistent, and the DSSP20 prediction is strongly divergent at pitch angles greater than about ± 20 degrees (although the absolute value of pitching moment is not great). Yaw results from these tests are discussed below.

In 1992, some very high incidence tests were done in a preliminary series of submarine rising stability experiments in the 1.5×1.5 m blowdown wind tunnel at IAR [36]. They included a number of runs with incidence up to -90 degrees angle of attack, and $+90$ degrees angle of drift. The model had sailplanes in addition to the standard cruciform tail and sail; this configuration is denoted HSsT.

As determined by comparison with HST data, the sailplanes had a significant effect on vertical plane loads in pitch, but a negligible effect on lateral loads in yaw. As there was no comparable HSsT data from any other test series in the database, the blowdown tunnel data are compared with only DSSP20 predictions in pitch, figures 102 to 104, and with both DSSP20 predictions and HST data (including 1991 STR high incidence results) in yaw, figures 105 to 108. High and moderate incidence data sets are reasonably consistent with each other; predictions from DSSP20 start to diverge at about ± 30 degrees for the forces and about ± 20 degrees for the moments.

5.6 Review

The foregoing comparisons with DSSP20 demonstrate that the in-plane force and moment are modeled reasonably well for this submarine, within a moderate range of incidence. Nevertheless, a number of areas for further improvement can be identified, including:

- Deficiencies in the hull model, such as the ratio of linear to nonlinear terms, and high- α hydrodynamics;

- Modeling appendage stall inception and post-stall characteristics;
- Accounting for tailplane efficiency — this area is starting to be better understood [67], but the simple model in DSSP20 has not yet been revised; and
- In general, modeling the effects of very high incidence such as encountered in emergency recovery.

6 Concluding Remarks

The comparison of results obtained for the Standard Submarine Model in a number of different hydrodynamic test facilities demonstrates the uncertainty barrier encountered in experimental investigations despite the best efforts of the experimenter. There are several consequences of this, one being that it may be easy to become focused on apparent trends when dealing with data from only one source when other data might not corroborate, or might even contradict, the observations. On the other hand, trends can become obscured by differences between facilities and procedures, so care has to be taken before rejecting observations made from one set of data that are not found in another.

In general, agreement between the experimental results was fairly good, while some expected deviations, notably in sail stall inception, were observed. However, other Reynolds number effects were obscured by facility and procedural differences. For the measurements compared here, there is no “best” set of data. No additional corrections were applied in making the comparisons, although in a few of the results there were relatively large systematic errors uncorrected for. For the DERA data this arose because an objective of the experiment was to provide support and other interference components for the validation of CFD corrections.

For the purpose of comparing experimental results with the semiempirical prediction methods used in DSSP20, all available pertinent data were used, omitting only those that were clearly deficient in some respect. In-plane forces and moments are modeled reasonably well in the predictions at the moderate flow incidences encountered in normal operational manoeuvres. Nevertheless, there are some deficiencies to be addressed in the code, many of which become significant at the extreme incidence angles associated with emergency recovery. It should be noted that because of the difficulties of model testing at high incidence, the same problems are generally present, but rarely acknowledged, in other submarine simulation programs.

References

1. Mackay, M. (1986). Flow Visualization Experiments with Submarine Models in a Water Tunnel. (DREA TM 86/220). Defence R&D Canada – Atlantic.
2. Mackay, M. (1988). Flow Visualization Experiments with Submarine Models in a Wind Tunnel. (DREA TM 88/204). Defence R&D Canada – Atlantic.
3. Mackay, M. (1990). Static Pressure Measurement with Surface-Mounted Disc Probes. *Experiments in Fluids*, Vol. 9 No. 1/2.
4. Hooft, J.P. (1985). Hydrodynamic Forces on an Axi-Symmetric Submerged Body. (NSMB Report No. 46562–2–NS). Netherlands Ship Model Basin. Restricted.
5. Hooft, J.P. (1986). Hydrodynamic Forces on an A-Symmetric Submerged Body. (MARIN Report No. 46562–3–MO). Maritime Research Institute Netherlands. Restricted.
6. Hooft, J.P. (1986). The Near Surface Hydrodynamic Properties of Two Submerged Streamlined Bodies. (MARIN Report No. 46562–4–MO, also DREA CR/87/421). Maritime Research Institute Netherlands. Restricted.
7. Hooft, J.P. (1986). Hydrodynamic Reaction Forces on an Axi-Symmetric Hull with Sail. (MARIN Report No. 47344–1–MO, also DREA CR/87/420). Maritime Research Institute Netherlands. Restricted.
8. Hooft, J.P. (1987). Hydrodynamic Reaction Forces on an Axi-Symmetric Hull with Sail, Part 2. (MARIN Report No. 47344–4–MO, also DREA CR/87/433). Maritime Research Institute Netherlands. Restricted.
9. Hooft, J.P. (1987). Complementary Tests on the Hull-Sail Interaction. (MARIN Report No. 47994–1–MO). Maritime Research Institute Netherlands. Confidential.
10. Hooft, J.P. (1988). Vertical Force on a Submerged Body due to Sway. (MARIN Report No. 47994–2–MO, also DREA CR/88/416). Maritime Research Institute Netherlands. Confidential.
11. Hooft, J.P. (1988). Influence of Appendages on Submarine Hydrodynamics. (MARIN Report No. 47994–3–MO, also DREA CR/88/417). Maritime Research Institute Netherlands. Confidential.
12. Hooft, J.P. (1989). Results of the Model Tests on Submarine Rudders. (MARIN Report No. 48869–1–MO, also DREA CR/89/446). Maritime Research Institute Netherlands. Confidential.

13. Hooft, J.P. (1989). Hydrodynamic Forces on Submarine Rudders. (MARIN Report No. 48869-2-MO, also DREA CR/89/447). Maritime Research Institute Netherlands. Confidential.
14. Hooft, J.P. (1989). Error Analysis of the Model Test Results for Submarine Hydrodynamics. (MARIN Report No. 48869-3-MO, also DREA CR/89/448). Maritime Research Institute Netherlands. Confidential.
15. Hooft, J.P. (1990). Near Surface Effects on Submarine Hydrodynamics (in three volumes), Part 1: Main Hull Alone, Part 2: Main Hull with Sail, and Part 3: Main Hull with Sail and Rudders. (MARIN Report No. 49446-1-MO, also DREA CR/91/421). Maritime Research Institute Netherlands. Confidential.
16. Hooft, J.P. (1991). Analysis of Near Surface Effects on a Submarine. (MARIN Report No. 49446-2-MO, also DREA CR/91/452). Maritime Research Institute Netherlands. Confidential.
17. Hooft, J.P. (1992). Static Near Surface Effects on Submarine Hydrodynamics; 1991 Research. (MARIN Report No. 410737-1-MO, also DREA CR/93/403). Maritime Research Institute Netherlands. Confidential.
18. Hooft, J.P. (1994). Oscillation Tests with a Submarine Model near the Free Water Surface. (MARIN Report No. 410737-2-MO, also DREA CR/94/456). Maritime Research Institute Netherlands. Confidential.
19. RWDI Inc. (1989). Flow Visualization Test of DREA Standard Submarine Model, October–November 1988. (DREA CR/89/435). Defence R&D Canada – Atlantic.
20. RWDI Inc. (1991). Fall 1988 Wind Tunnel Tests of the DREA Six Metre Long Submarine Model – Force Data Analysis. (DREA CR/91/422). Defence R&D Canada – Atlantic. Limited Distribution.
21. Whickens, R.H. and de Souza, F. (1993). Flow Visualization Analysis and Flow Field Survey on the DREA Mark 1 Generic Submarine Model. (NRC-IAR LTR-HA-94, also DREA CR/93/455). Defence R&D Canada – Atlantic. Limited Distribution.
22. Drolet, Y. (1995). Circulation in the Vortex Field of a Submarine. (DREA CR/95/420). Defence R&D Canada – Atlantic. Limited Distribution.
23. Nguyen, V.D. and Tanguay, B. (1992). Wind Tunnel Investigation of the Strut Interference Effect for the DREA Mk 2 Static Test Rig. (NRC-IAR LTR-HA-30/6127, also DREA CR/92/460). Defence R&D Canada – Atlantic. Limited Distribution.
24. Nguyen, V.D., Drolet, Y., and Watt, G.D. (1995). Interference of Various Support Strut Configurations in Wind Tunnel Tests on a Model Submarine. (AIAA paper 95-0443). AIAA 33rd Aerospace Sciences Meeting, Reno, Nevada.

American Institute of Aeronautics and Astronautics. American Institute for Aeronautics and Astronautics.

25. Fournier, E. and Nguyen, V.D. (1993). Wind Tunnel Investigation of the DREA Powered Mk 1 Submarine Model (in two volumes). (NRC-IAR LTR-HA-30/6130, also DREA CR/93/459). Defence R&D Canada – Atlantic. Limited Distribution.
26. Fournier, E. and Drolet, Y. (1995). Effects of Propulsion on the Overall Forces of a Submarine (in two volumes). (DREA CR/95/409). Defence R&D Canada – Atlantic. Volume 1 Limited Distribution, Volume 2 Confidential.
27. Watt, G.D. (1995). Re-Evaluating the Thrust and Torque Measurement Capability of the Mark 1 Propulsion System for the DREA Static Test Rig. (DREA TM 95/209). Defence R&D Canada – Atlantic.
28. Watt, G.D. (1996). Submarine Rising Stability Tests at IAR: Sting Support Tare and Interference Corrections for the Steady State Roll Sweep Data from the 9 m Wind Tunnel. (DREA TM 96/231). Defence R&D Canada – Atlantic. Limited Distribution.
29. Aboulazm, A.F. (1991). Exploratory Fluid Visualization Tests at the Marine Institute Flume Tank. (DREA CR/91/419). Defence R&D Canada – Atlantic.
30. Nguyen, V.D. (1991). Preliminary Assessment of the Single Strut Support System for a 0.6 metre long DREA Standard Submarine Model. (NRC-IAR LTR-HA-84, also DREA CR/92/426). Defence R&D Canada – Atlantic. Limited Distribution.
31. Butterworth, P.J. (1993). The Measurement of Forces, Moments, and Static Pressures on a Model Submarine. (DRA/AWMH/TR93023). Defence Research Agency. Limited Distribution.
32. Hooft, J.P. (1992). Wave Excited Forces on a Submarine, Part 1. Experimental Results with a Streamlined Hull with Appendages. (MARIN Report No. 411043-1-ZT, also DREA CR/93/401/Pt.1). Maritime Research Institute Netherlands. Limited Distribution.
33. Hooft, J.P. (1992). Wave Excited Forces on a Submarine, Part 2. Analysis of the Experiments with a Streamlined Hull with Appendages. (MARIN Report No. 411043-2-ZT, also DREA CR/93/401/Pt.2). Maritime Research Institute Netherlands. Limited Distribution.
34. Hooft, J.P. (1992). Wave Excited Forces on a Submarine, Part 3. Experimental Results with a Bare Streamlined Hull. (MARIN Report No. 411043-3-ZT, also DREA CR/93/401/Pt.3). Maritime Research Institute Netherlands. Limited Distribution.

35. Hooft, J.P. (1992). Wave Excited Forces on a Submarine, Part 4. Analysis of the Experiments with a Bare Streamlined Hull. (MARIN Report No. 411043-4-ZT, also DREA CR/93/401/Pt.4). Maritime Research Institute Netherlands. Limited Distribution.
36. Watt, G.D. (1993). Submarine Rising Stability Tests at IAR: Preliminary Steady State Test Results from the 5 Foot Blowdown Tunnel. (DREA TM 93/212). Defence R&D Canada – Atlantic. Limited Distribution.
37. Nienhuis, U. and Radstaat, G. (1994). Submarine Model Wake Survey and Propulsion Test, Phase 2: Presentation and Discussion of LDV Test Results. (MARIN Report No. 411288-2-DT, also DREA CR/95/408). Maritime Research Institute Netherlands. Limited Distribution.
38. van Wijngaarden, H.C.J. and Bruning, H. (1997). Model Tests in Calm Water for Shaft Bearing Forces on a Submarine Model. (MARIN Report No. 411288-3-VT, also DREA CR/97/433). Maritime Research Institute Netherlands. Limited Distribution.
39. Datta, I., Williams, C.D., and Pond, J. (1996). Use of the Marine Dynamic Test Facility to Measure Hydrodynamic Coefficients for a Generic Submarine Model. (NRC-IMD TR-1996-23). Institute for Marine Dynamics. Limited Distribution.
40. Mackay, M. (1996). Submarine Turning Circle Experiments in a Towing Tank. In *Warship '96 International Symposium on Naval Submarines 5*. London: The Royal Institution of Naval Architects.
41. Atkins, D.J. (1999). The Application of Computational Fluid Dynamics to the Hydrodynamic Design of Submarines. In *Warship '99 International Symposium on Naval Submarines 6*. London: The Royal Institution of Naval Architects.
42. Mackay, M. (1999). DSSP20 (Beta Edition) User Guide to the Preprocessing Modules. (DREA TM 1999-108). Defence R&D Canada – Atlantic.
43. Mackay, M. (1999). DSSP20 (Beta Edition) User Guide to the Simulation Modules. (DREA TM 1999-109). Defence R&D Canada – Atlantic.
44. ITTC (1990). Report of the Panel on Validation Procedures. In *Proceedings of the 19th ITTC*. Madrid: International Towing Tank Conference.
45. Hermanski, G., Derradji-Aouat, A., and Hackett, P. (2001). Uncertainty Analysis — Preliminary Data Error Estimation for Ship Model Experiments. In *Sixth Canadian Marine Hydromechanics and Structures Conference*. Vancouver: University of British Columbia.
46. Watt, G.D. (1989). Correcting Wind Tunnel Force Measurements for Wind Loading Deflections of the Model. (DREA TM 89/225). Defence R&D Canada – Atlantic.

47. Brown, T.R. and Hansen, K. (1987). A User Manual for Aeronautical Research Facilities in Building M-2. (Comprising Laboratory Reports LTR-LA-285, LTR-LA-286, and LTR-LA-287.) Low Speed Aerodynamics Laboratory, National Research Council.
48. Mackay, M. (1988). The Prediction of Submarine Out-of-Plane Force and Moment using a Panel Method. In *Warship '88 International Symposium on Conventional Naval Submarines*. London: The Royal Institution of Naval Architects.
49. Conway, J.T. and Mackay, M. (1990). Prediction of the Effects of Body Separation Vortices on Submarine Configurations using the CANAERO Panel Method. (AIAA paper 90-0302). AIAA 28th Aerospace Sciences Meeting, Reno, Nevada. American Institute of Aeronautics and Astronautics.
50. Mackay, M. and Conway, J.T. (1991). Modelling the Crossflow Body Separation on a Submarine using a Panel Method. In *Warship '91 International Symposium on Naval Submarines 3*. London: The Royal Institution of Naval Architects.
51. Glansdorp, C.C. (1982). A New Planar Motion Mechanism for Model Testing. In *Symposium on Advanced Hydrodynamic Testing Facilities*. (NATO DS/A/DR(83)252). NATO Defence Research Group.
52. Watt, G.D. (1994). The DREA Static Test Rig for Wind Tunnel Tests on Submarine Models – Development History and Future Options. (DREA Report 94/102). Defence R&D Canada – Atlantic. Limited Distribution.
53. Hooft, J.P. (1986). Hydrodynamic Forces on Tear-Drop Bodies. (MARIN Report No. 07659-1-MO). Maritime Research Institute Netherlands. Limited Distribution.
54. Hooft, J.P.(1996). Hydrodynamic Effects in Submarine Manoeuvring Models. In *Proceedings of the International Workshop on Submarine Hydromechanics* (Mackay, M., ed.). (DREA Special Report 96/2). Defence R&D Canada – Atlantic. Limited Distribution.
55. Allen, J.H. and Perkins, E.W. (1951). Characteristics of Flow over Inclined Bodies of Revolution. (NACA Research Memorandum A50L07). National Advisory Committee for Aeronautics.
56. Allen, J.H. and Perkins, E.W. (1951). A Study of Effects of Viscosity on Flow over Slender Inclined Bodies of Revolution. (NACA Report 1048). National Advisory Committee for Aeronautics.
57. Goldstein, S., ed. (1938). *Modern Developments in Fluid Dynamics*, Volume II. Oxford: OUP.
58. Ward, B. and Lloyd, A.R.J.M. (1990). Experiments to Measure Forces and Moments on Bodies of Revolution of Varying Fineness Ratios in Rectilinear

- Flow. (ARE TR90308). Admiralty Research Establishment. Limited Distribution.
59. Hoerner, S.F. (1958). *Fluid Dynamic Drag*. Midland Park NJ: published by the author.
 60. Mackay, M. (1995). A Review of Semiempirical Methods for Predicting Appendage Forces. (DREA Report 95/102). Defence R&D Canada – Atlantic. Limited Distribution.
 61. Mackay, M. (1995). Estimation of the Force due to a Submarine Sail or Similar Appendage. In *Third Canadian Marine Hydrodynamics and Structures Conference*. Halifax: Technical University of Nova Scotia.
 62. Aucher, M. (1981). Dynamique des Sous-Marins. In *Sciences et Techniques de l'Armement, 4^e fascicule*. Paris: Imprimerie Nationale.
 63. Lawrence, H.R. and Flax, A.H. (1954). Wing–Body Interference at Subsonic and Supersonic Speeds — Survey and New Developments. *Journal of the Aeronautical Sciences*, Vol. 21, No. 5.
 64. Pitts, W.C., Nielsen, J.N., and Kaatari, G.E. (1957). Lift and Center of Pressure of Wing–Body–Tail Combinations at Subsonic, Transonic, and Supersonic Speeds. (NACA Report 1307). National Advisory Committee for Aeronautics.
 65. Mackay, M. (2000). Some Effects of Tailplane Efficiency on Submarine Stability and Manoeuvring. (DREA TM 2001–031). Defence R&D Canada – Atlantic.
 66. Dempsey, E.M. (1977). Static Stability Characteristics of a Systematic Series of Stern Control Surfaces on a Body of Revolution. (DTNSRDC Report 77–0085). David Taylor Naval Ship Research and Development Center.
 67. Mackay, M., Bohlmann, H.J., and Watt, G.D. (2002). Modeling Submarine Tailplane Efficiency. In *Challenges in Dynamics, System Identification, Control and Handling Qualities for Land, Air, Sea, and Space Vehicles*. (RTO–MP–095). Paris: NATO RTO.

Table 1. Estimates of nondimensionalized symmetry error S'_x , in percent, for the HS configuration in yaw.

(HS in yaw)	R_e , million	X	Y	Z	K	M	N
NAE	7.0	1.1	0.5	6.0	4.2	4.1	3.5
MARIN	6.5	1.4	0.2	0.9	3.4	4.0	0.3
	9.75	6.9	0.9	1.3	4.0	6.0	0.3
STR	23.0	5.5	6.7	1.2	7.9	9.5	2.2
DERA	7.6	9.3	9.0	16.7	12.3	5.6	8.9
	11.4	6.8	9.9	21.0	14.3	7.7	11.7
MDTF	11.5	9.7	3.2	3.8	3.8	3.3	2.3

Table 2. Estimates of nondimensionalized symmetry error S'_x , in percent, for the HST configuration in yaw.

(HST in yaw)	R_e , million	X	Y	Z	K	M	N
STR	11.0	9.4	2.6	10.5	3.2	3.5	1.7
	16.0	8.8	3.8	12.1	2.9	2.6	1.8
	23.0	8.2	5.0	13.1	4.8	1.2	4.4
(see note)	23.0	8.2	5.0	5.4	2.6	4.8	4.4
DERA	7.6	8.9	7.5	12.0	14.3	5.3	12.8
	11.4	5.3	6.2	15.8	14.4	4.9	17.4
	15.2	9.0	18.4	31.0	28.1	12.3	36.8
MDTF	11.5	9.0	3.2	2.8	4.6	1.4	4.3

Note: the first three rows of STR data do not have the 1991 corrections applied, see section 3.3. The last row has corrections applied for the Z , K , and M data.

Table 3. Estimates of neutral point x'_n for hull alone.

(H)	R_e , million	x'_n
NAE	7.0	0.710
MARIN	6.5	1.478
	13.0	1.562
STR	23.0	0.976
DERA	7.6	1.542
	11.4	1.796
	15.2	1.603
MDTF	11.5	1.470

Table 4. Estimates of vertical plane neutral point x'_{vn} for hull and sail.

(HS in pitch)	R_e , million	x'_{vn}
MARIN	6.5	0.704
	9.75	0.760
STR	23.0	0.925
DERA	7.6	1.306
	11.4	1.274
MDTF	11.5	1.208

Table 5. Estimates of horizontal plane neutral point x'_{hn} for hull and sail.

(HS in yaw)	R_e , million	x'_{hn}
NAE	7.0	0.168
MARIN	6.5	0.293
	9.75	0.282
STR	23.0	0.219
DERA	7.6	0.275
	11.4	0.279
MDTF	11.5	0.290

Table 6. Estimates of neutral point x'_n for hull and tail.

(HT)	R_e , million	x'_n
STR	23.0	0.132
DERA	7.6	0.315
	11.4	0.316
MDTF	11.5	0.375

Table 7. Estimates of vertical plane neutral point x'_{vn} for hull, sail, and tail.

(HST in pitch)	R_e , million	x'_{vn}
STR	23.0	0.186
DERA	7.6	0.273
	11.4	0.283
	15.2	0.201
MDTF	11.5	0.275

Table 8. Estimates of horizontal plane neutral point x'_{hn} for hull, sail, and tail.

(HST in yaw)	R_e , million	x'_{hn}
STR	11.0	0.199
	16.0	0.186
	23.0	0.182
DERA	7.6	0.191
	11.4	0.207
	15.2	0.182
MDTF	11.5	0.194

Table 9. Hull alone: ratios of slopes $Z'_{w'}$ and $M'_{w'}$ to the regressed¹ DSSP20 values.

(H)	R_e , million	$Z'_{w'}$ ratio	$M'_{w'}$ ratio
NAE	7.0	1.430	0.827
MARIN	6.5	0.876	0.967
	13.0	0.860	1.004
	All ²	0.881	1.098
STR	23.0	1.281	1.018
DERA	7.6	0.749	0.941
	11.4	0.677	0.991
	15.2	0.801	1.045
	All	0.708	0.972
MDTF	11.5	0.927	1.109
Data ³	All	0.911	0.995
Allen & Perkins	Regression ¹	0.407	1.320
	Nominal slopes ⁴	0.000	1.325
DSSP20 ⁵	Regression ¹	1.000	1.000
	HULFOR calculated	0.959	1.014
	HULFOR empirical	0.866	1.064
	SUBSIM	0.114	0.760

Notes:

1. All regression is order 3 over values in the range $-6 < \alpha < +6$ degrees.
2. The full set of MARIN data included some additional values for $R_e = 9.75 \times 10^6$ that are not shown on figure 11.
3. This is the complete concatenated set of experimental data at all Reynolds numbers.
4. Nominal slopes are from equation (4).
5. DSSP20 uses HULFOR calculated coefficients for its calculations; see section 5.1.

Table 10. Sail: ratios of apparent sail factor k_s to the DSSP20 value obtained from equation (7).

k_s ratio	(HS-H)	(HST-HT)
NAE	0.956	
MARIN	0.866	
STR	0.959	0.775
DERA	0.901	0.819
MDTF	0.952	0.810

Table 11. Sail: ratios of the roll moment arm as $\beta \rightarrow 0$ to the DSSP20 value $(4/3\pi)b$ obtained from equation (8).

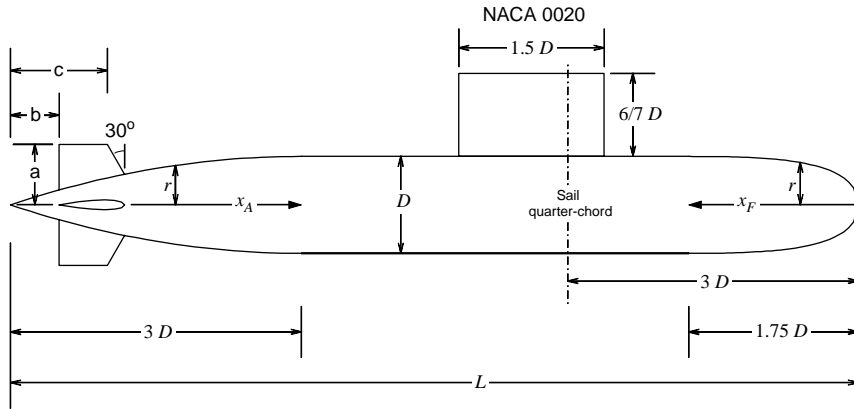
C_{P_b} ratio	(HS-H)	(HST-HT)
NAE	0.934	
MARIN	0.983	
STR	1.030	0.988
DERA	1.101	1.098
MDTF	1.104	1.135

Table 12. Sail: apparent chordwise center of pressure, C_{P_c} , as $\beta \rightarrow 0$, fraction of chordlength aft of the leading edge (i.e., negative forward of the leading edge).

C_{P_c}	(HS-H)	(HST-HT)
NAE	0.391	
MARIN	0.201	
STR	0.289	-0.415
DERA	0.159	-0.258
MDTF	-0.055	-0.327

Tail appendages,
four identical, NACA 0015
Dimensions,
a: $0.625 D$
b: $0.5 D$
c: $1.0 D$

$L = 8.75 D$
Hull offsets r
given in text



The Standard Model hull is specified in three sections: nose, midbody, and tail. The parent hull has $L/D = 8.75$, and

- Nose:
- Length, $1.75D$
 - Axisymmetric profile defined by:

$$\frac{r}{D} = 0.8685\sqrt{\frac{x_F}{D}} - 0.3978\frac{x_F}{D} + 0.006511\left(\frac{x_F}{D}\right)^2 + 0.005086\left(\frac{x_F}{D}\right)^3$$

where x_F is distance measured aft from the FP

- Midbody:
- Length, $4D$
 - Axisymmetric, with constant diameter D

- Tail:
- Length, $3D$
 - Axisymmetric parabolic profile:

$$\frac{r}{D} = \frac{1}{3}\left(\frac{x_A}{D}\right) - \frac{1}{18}\left(\frac{x_A}{D}\right)^2$$

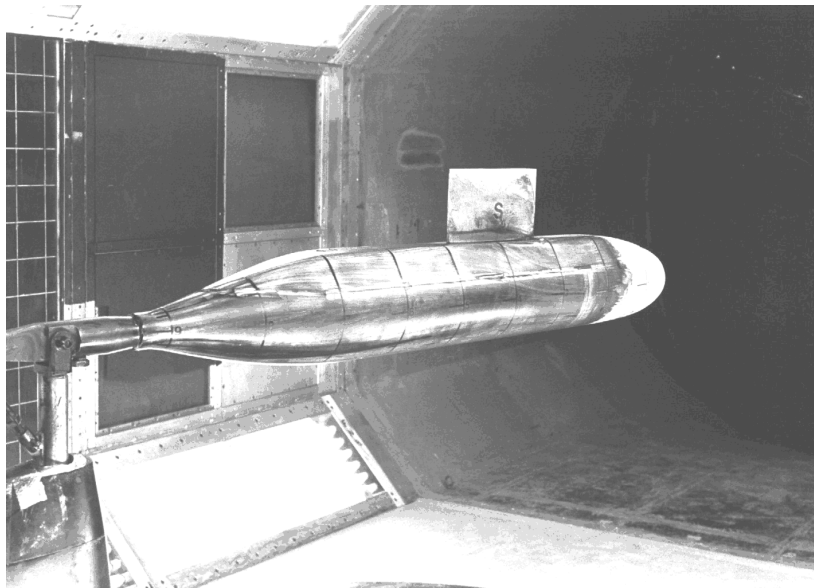
where x_A is distance measured forward from the AP

Tail appendage sections are defined parallel to the hull longitudinal axis.

Figure 1. The Standard Model: parent (HST) definition.

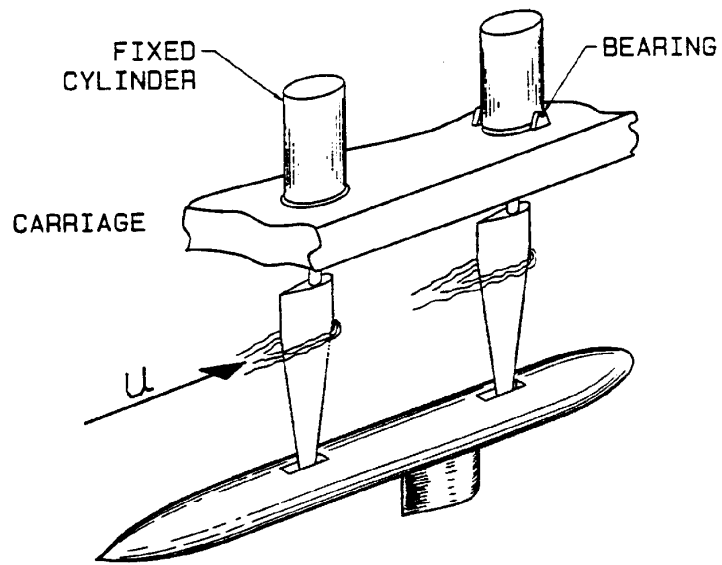


(a)

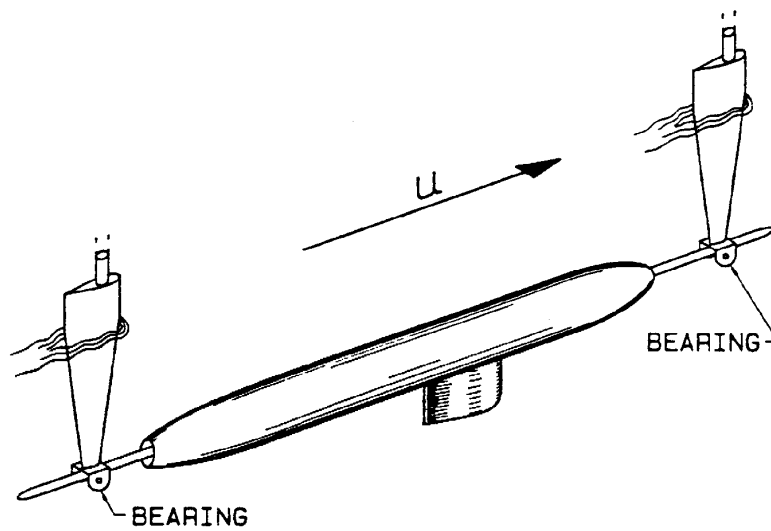


(b)

Figure 2. NAE 2 × 3 m wind tunnel: (a) general arrangement for sting-supported models; (b) oil flow visualization with a Hull + Sail + Deck Casing configuration.

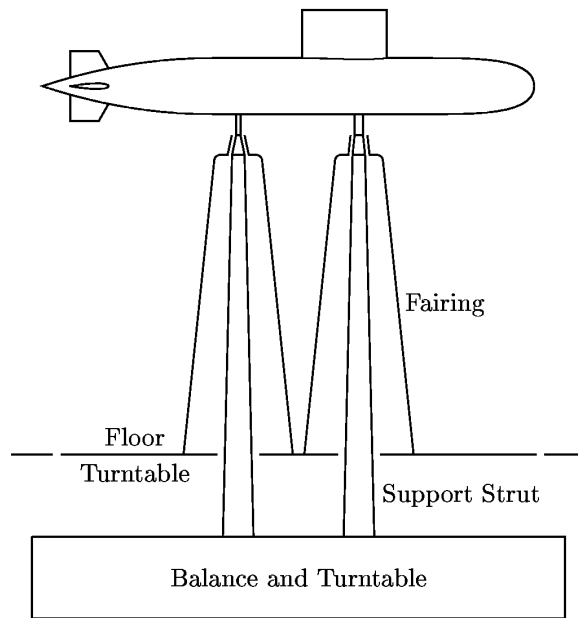


(a)

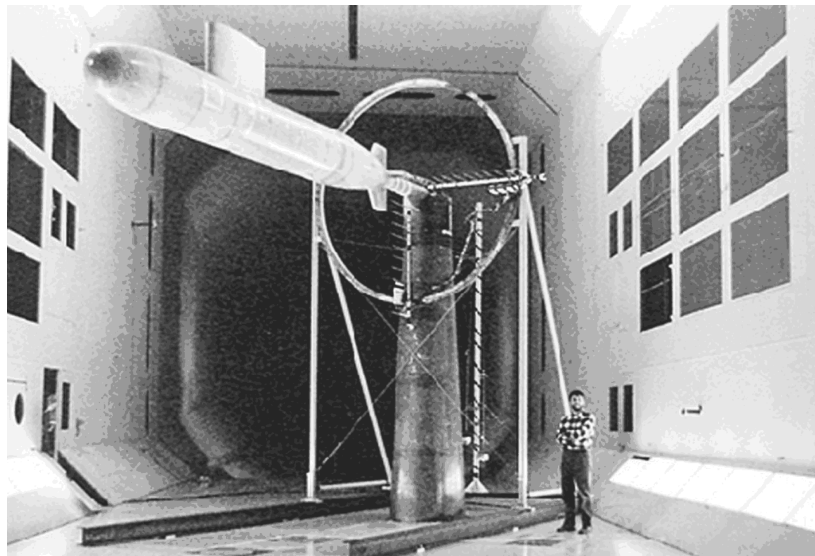


(b)

Figure 3. MARIN PMM: (a) conventional twin-sword model support;
(b) modified support arrangement.



(a)



(b)

Figure 4. STR (IAR 9 × 9 m wind tunnel): (a) standard twin strut support arrangement; (b) sting model support arrangement with wake survey rig.

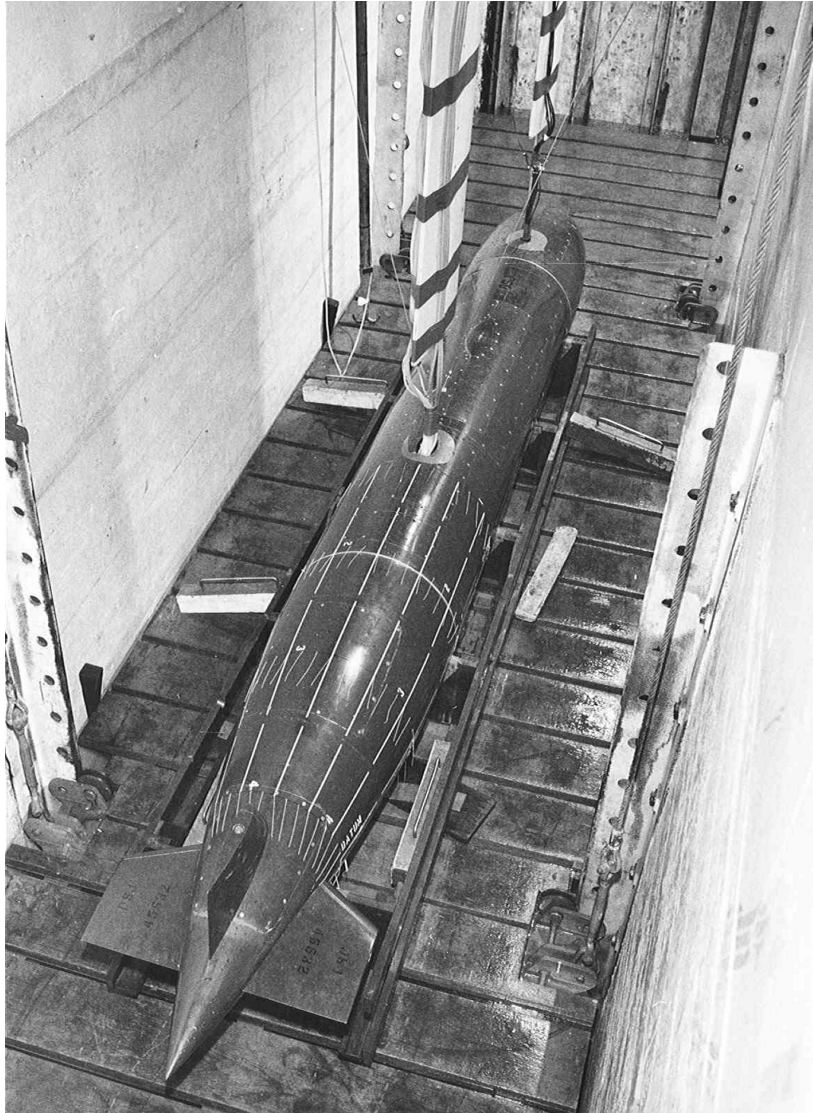
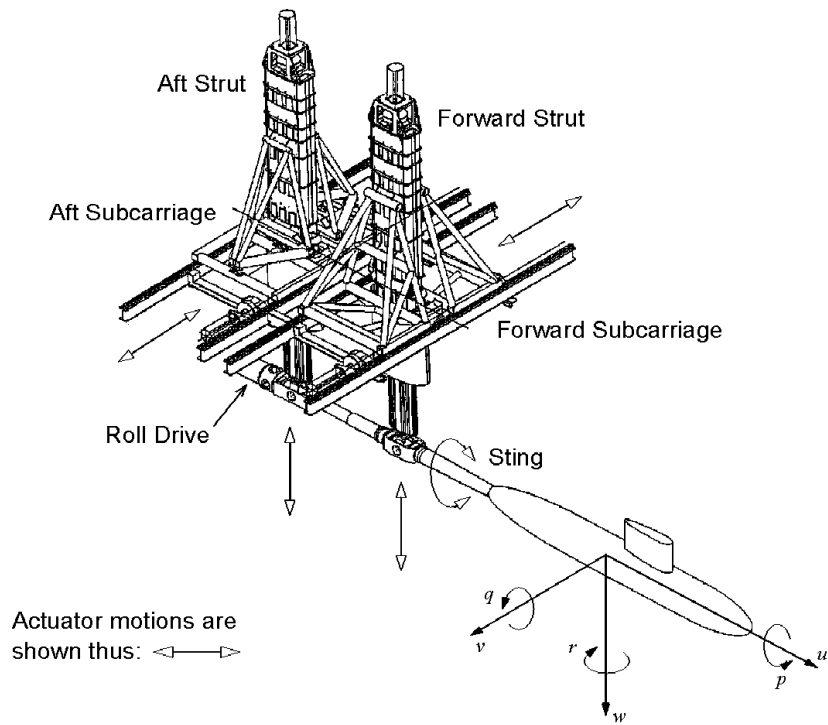
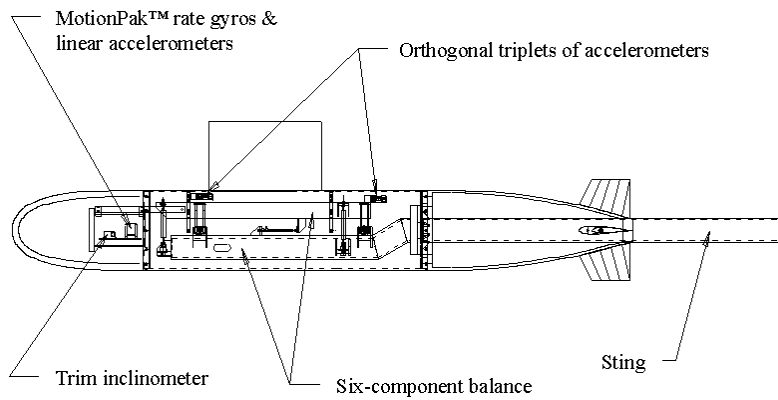


Figure 5. DERA (Haslar) Ship Tank: model DSJ Hull + Tail configuration on PMM twin-sword mounting [41]. © British Crown Copyright 1999/DERA.



(a)



(b)

Figure 6. MDTF (IMD 200 m towing tank): (a) general arrangement; (b) model internal balance arrangement.

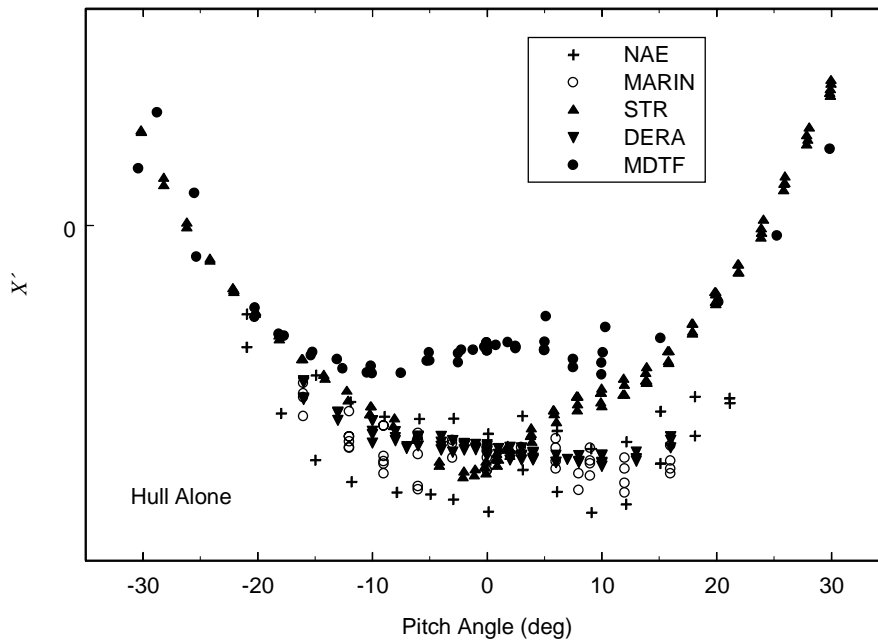


Figure 7. Hull alone axial force: all data sets.

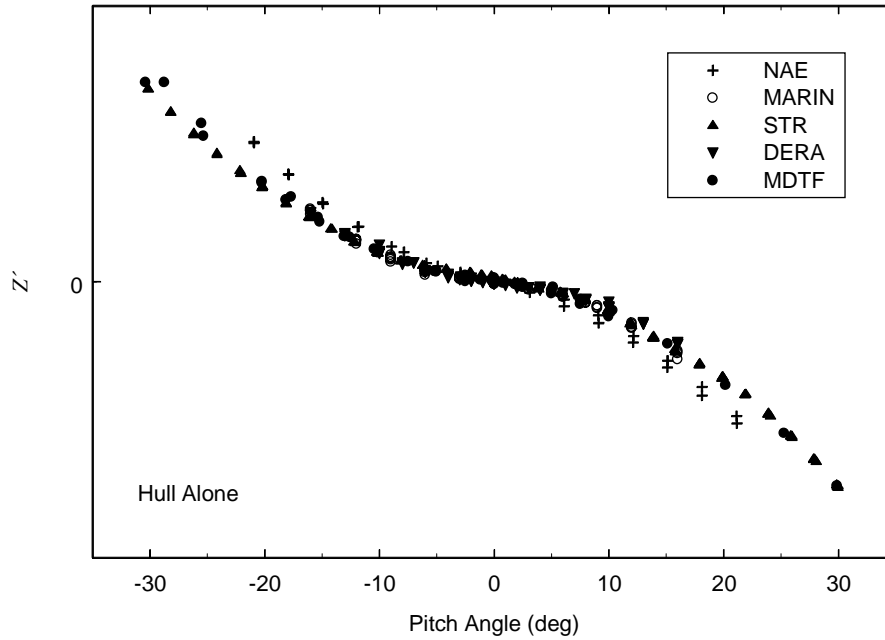


Figure 8. Hull alone normal force: all data sets.

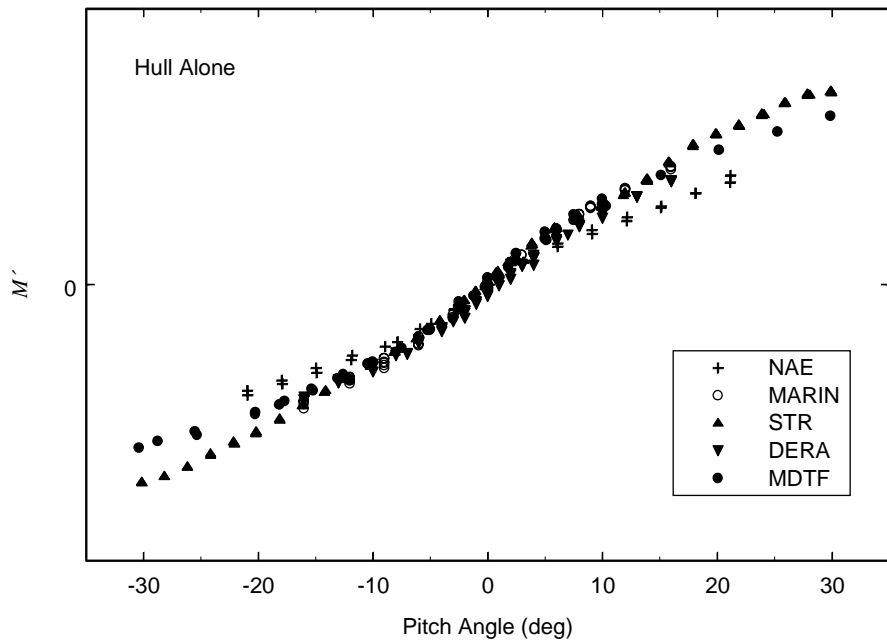


Figure 9. Hull alone pitching moment: all data sets.

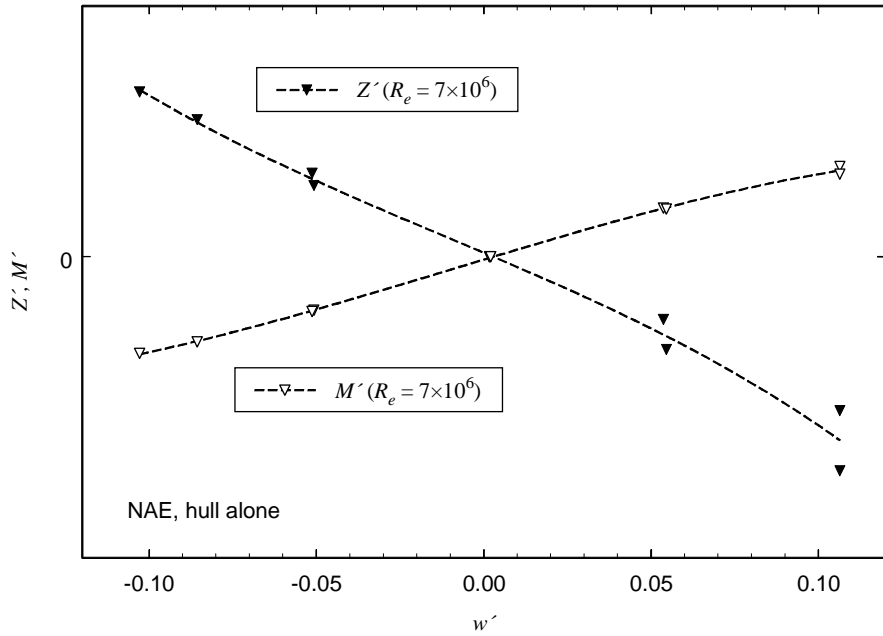


Figure 10. NAE normal force and pitching moment for hull alone at $-6 < \alpha < +6$ degrees.

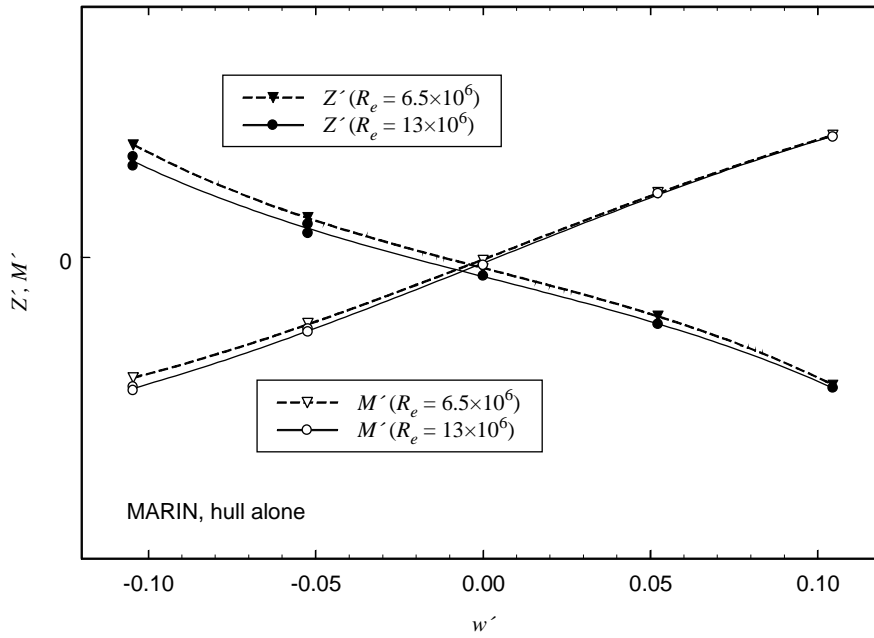


Figure 11. MARIN normal force and pitching moment for hull alone at $-6 < \alpha < +6$ degrees.

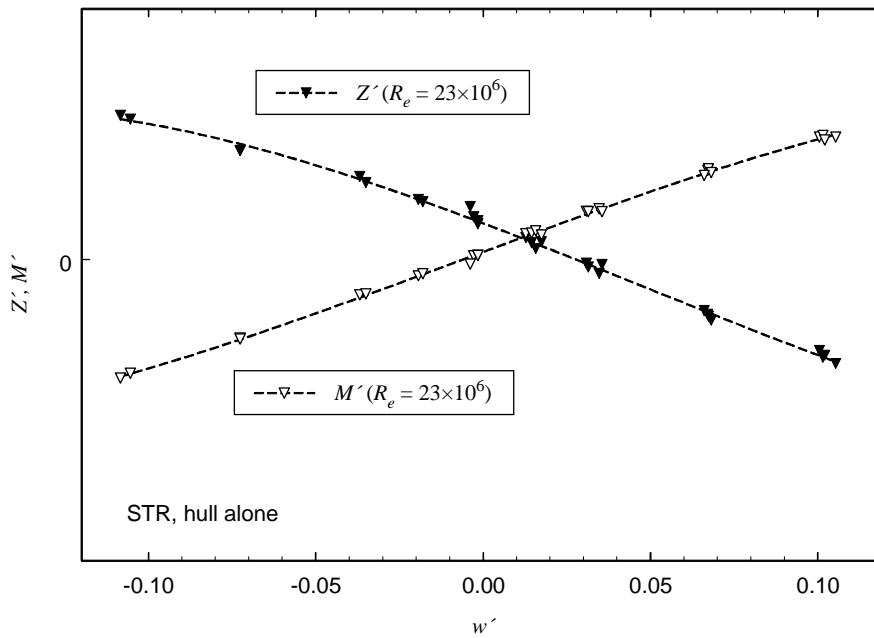


Figure 12. STR normal force and pitching moment for hull alone at $-6 < \alpha < +6$ degrees.

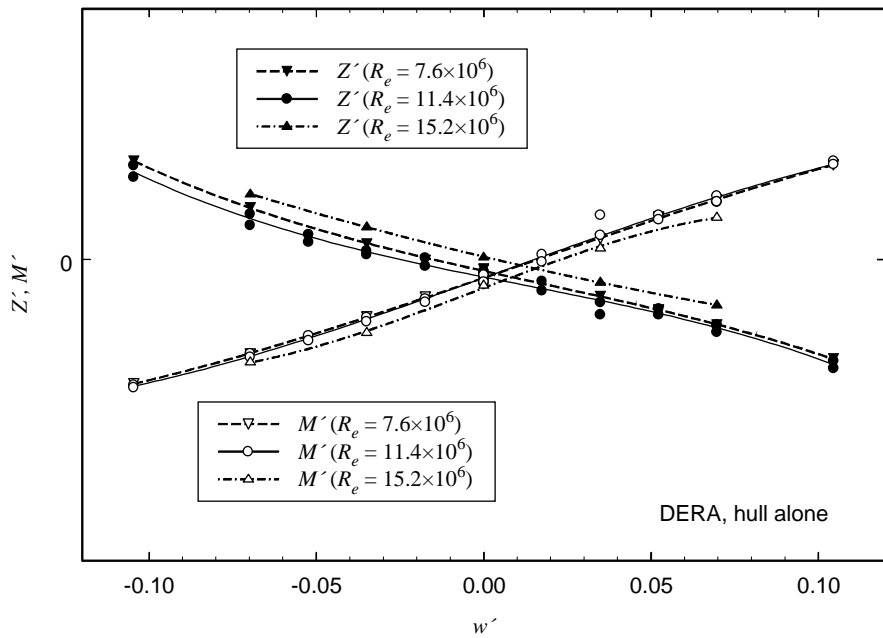


Figure 13. DERA normal force and pitching moment for hull alone at $-6 < \alpha < +6$ degrees.

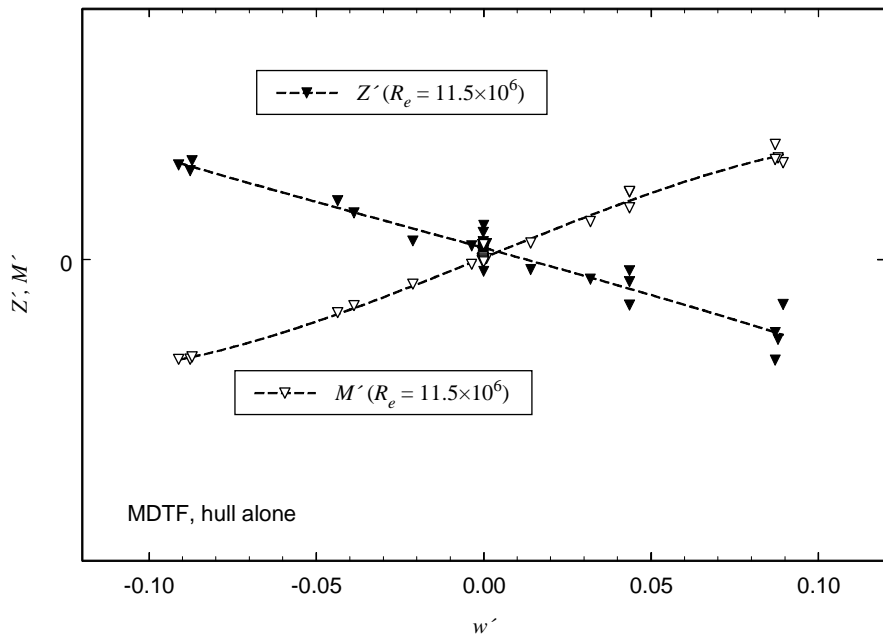


Figure 14. MDTF normal force and pitching moment for hull alone at $-6 < \alpha < +6$ degrees.

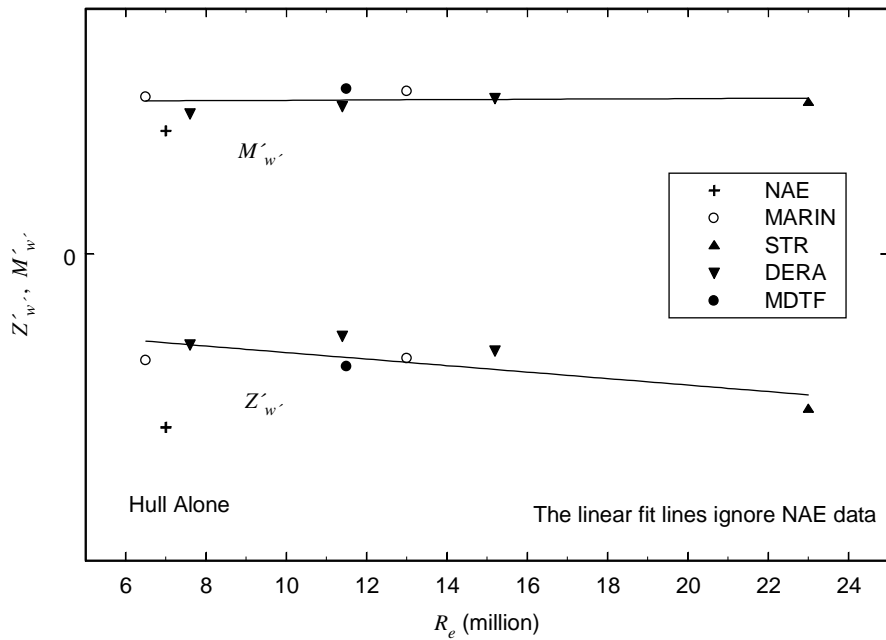


Figure 15. Hull alone $Z'_{w'}$ and $M'_{w'}$: all data sets.

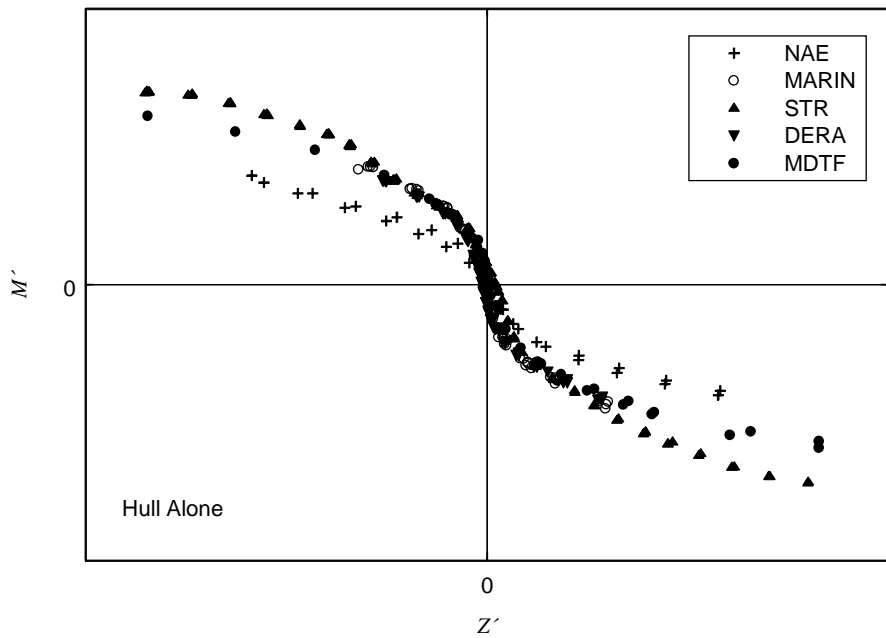


Figure 16. Hull alone pitching moment vs normal force: all data sets.

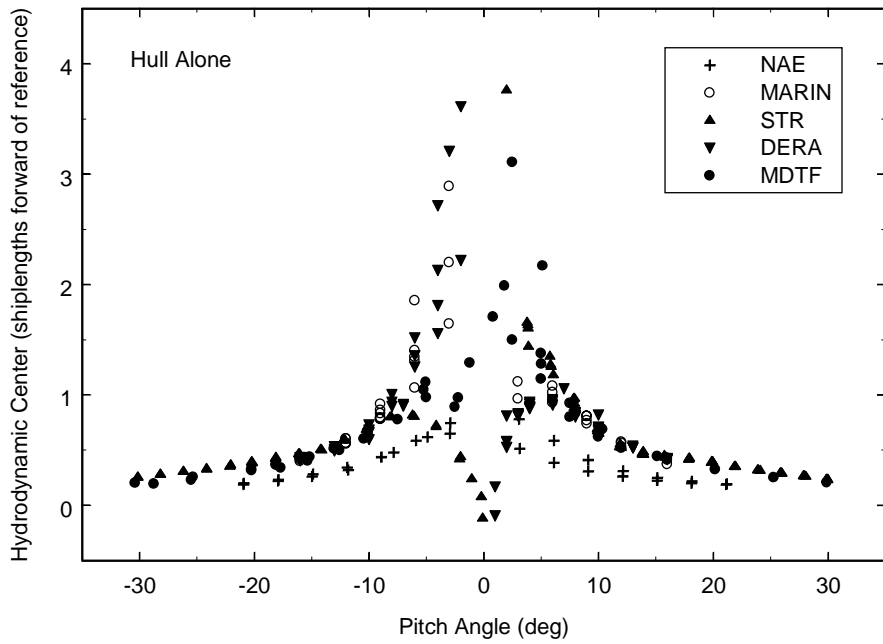


Figure 17. Hull alone hydrodynamic center: all data sets.

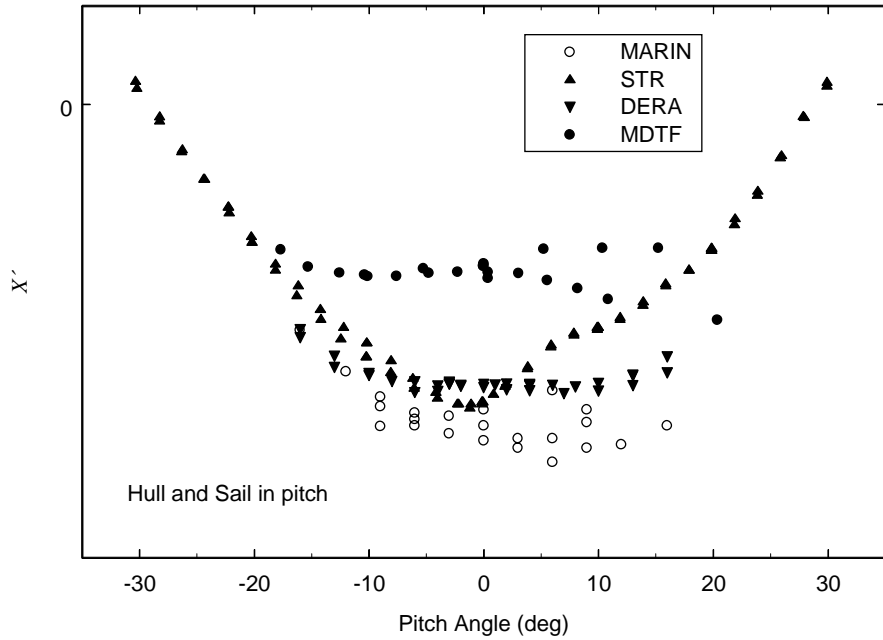


Figure 18. Hull and sail in pitch, axial force: all data sets.

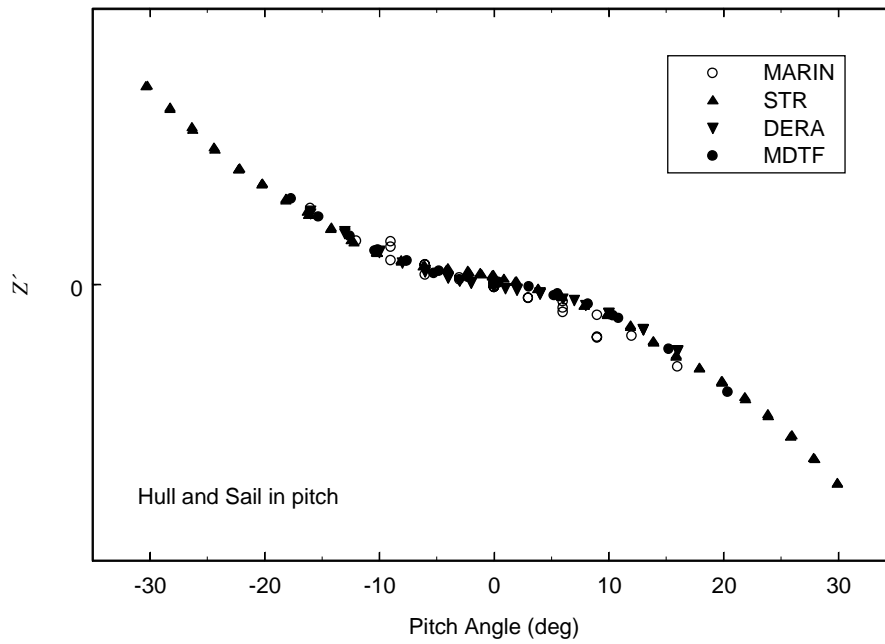


Figure 19. Hull and sail in pitch, normal force: all data sets.

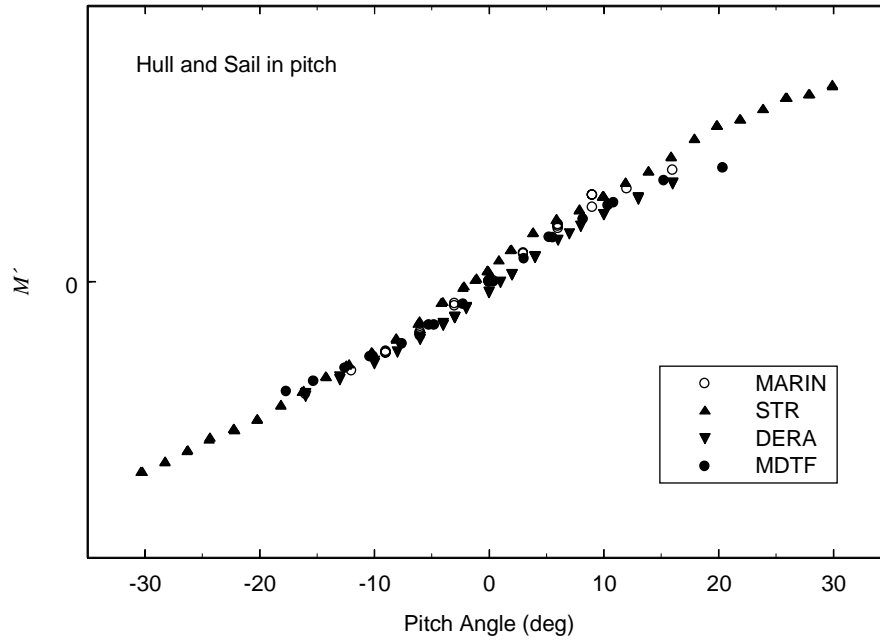


Figure 20. Hull and sail in pitch, pitching moment: all data sets.

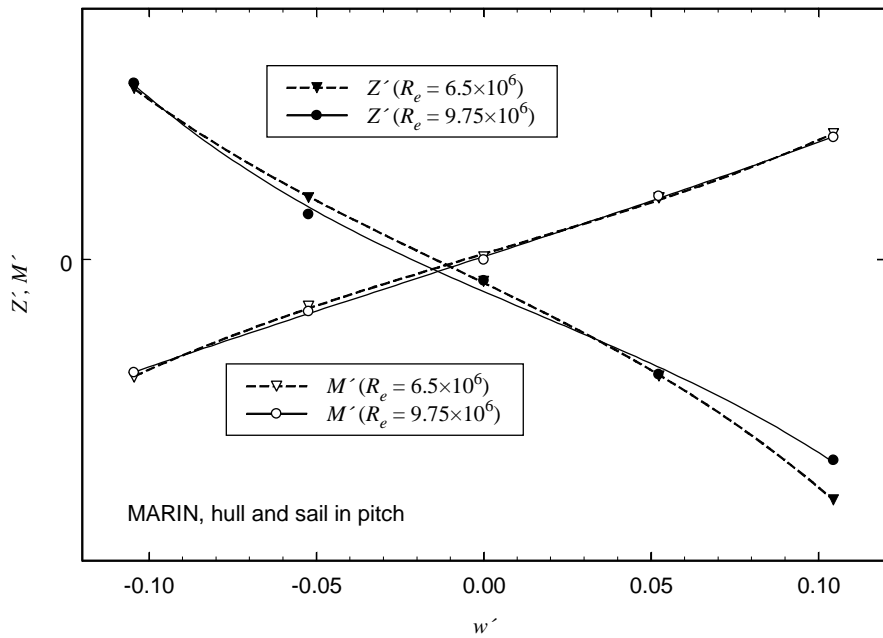


Figure 21. MARIN normal force and pitching moment for hull and sail at $-6 < \alpha < +6$ degrees.

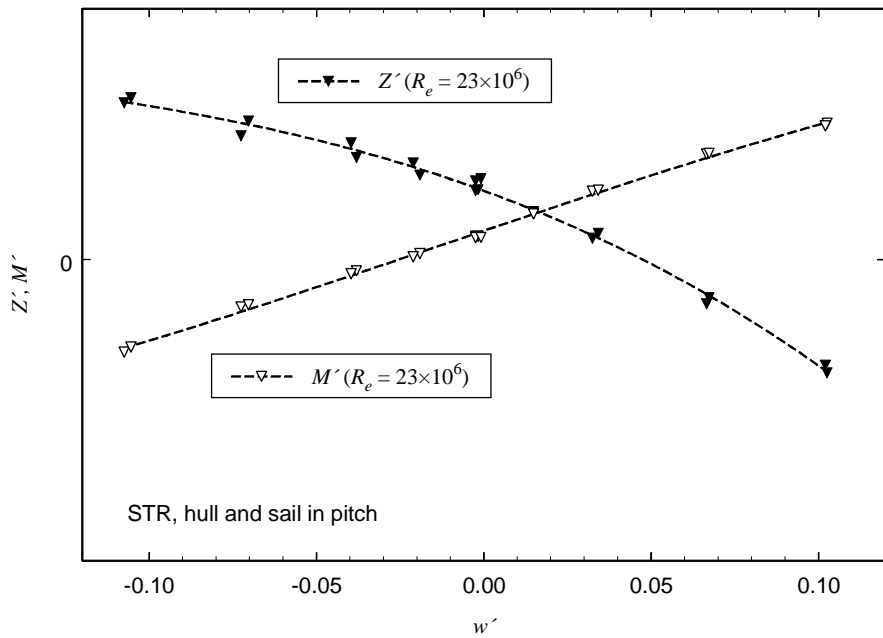


Figure 22. STR normal force and pitching moment for hull and sail at $-6 < \alpha < +6$ degrees.

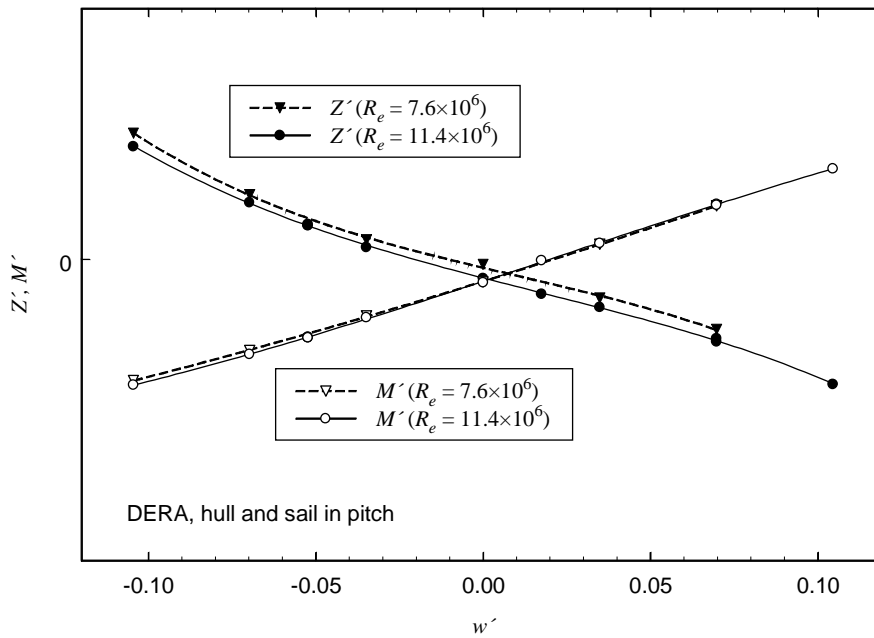


Figure 23. DERA normal force and pitching moment for hull and sail at $-6 < \alpha < +6$ degrees.

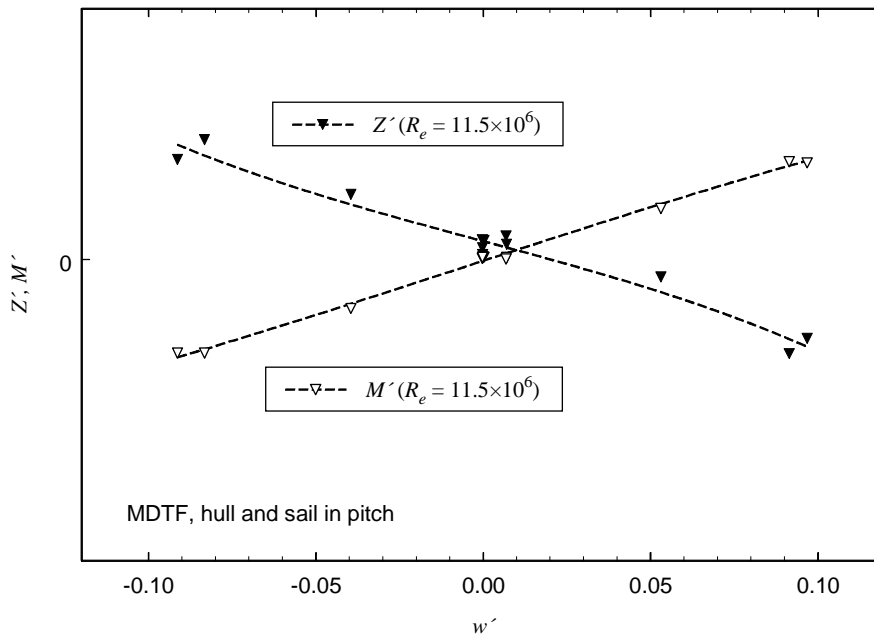


Figure 24. MDTF normal force and pitching moment for hull and sail at $-6 < \alpha < +6$ degrees.

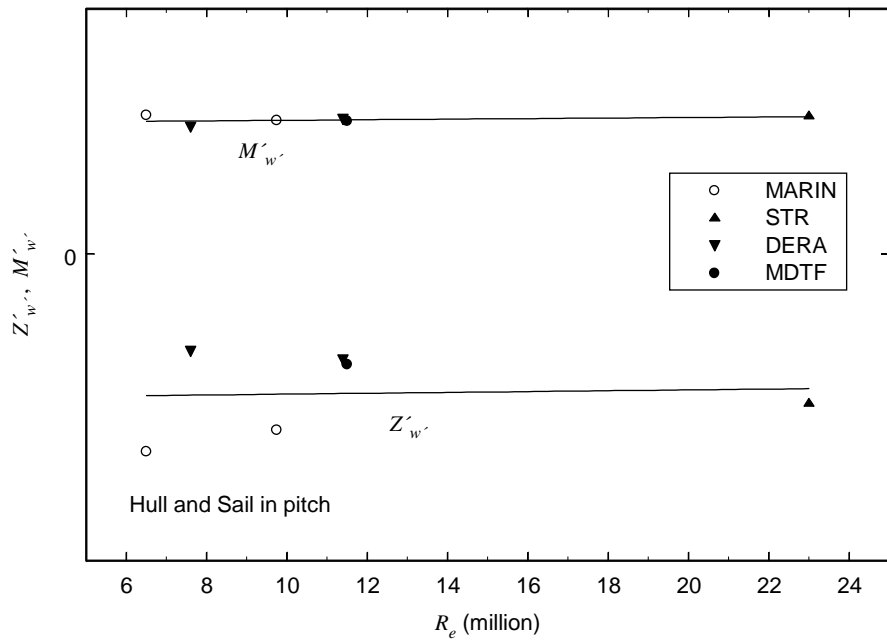


Figure 25. Hull and sail, $Z'_{w'}$ and $M'_{w'}$: all data sets.

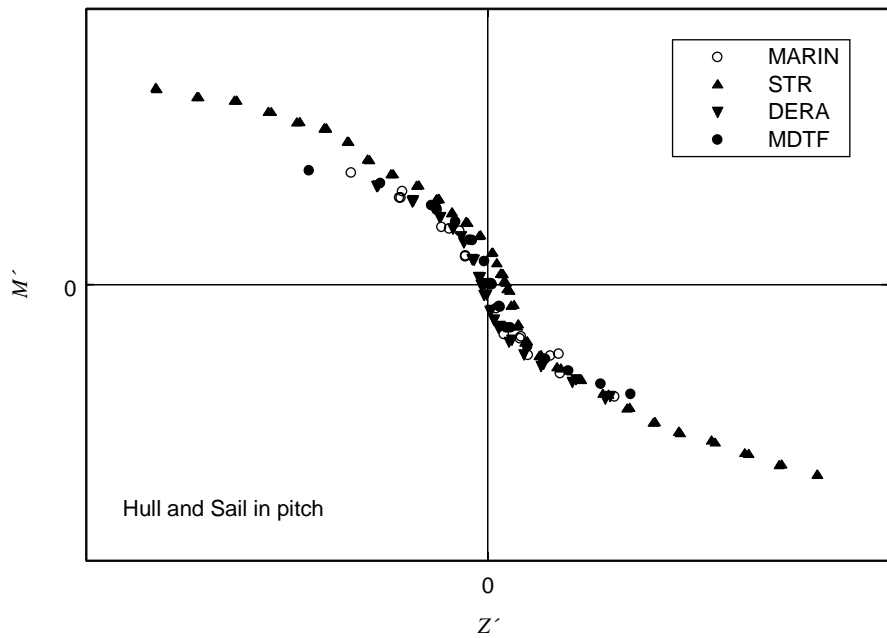


Figure 26. Hull and sail, pitching moment vs normal force: all data sets.

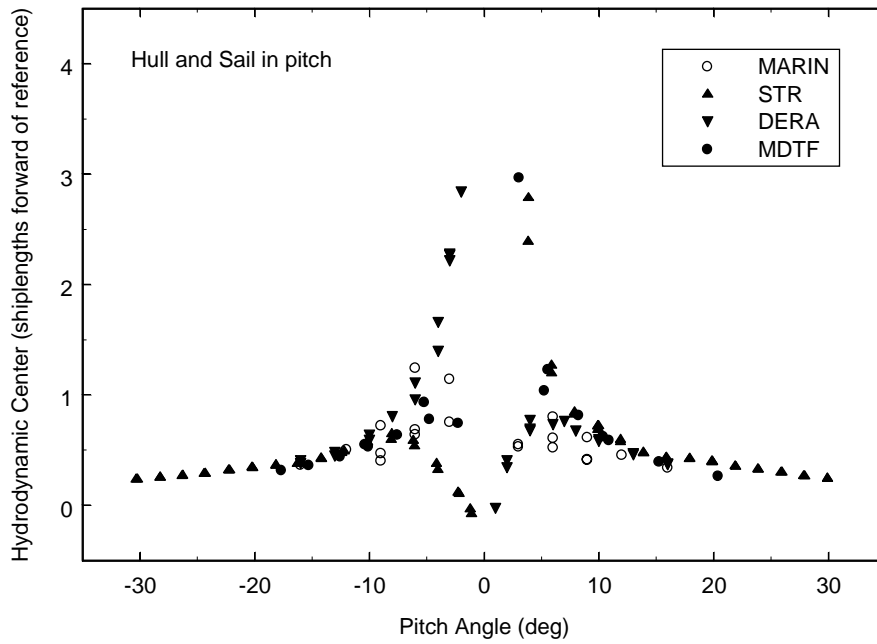


Figure 27. Hull and sail, vertical plane hydrodynamic center: all data sets.

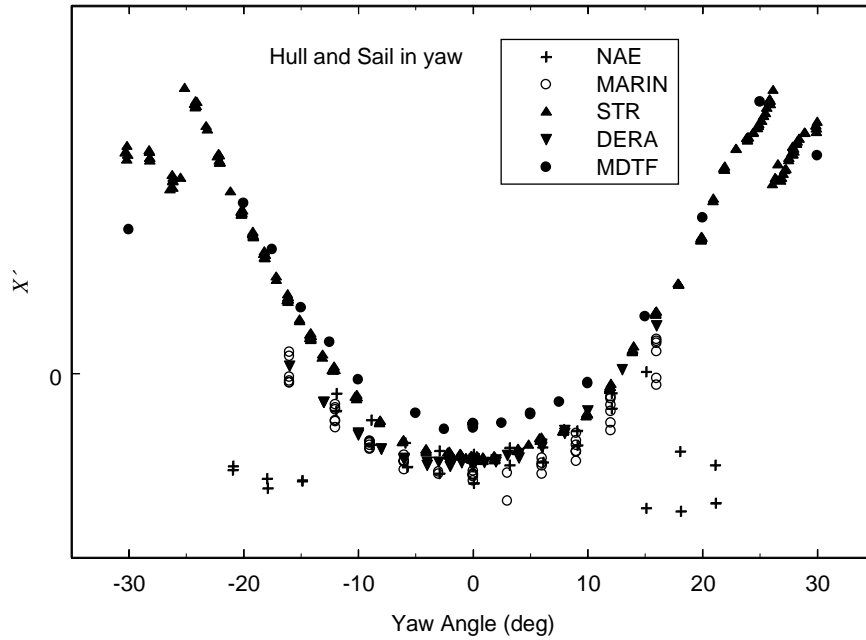


Figure 28. Hull and sail in yaw, axial force: all data sets.

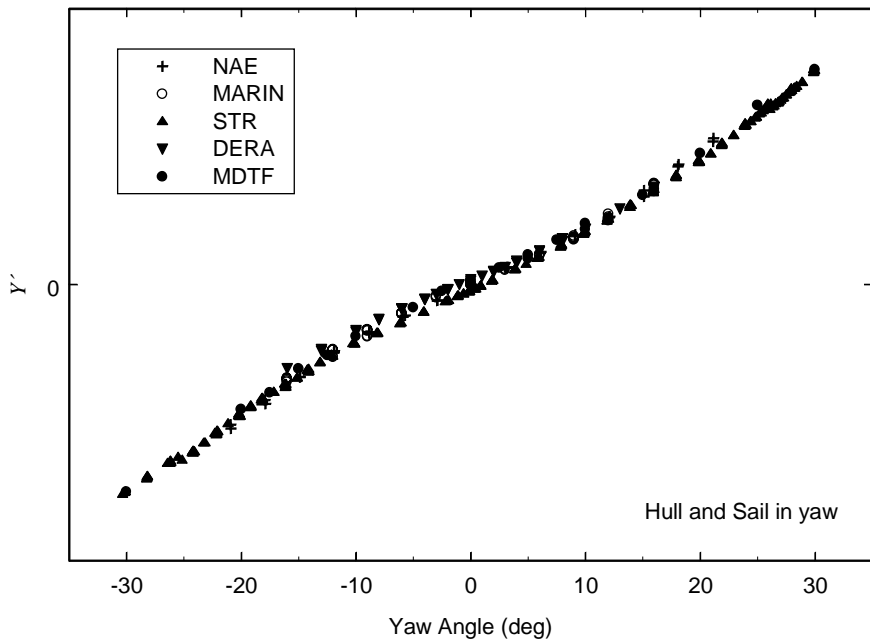


Figure 29. Hull and sail in yaw, side force: all data sets.

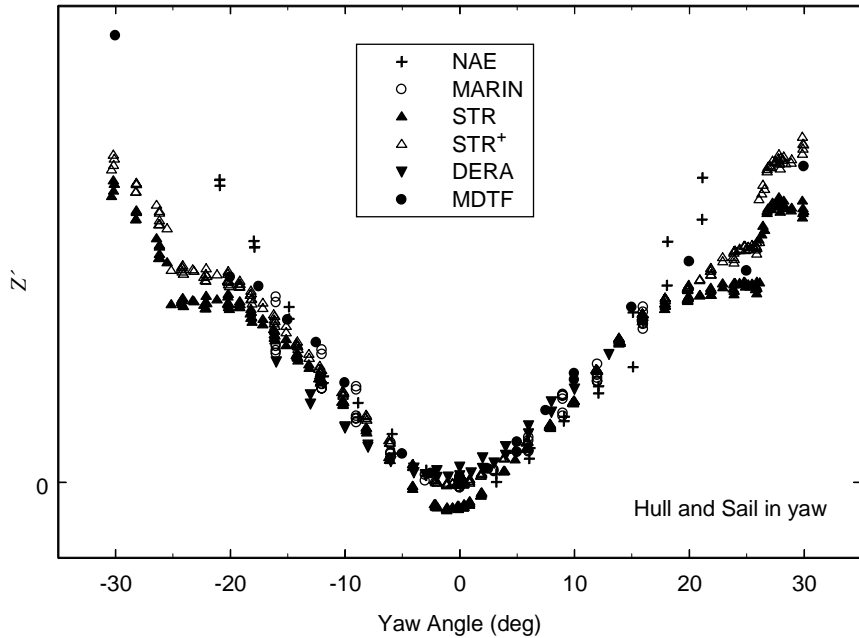


Figure 30. Hull and sail in yaw, normal force: all data sets. The notation STR⁺ denotes 1994 corrected data.

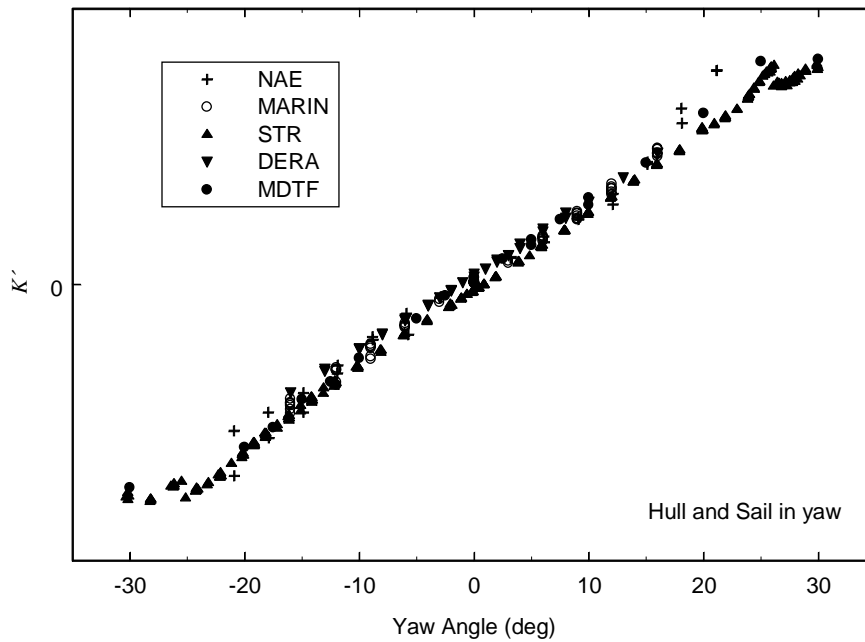


Figure 31. Hull and sail in yaw, rolling moment: all data sets. STR 1994 corrected data are indistinguishable from uncorrected data, and have been omitted from this figure.

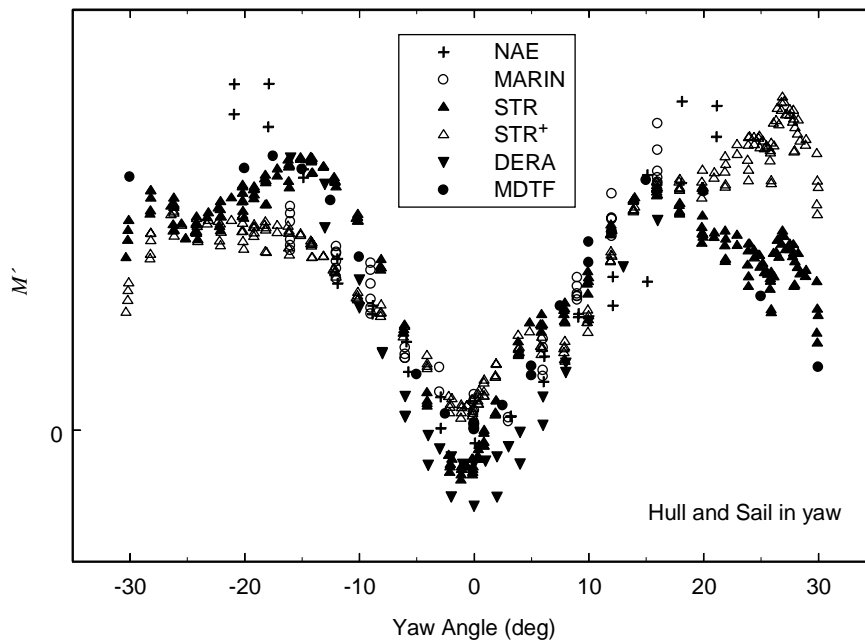


Figure 32. Hull and sail in yaw, pitching moment: all data sets. The notation STR⁺ denotes 1994 corrected data.

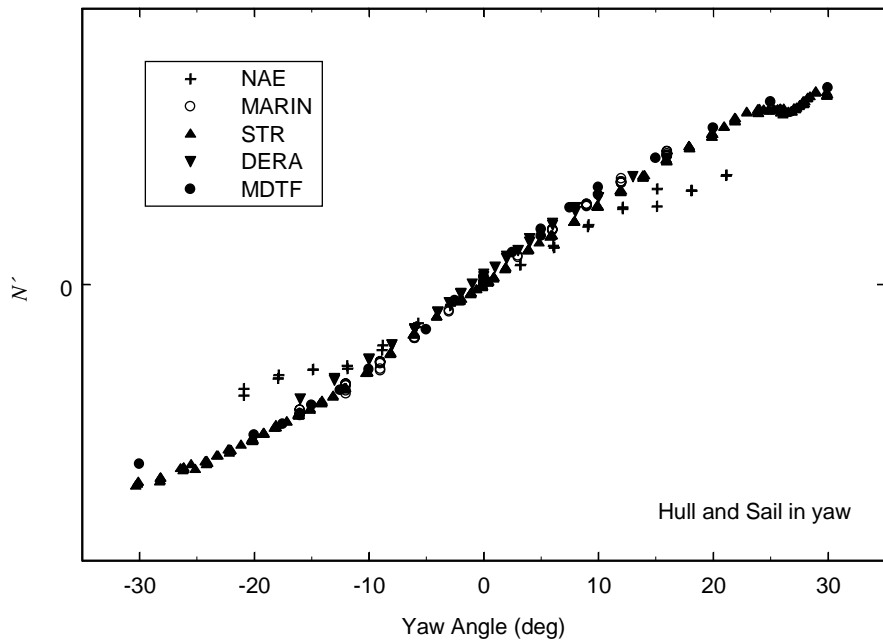


Figure 33. Hull and sail in yaw, yawing moment: all data sets.

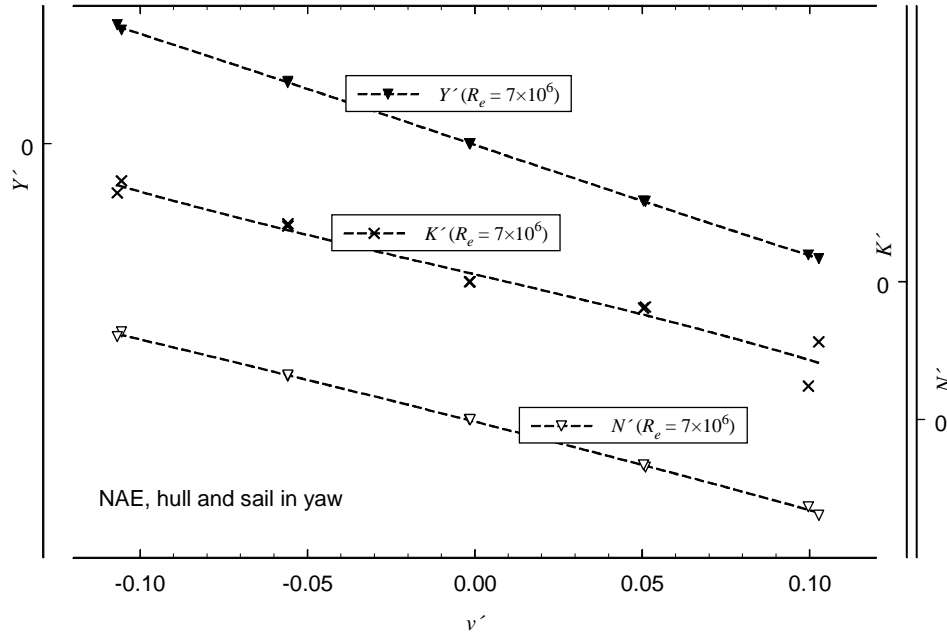


Figure 34. NAE in-plane force and moments for hull and sail at $-6 < \beta < +6$ degrees.

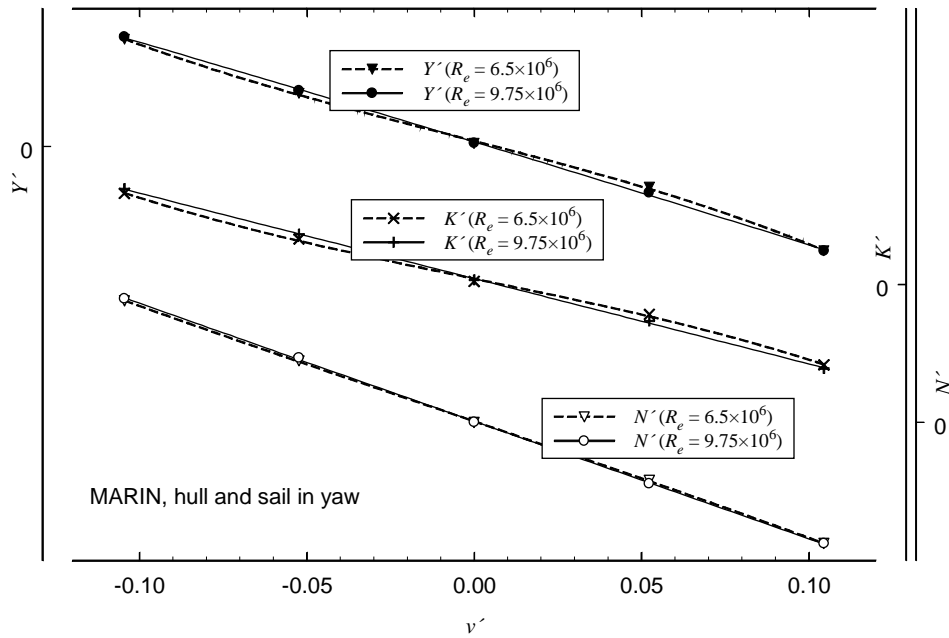


Figure 35. MARIN in-plane force and moments for hull and sail at $-6 < \beta < +6$ degrees.

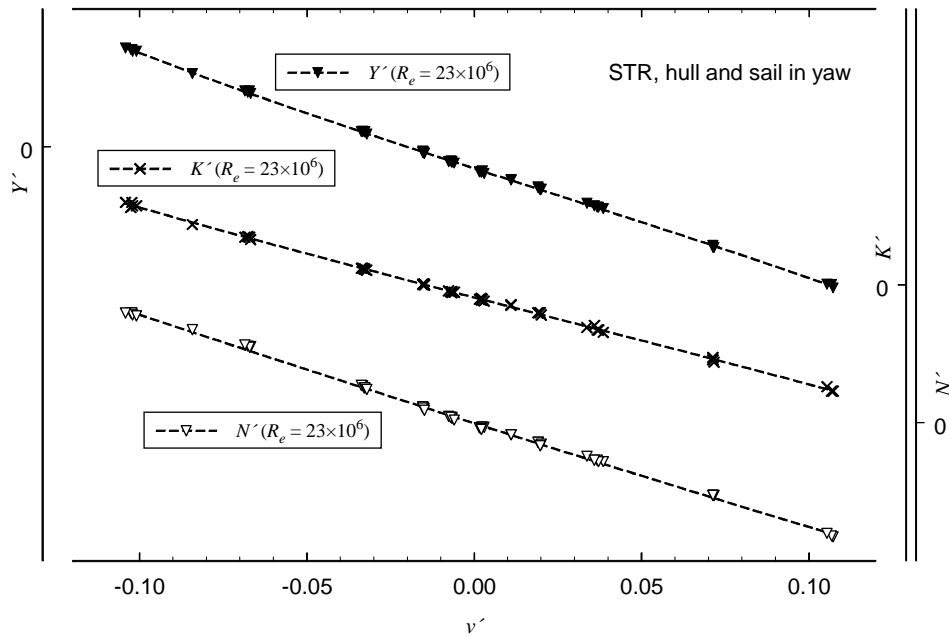


Figure 36. STR in-plane force and moments for hull and sail at $-6 < \beta < +6$ degrees.

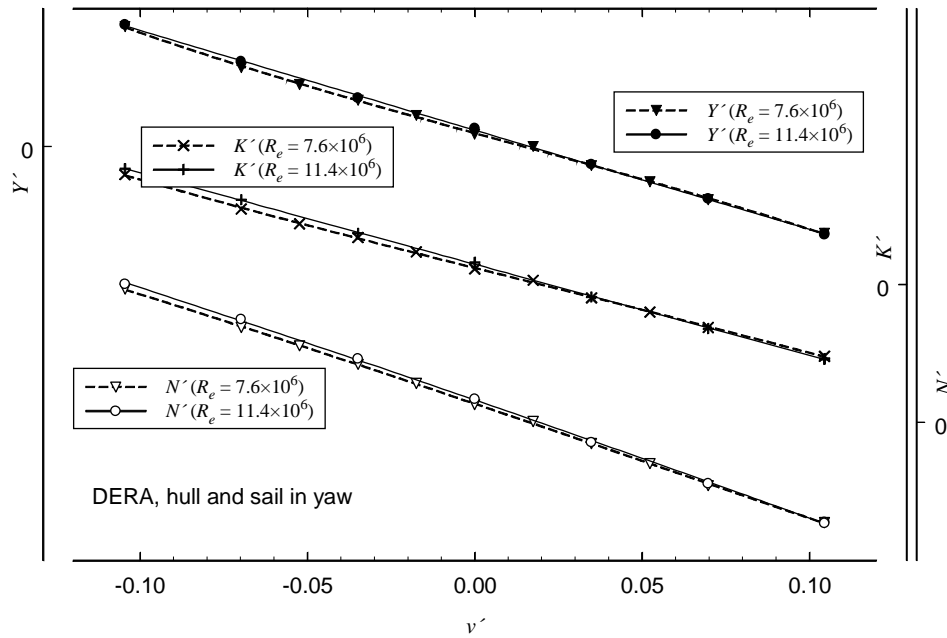


Figure 37. DERA in-plane force and moments for hull and sail at $-6 < \beta < +6$ degrees.

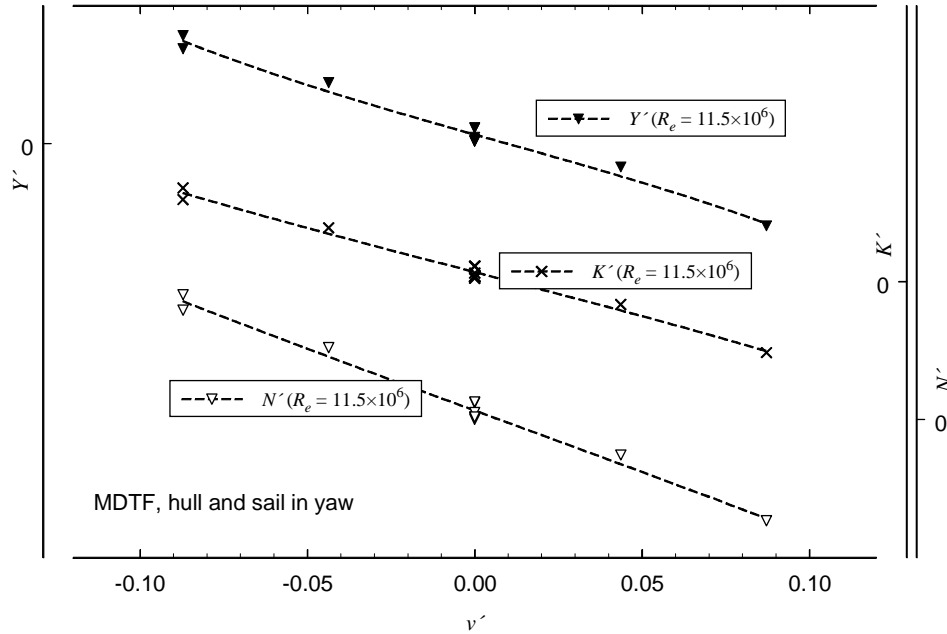


Figure 38. MDTF in-plane force and moments for hull and sail at $-6 < \beta < +6$ degrees.

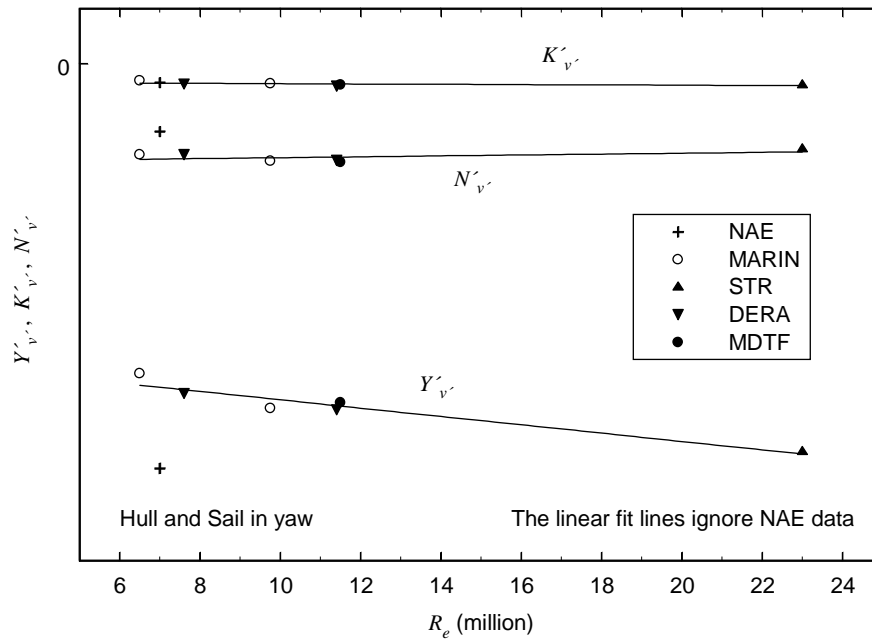


Figure 39. Hull and sail, $Y'_{v'}$, $K'_{v'}$ and $N'_{v'}$: all data sets.

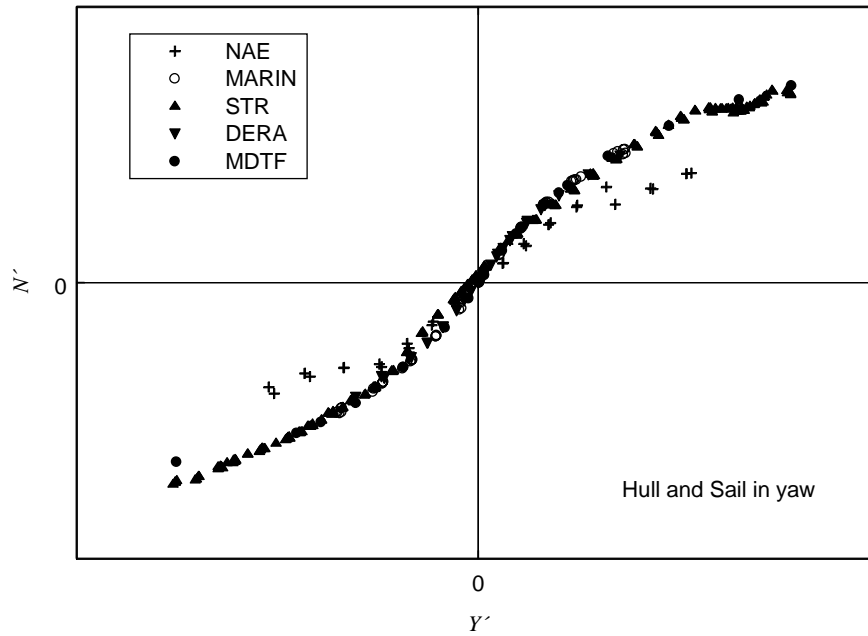


Figure 40. Hull and sail, yawing moment vs side force: all data sets.

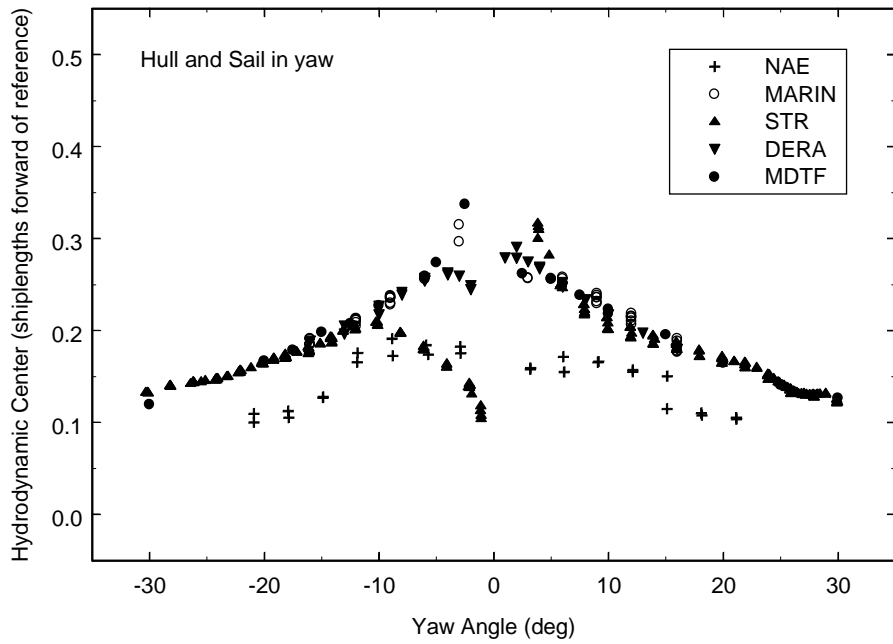


Figure 41. Hull and sail, horizontal plane hydrodynamic center: all data sets.

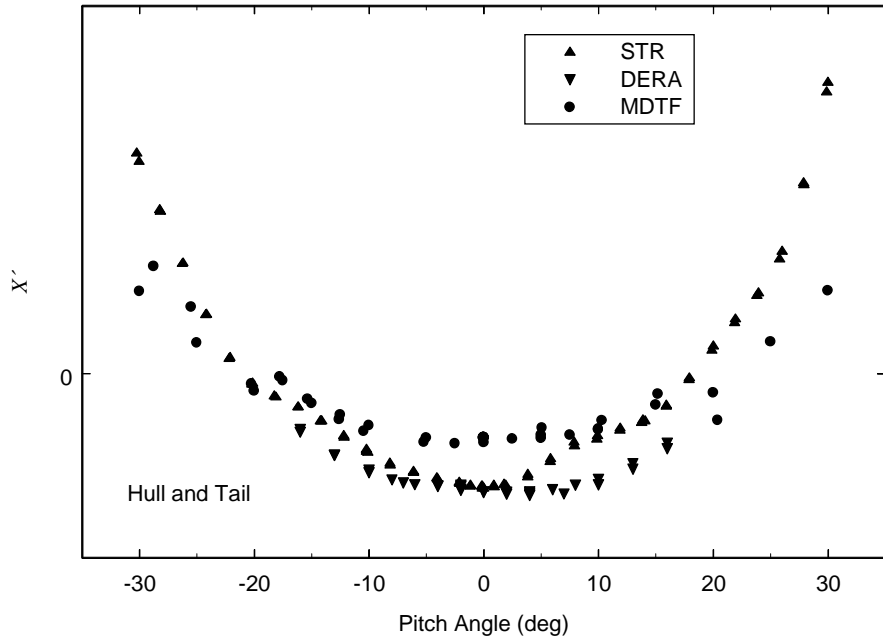


Figure 42. Hull and tail axial force: all data sets.

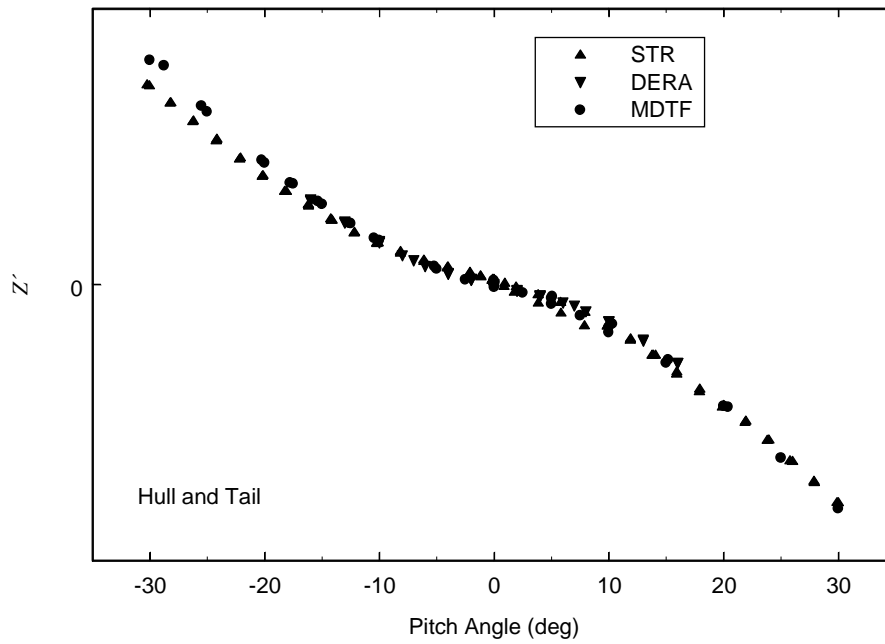


Figure 43. Hull and tail normal force: all data sets.

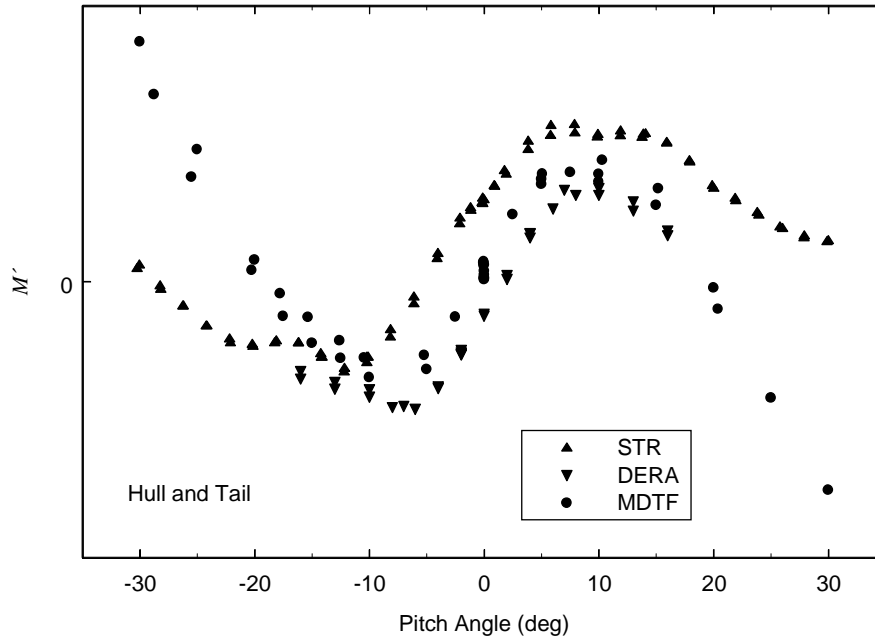


Figure 44. Hull and tail pitching moment: all data sets.

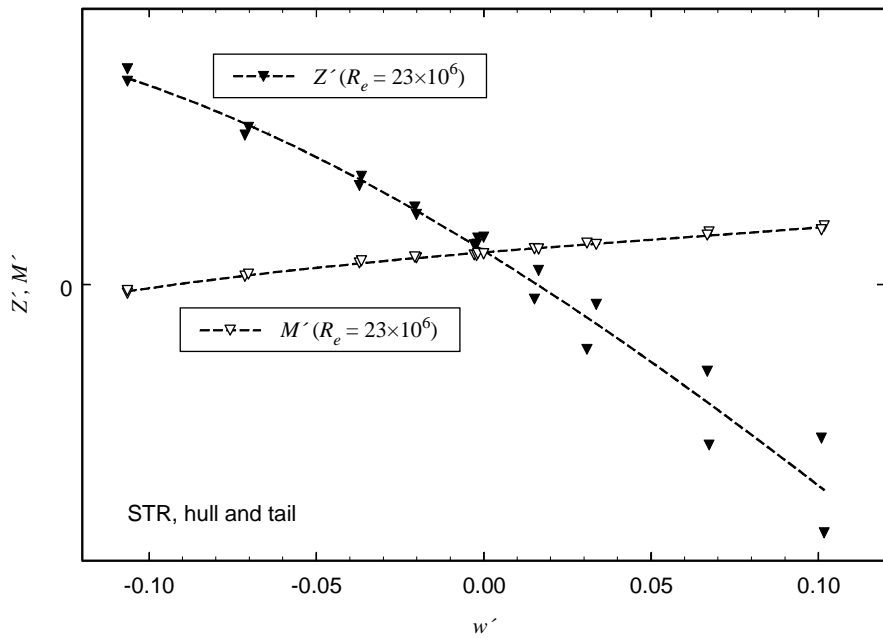


Figure 45. STR normal force and pitching moment for hull and tail at $-6 < \alpha < +6$ degrees.

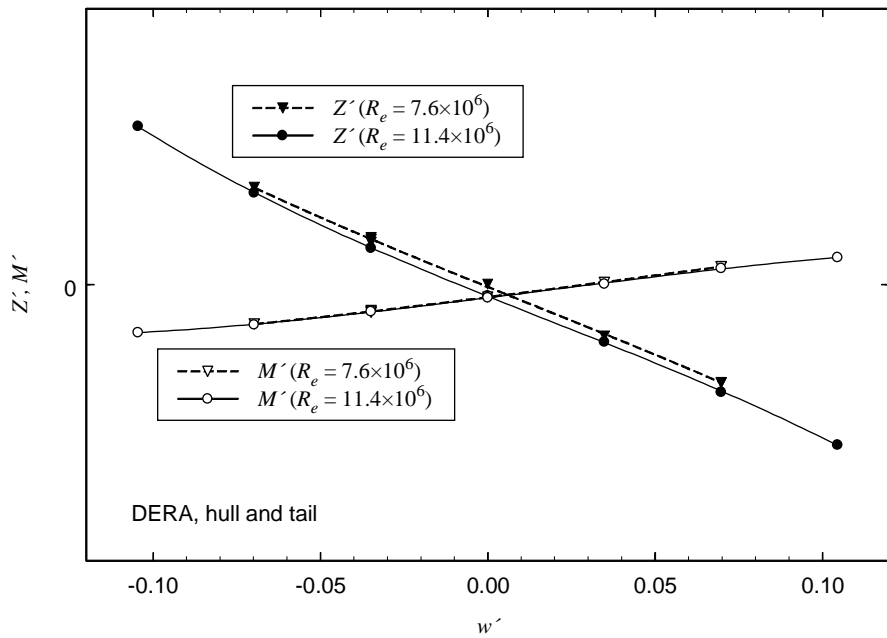


Figure 46. DERA normal force and pitching moment for hull and tail at $-6 < \alpha < +6$ degrees.

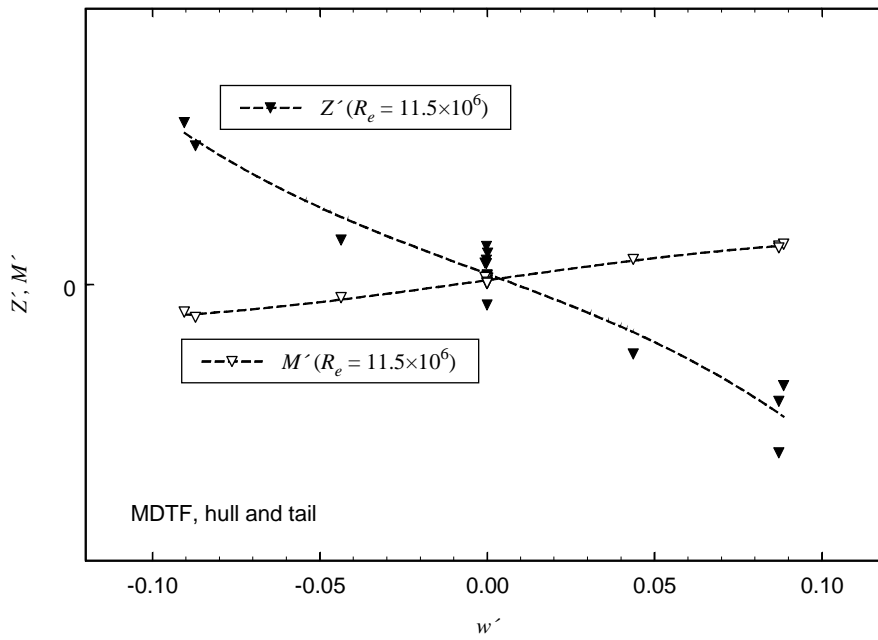


Figure 47. MDTF normal force and pitching moment for hull and tail at $-6 < \alpha < +6$ degrees.

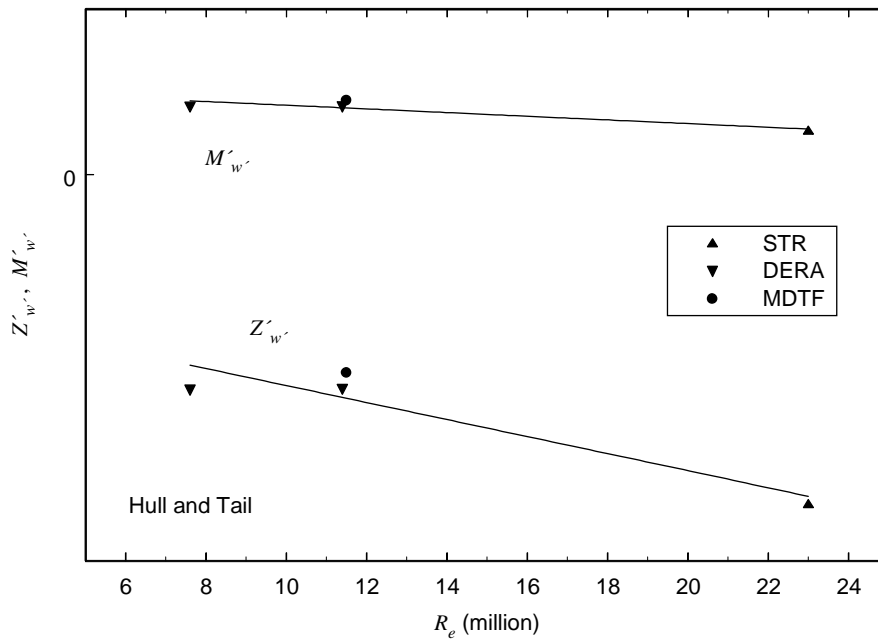


Figure 48. Hull and tail, $Z'_{w'}$ and $M'_{w'}$: all data sets.

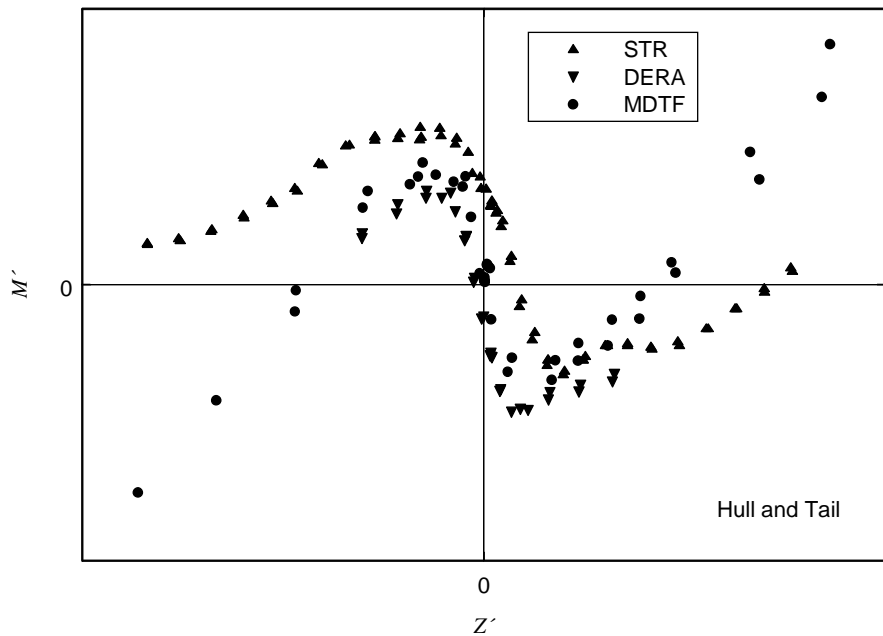


Figure 49. Hull and tail, pitching moment vs normal force: all data sets.

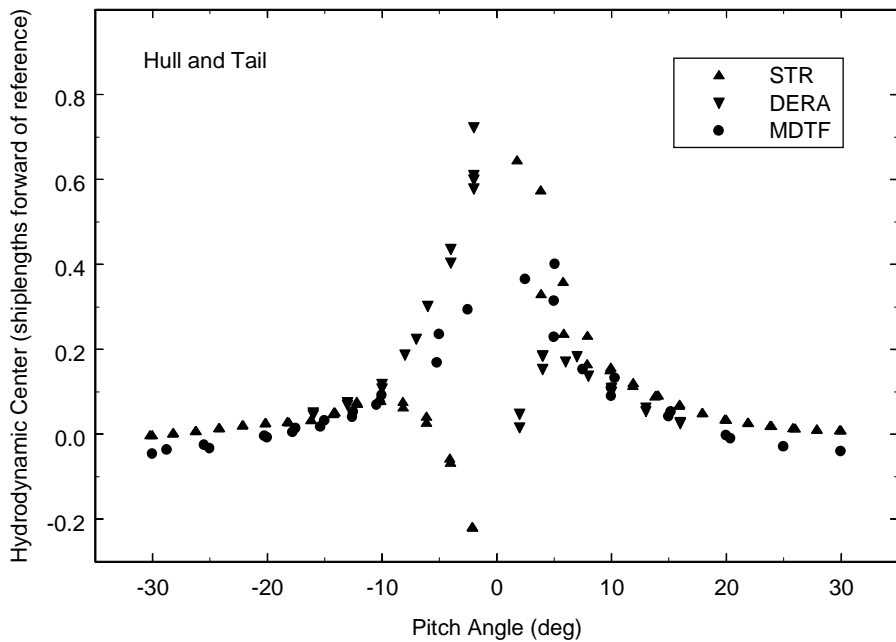


Figure 50. Hull and tail, hydrodynamic center: all data sets.

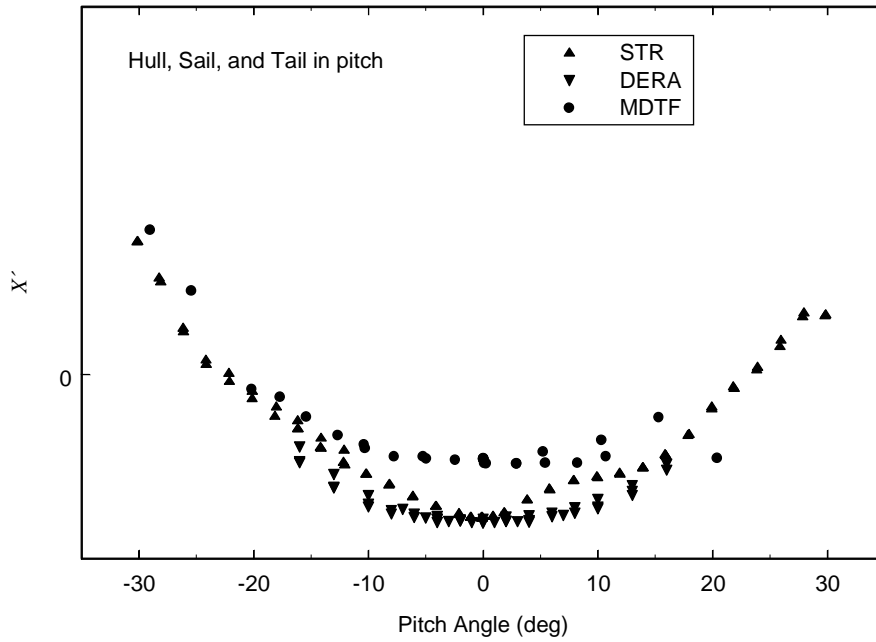


Figure 51. Hull, sail, and tail in pitch, axial force: all data sets.

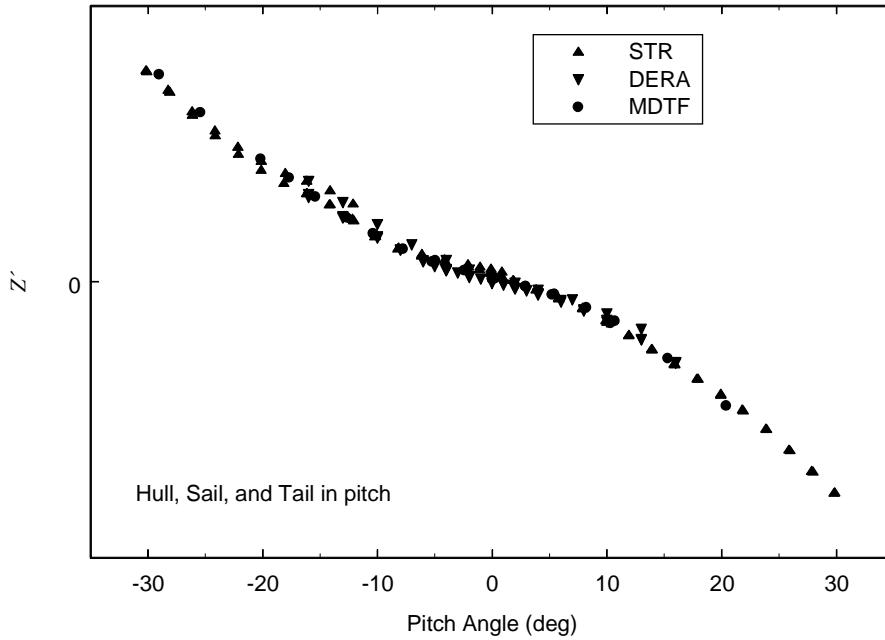


Figure 52. Hull, sail, and tail in pitch, normal force: all data sets.

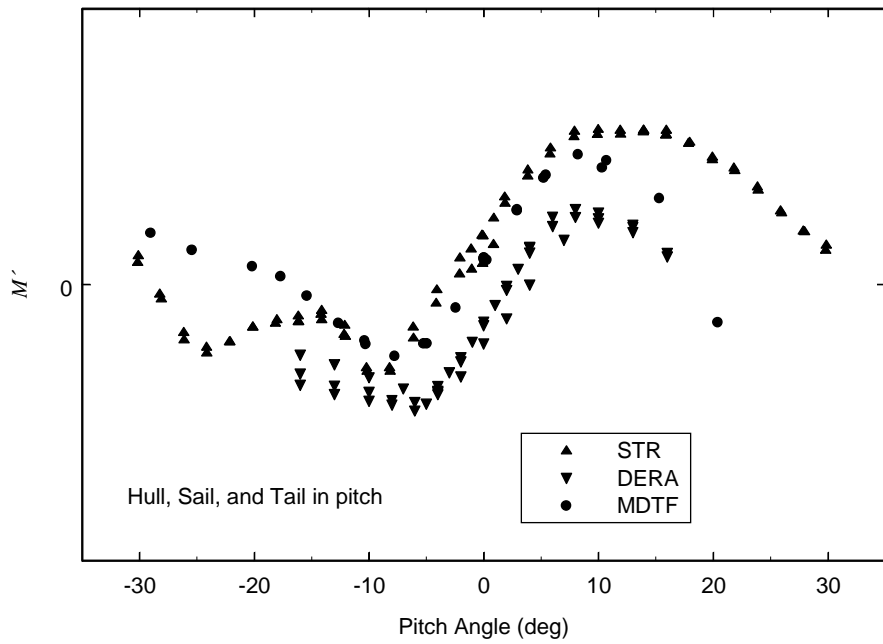


Figure 53. Hull, sail, and tail in pitch, pitching moment: all data sets.

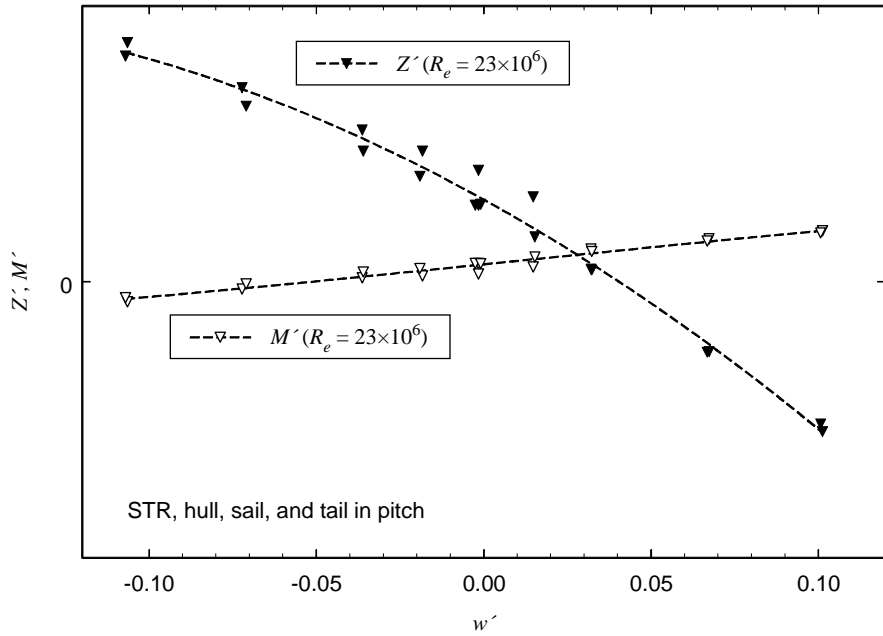


Figure 54. STR normal force and pitching moment for hull, sail, and tail at $-6 < \alpha < +6$ degrees.

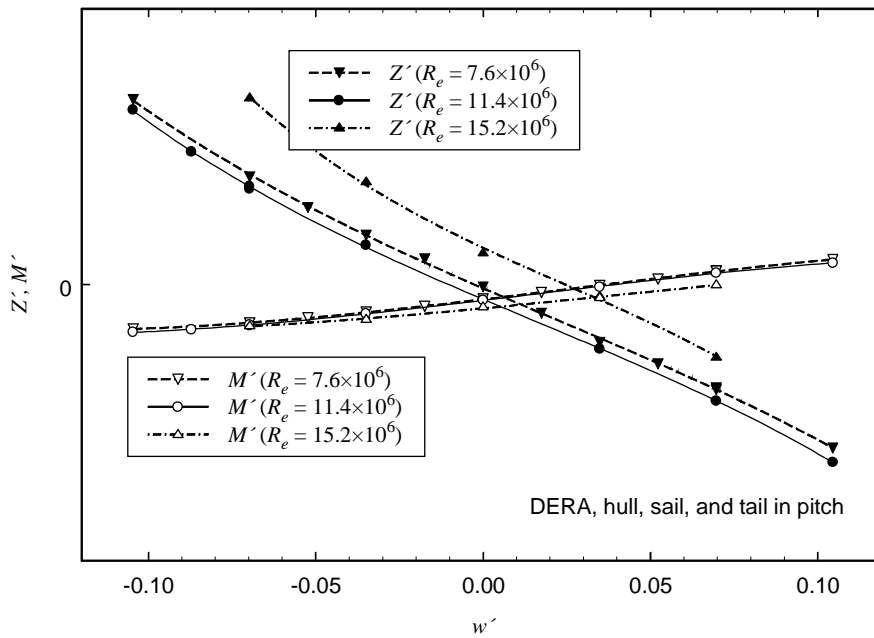


Figure 55. DERA normal force and pitching moment for hull, sail, and tail at $-6 < \alpha < +6$ degrees.

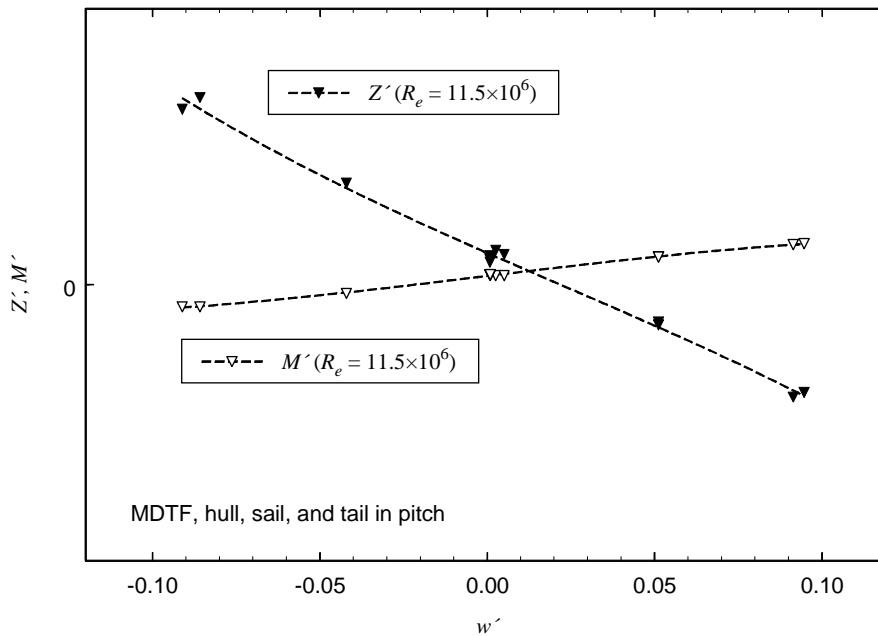


Figure 56. MDTF normal force and pitching moment for hull, sail, and tail at $-6 < \alpha < +6$ degrees.

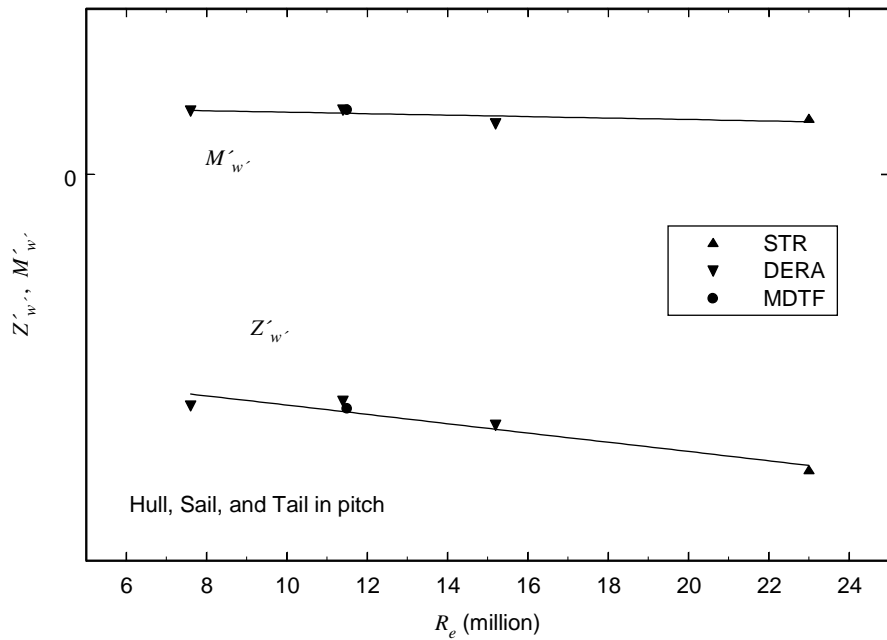


Figure 57. Hull, sail, and tail, $Z'_{w'}$ and $M'_{w'}$: all data sets.

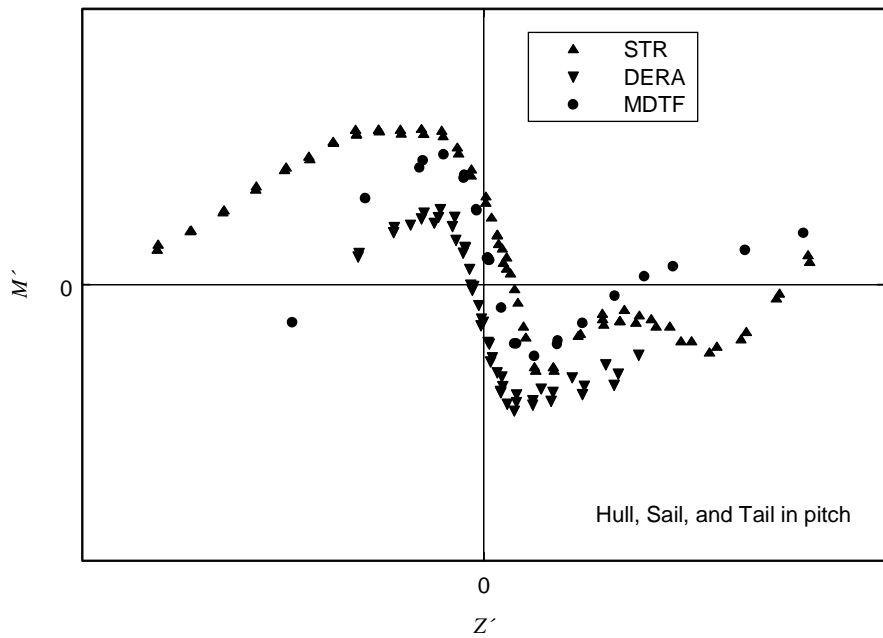


Figure 58. Hull, sail, and tail, pitching moment vs normal force: all data sets.

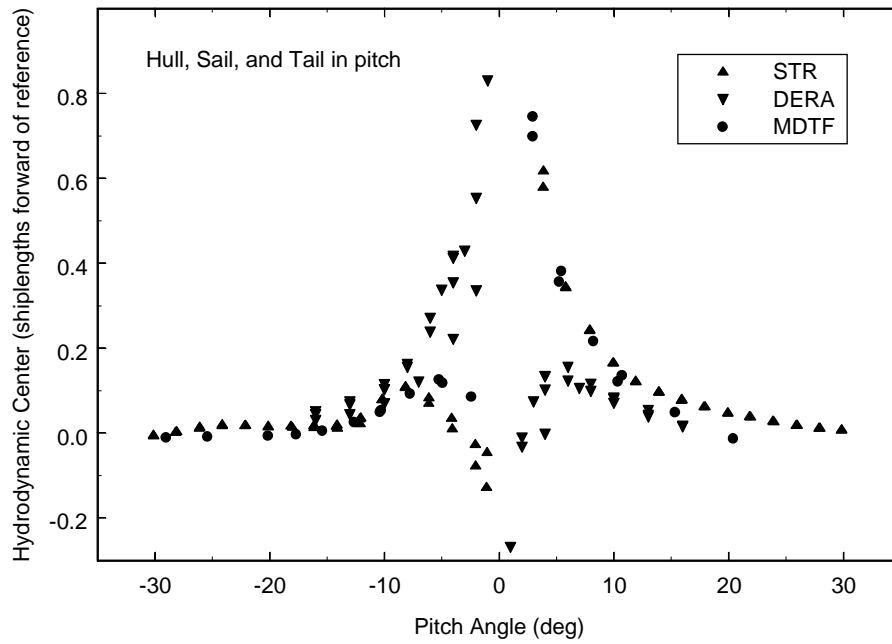


Figure 59. Hull, sail, and tail, vertical plane hydrodynamic center: all data sets.

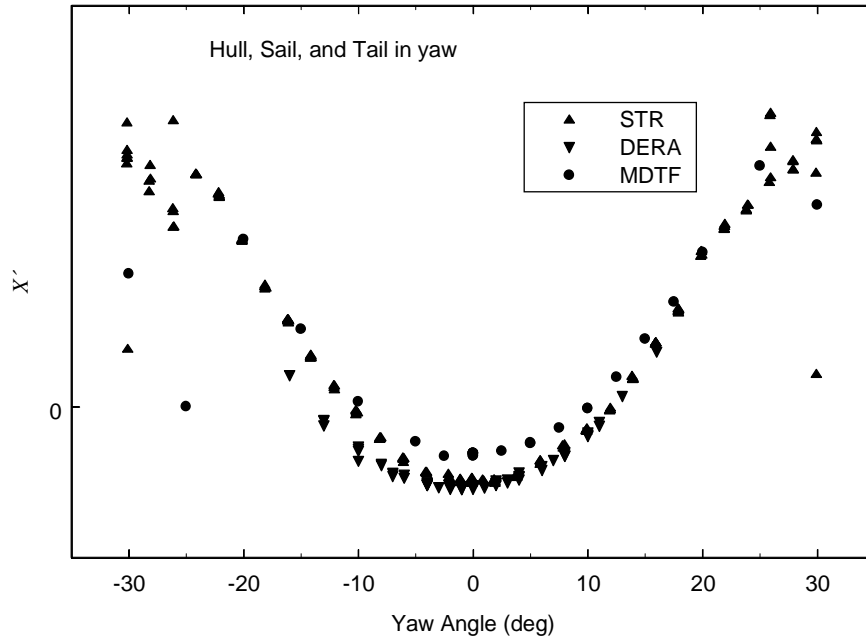


Figure 60. Hull, sail, and tail in yaw, axial force: all data sets.

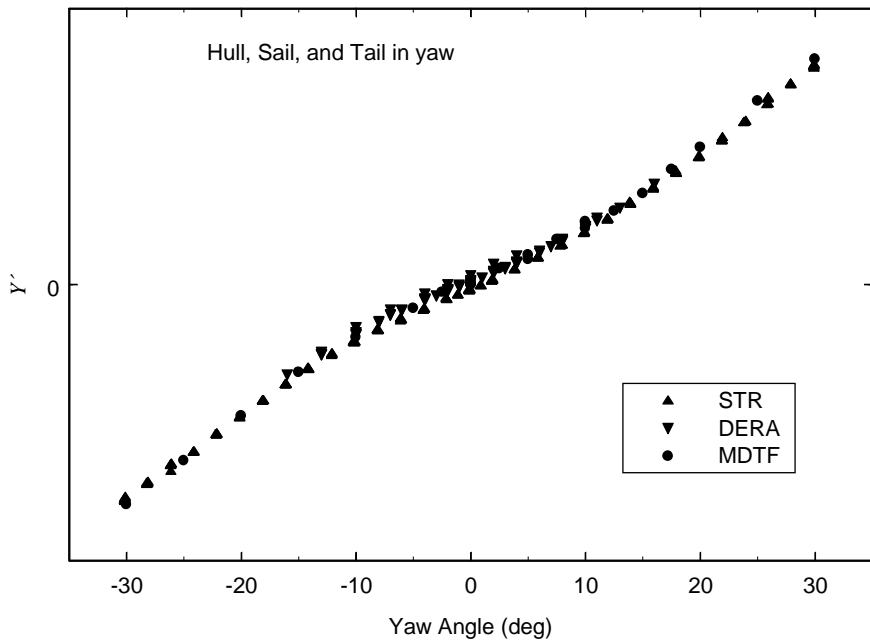


Figure 61. Hull, sail, and tail in yaw, side force: all data sets.

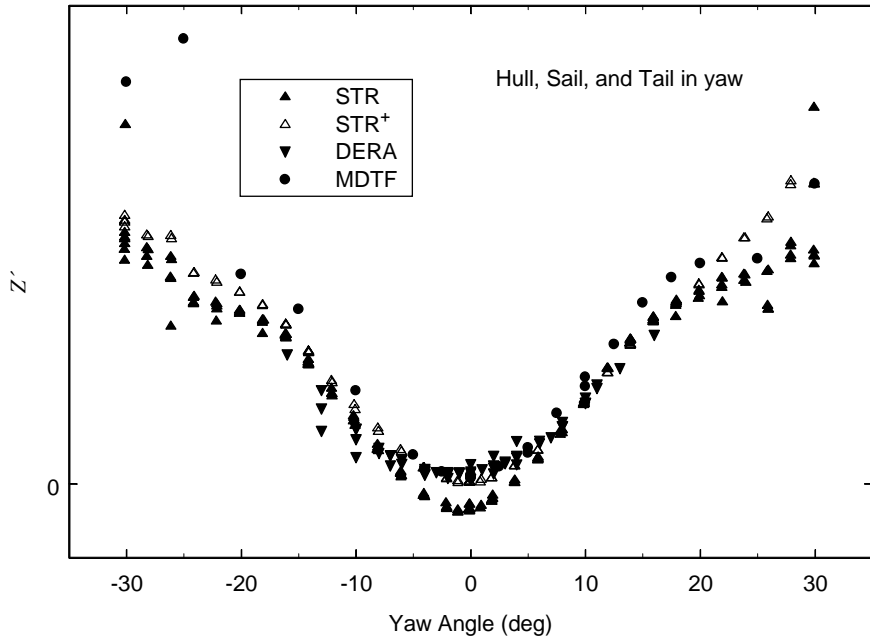


Figure 62. Hull, sail, and tail in yaw, normal force: all data sets. The notation STR⁺ denotes 1994 corrected ($R_e = 23 \times 10^6$) data.

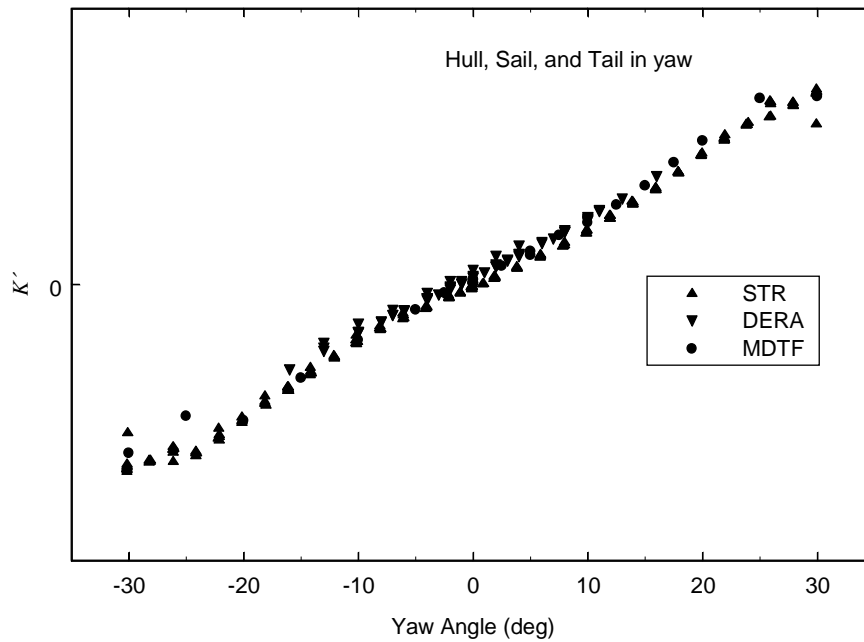


Figure 63. Hull, sail, and tail in yaw, rolling moment: all data sets. STR 1994 corrected data are indistinguishable from uncorrected data, and have been omitted from this figure.

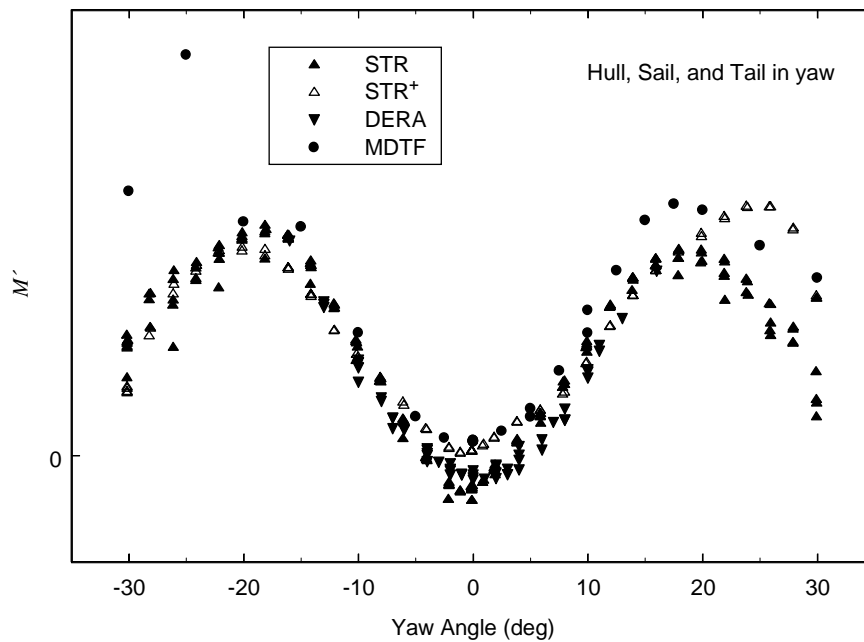


Figure 64. Hull, sail, and tail in yaw, pitching moment: all data sets. The notation STR⁺ denotes 1994 corrected ($R_e = 23 \times 10^6$) data.

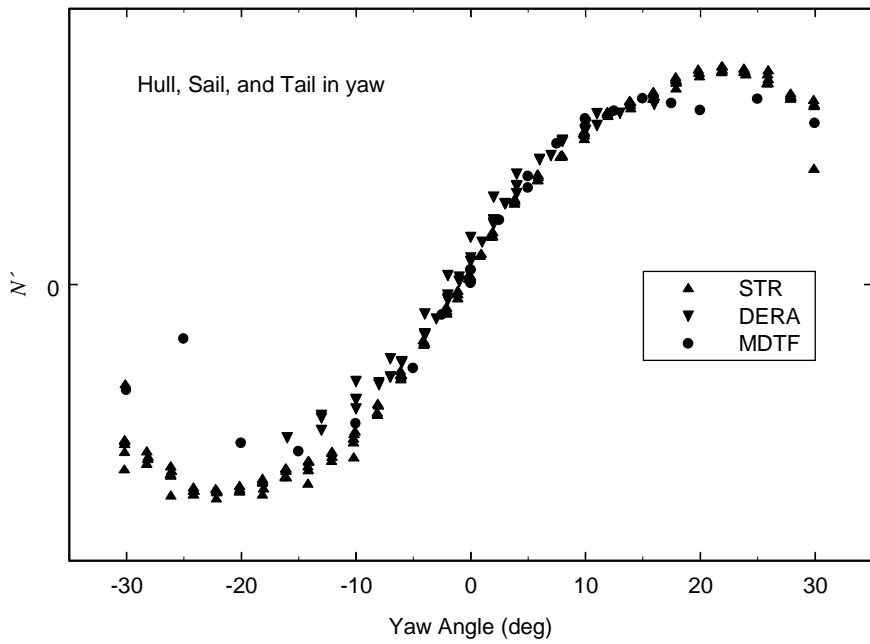


Figure 65. Hull, sail, and tail in yaw, yawing moment: all data sets.

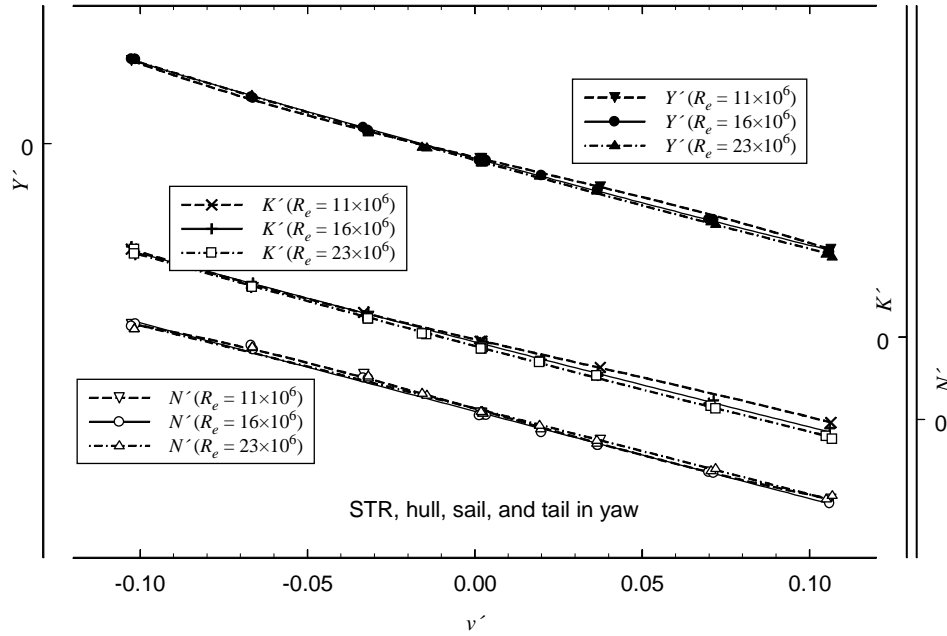


Figure 66. STR in-plane force and moments for hull, sail, and tail at $-6 < \beta < +6$ degrees.

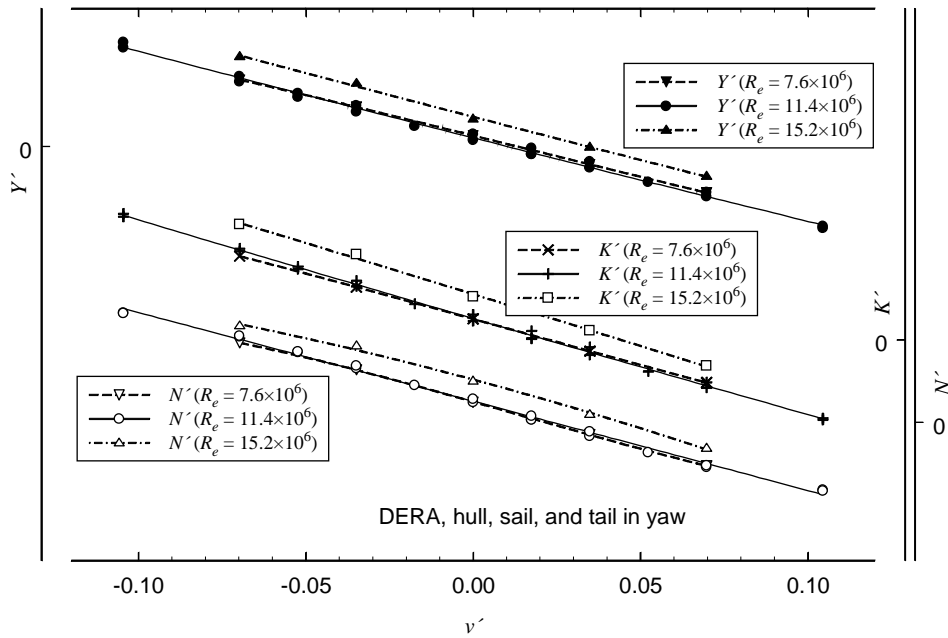


Figure 67. DERA in-plane force and moments for hull, sail, and tail at $-6 < \beta < +6$ degrees.

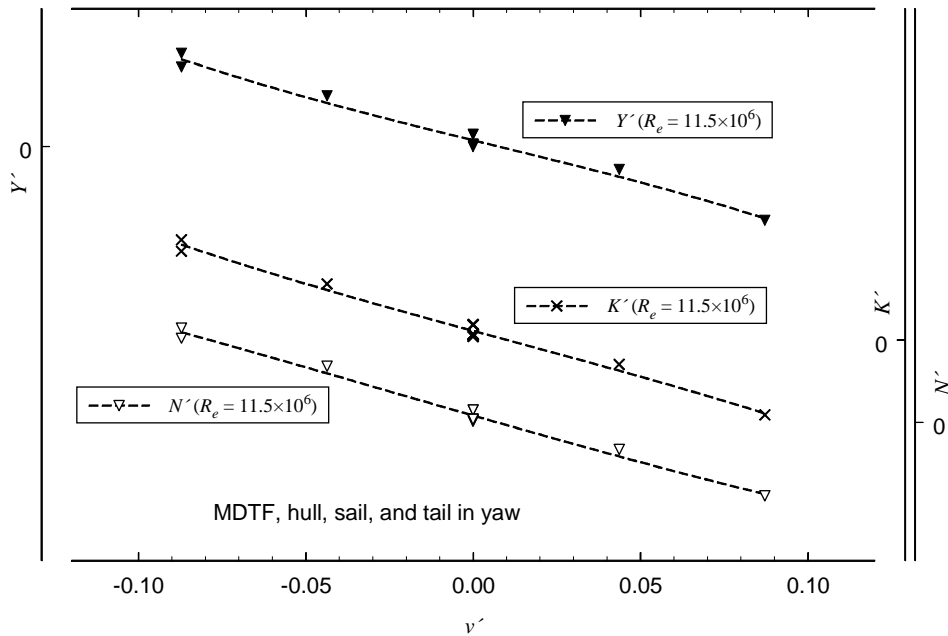


Figure 68. MDTF in-plane force and moments for hull, sail, and tail at $-6 < \beta < +6$ degrees.

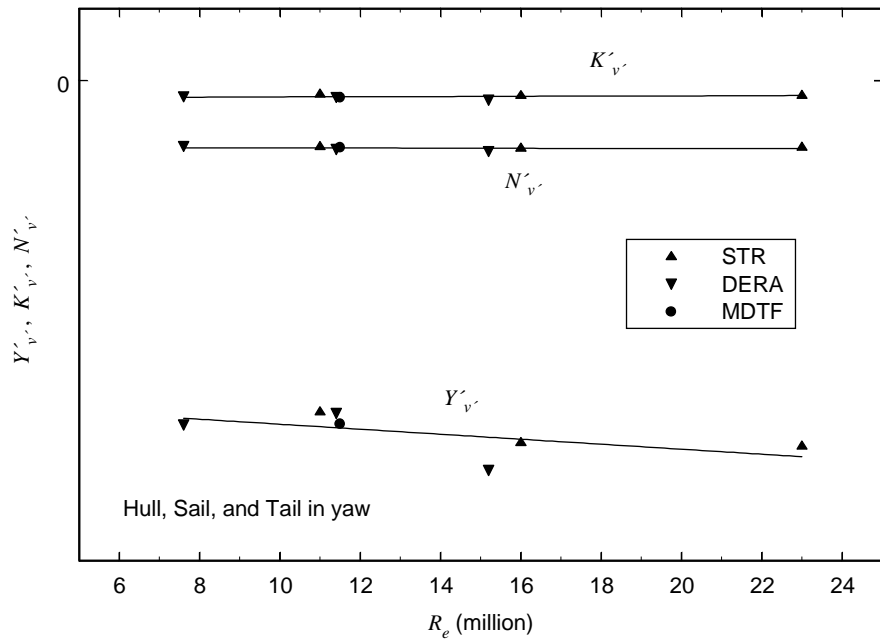


Figure 69. Hull, sail, and tail, $Y'_{v'}$, $K'_{v'}$, and $N'_{v'}$: all data sets.

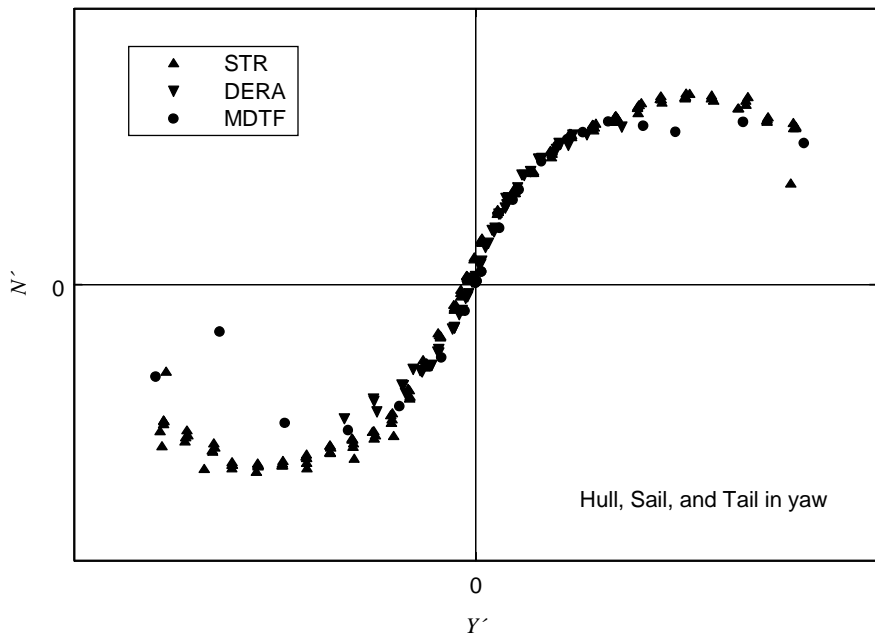


Figure 70. Hull, sail, and tail, yawing moment vs side force: all data sets.

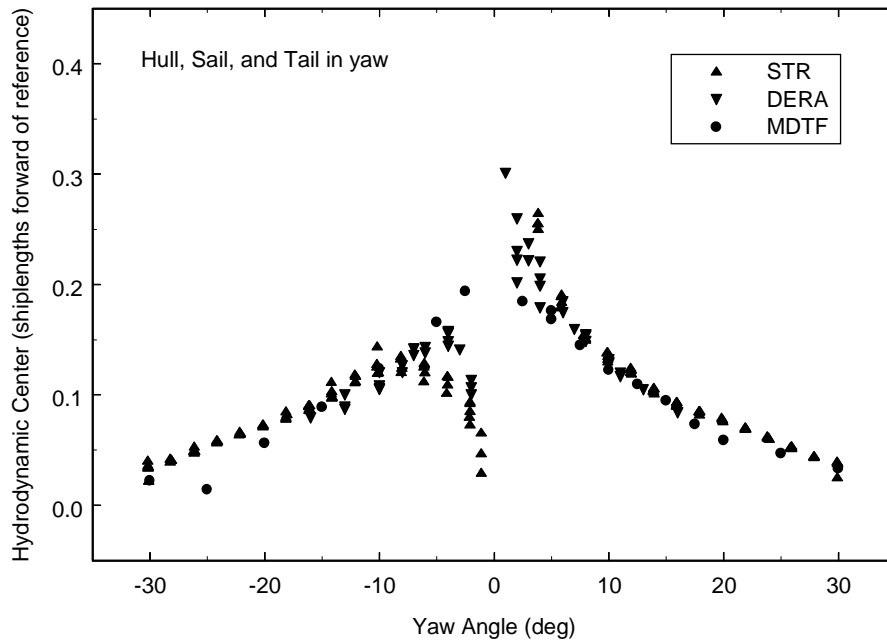


Figure 71. Hull, sail, and tail, horizontal plane hydrodynamic center: all data sets.

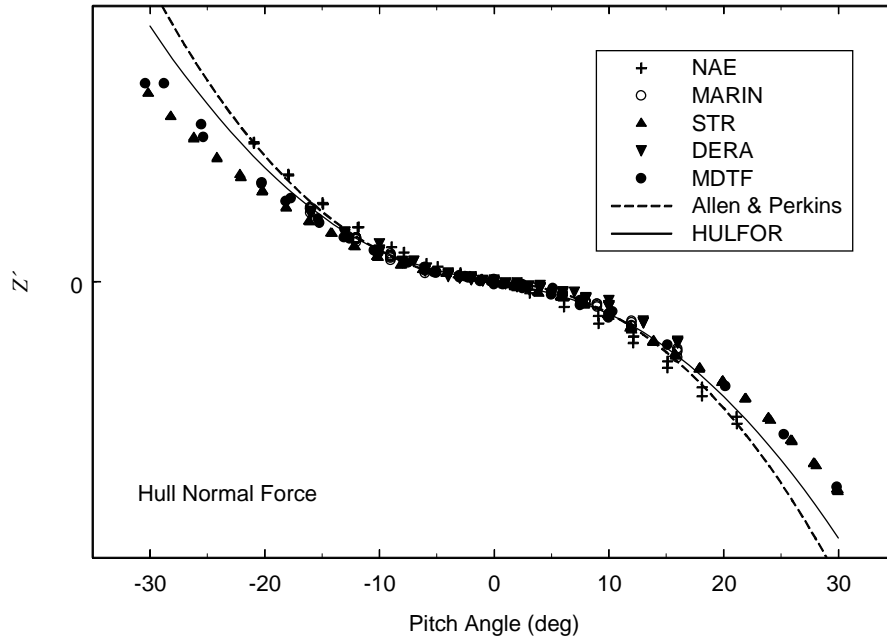


Figure 72. Hull normal force: adjusted offsets.

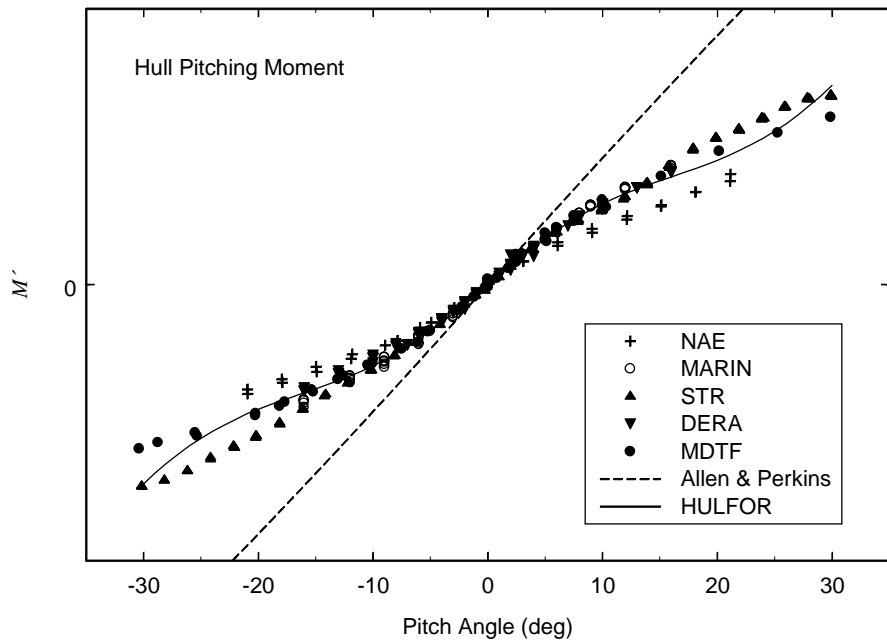


Figure 73. Hull pitching moment: adjusted offsets.

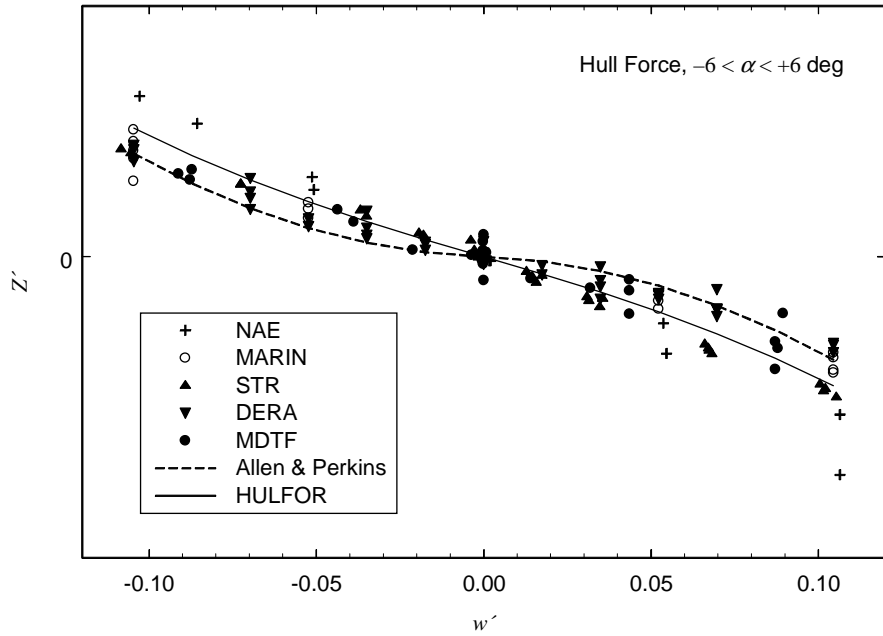


Figure 74. Hull normal force for $-6 < \alpha < +6$ degrees: adjusted offsets.

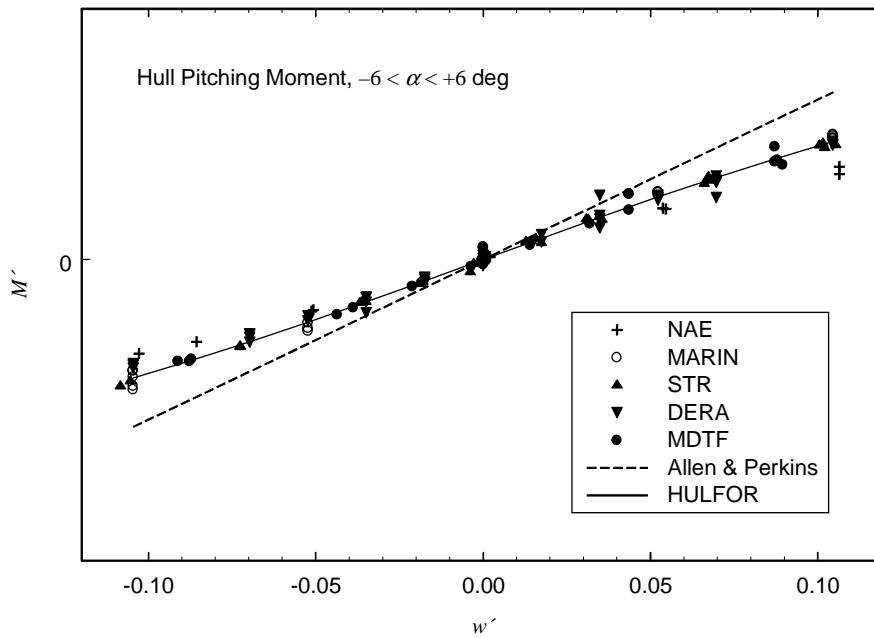


Figure 75. Hull pitching moment for $-6 < \alpha < +6$ degrees: adjusted offsets.

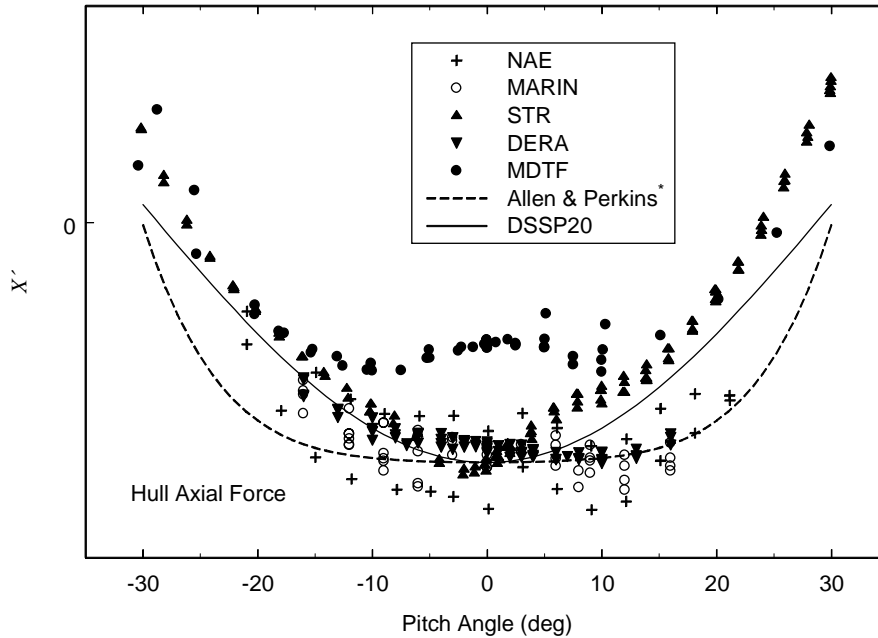


Figure 76. Hull axial force; the Allan and Perkins* estimate uses the DSSP20 value of the zero-lift drag coefficient, D'_0 .

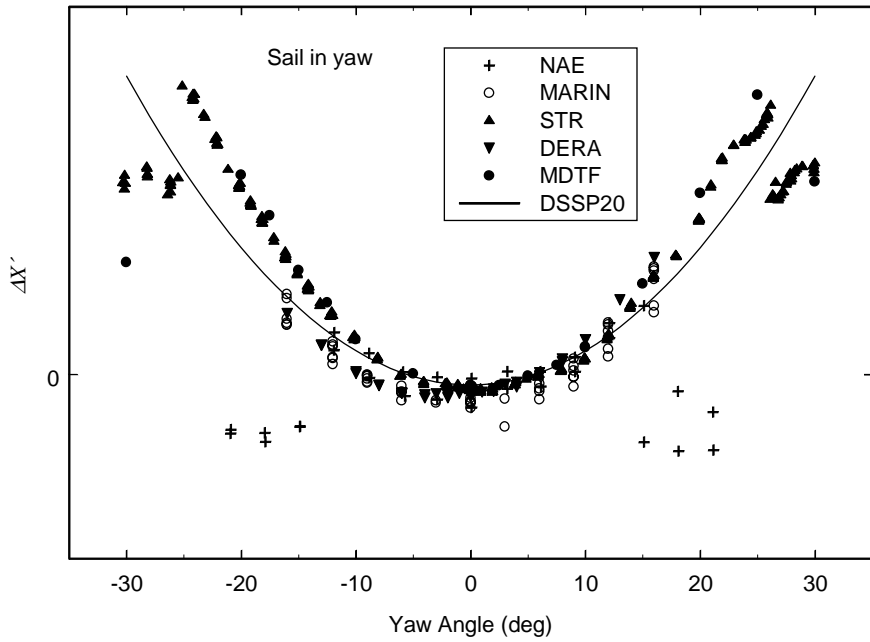


Figure 77. Sail incremental axial force (HS-H).

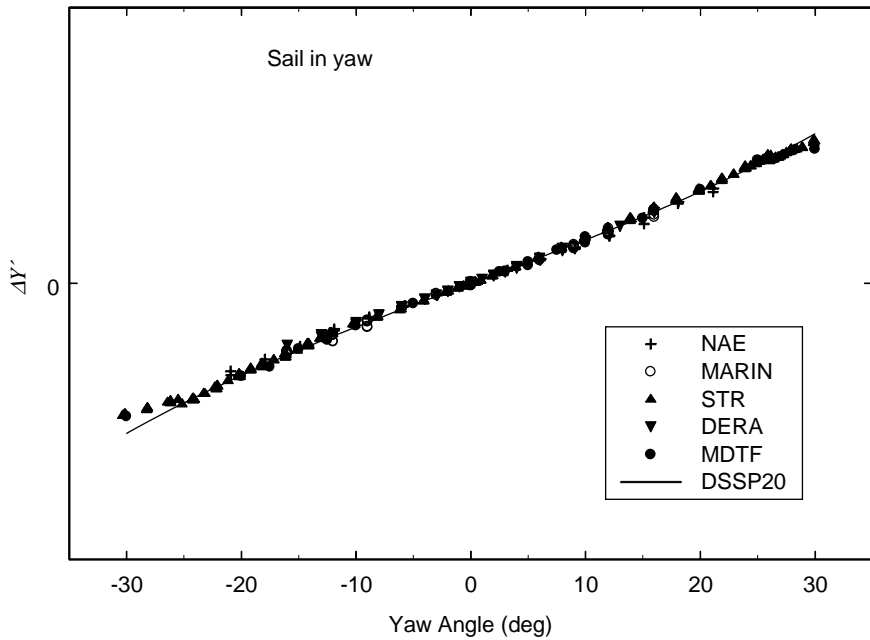


Figure 78. Sail incremental sideforce (sail lift, HS-H); zero offsets removed.

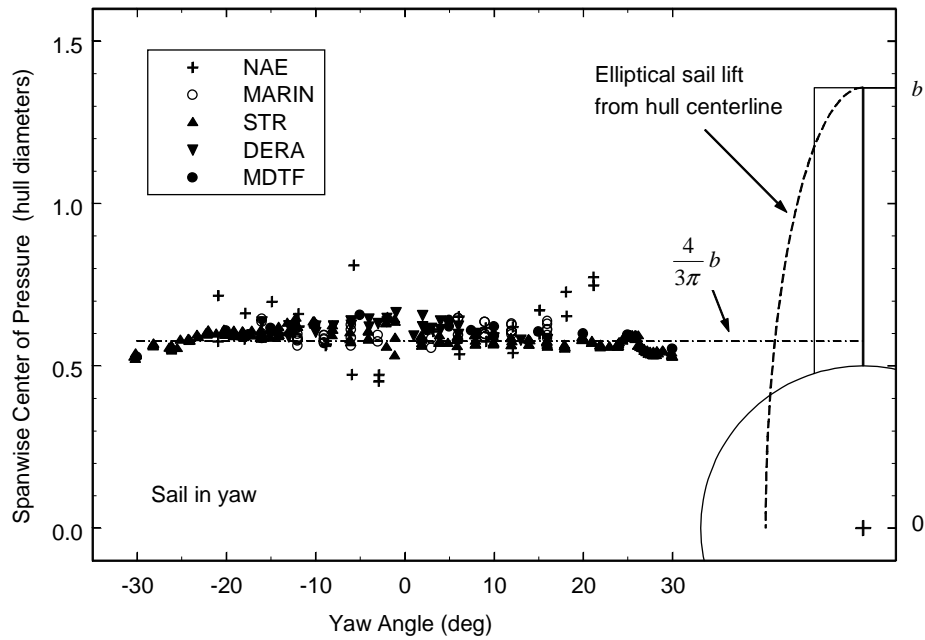


Figure 79. Rolling moment arm of sail incremental sideforce (HS-H); zero offsets removed.

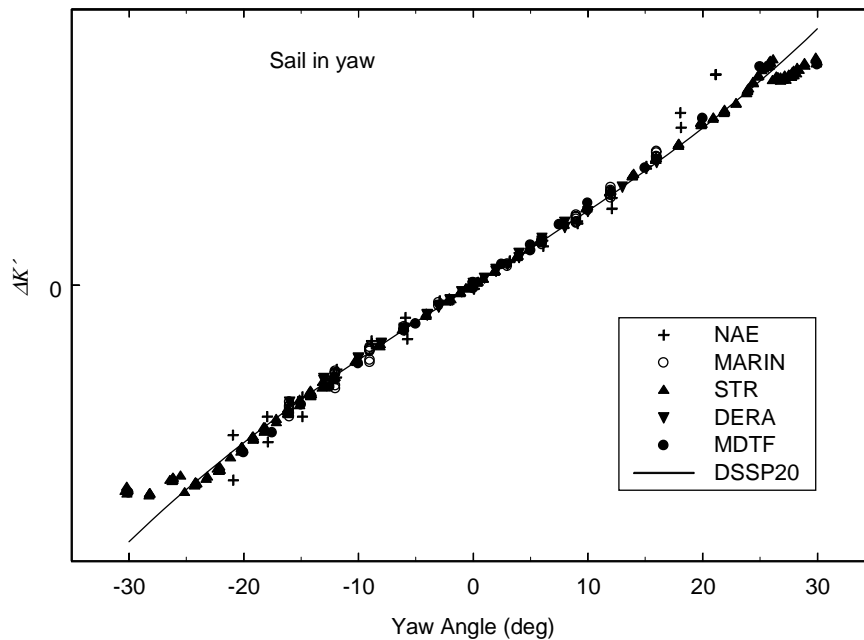


Figure 80. Sail rolling moment; zero offsets removed.

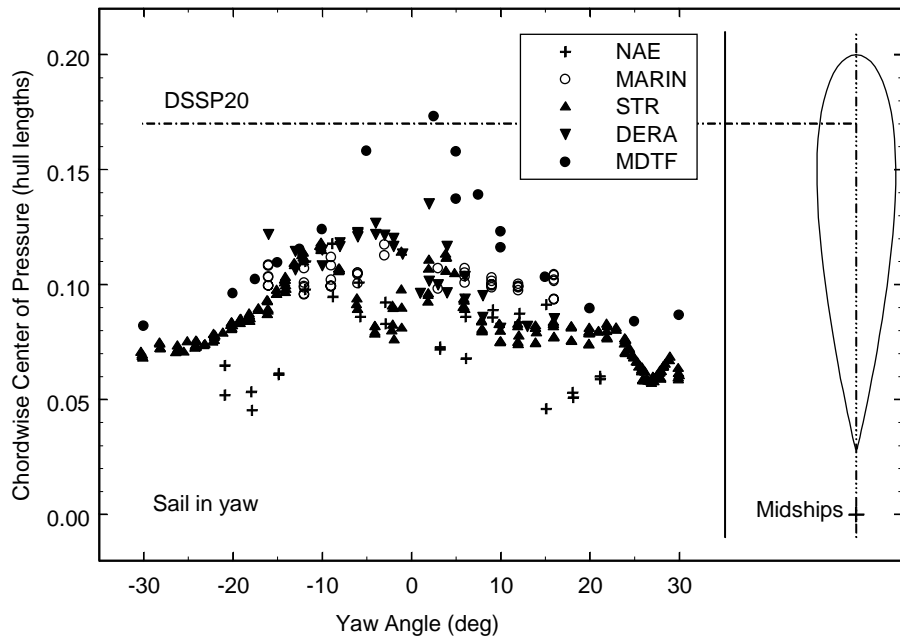


Figure 81. Yawing moment arm of sail incremental sideforce (HS-H); zero offsets removed.

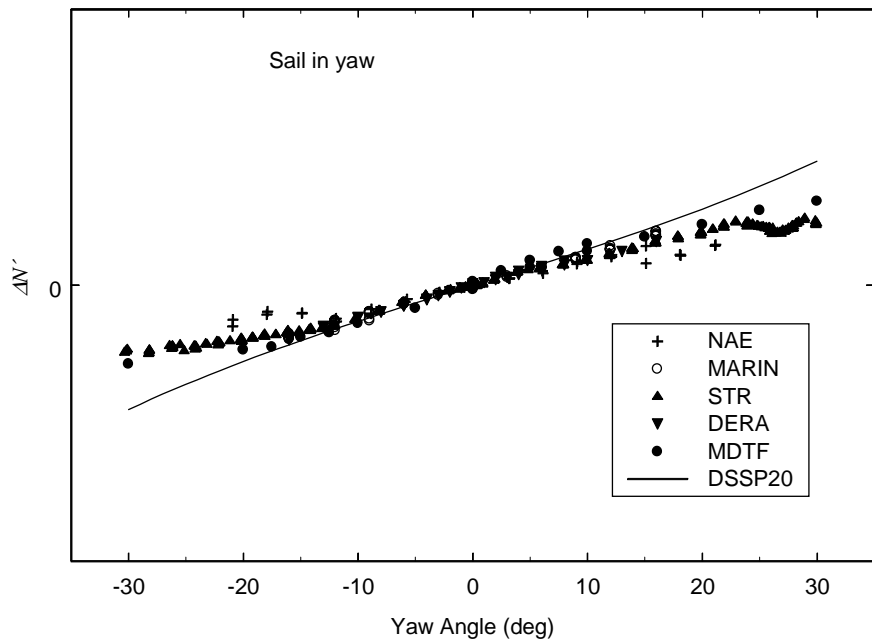


Figure 82. Sail incremental yawing moment (HS-H); zero offsets removed.

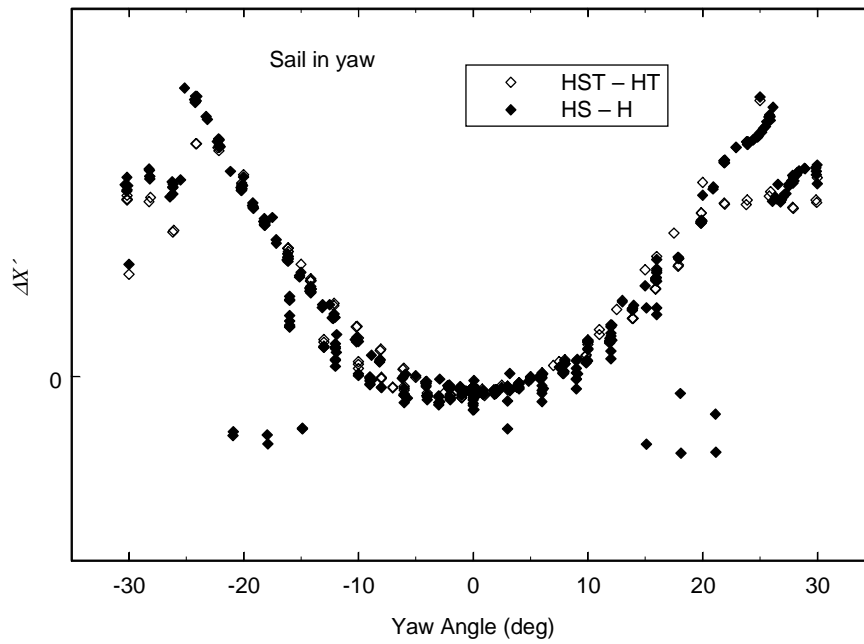


Figure 83. Sail incremental axial force; (HST-HT) and (HS-H).

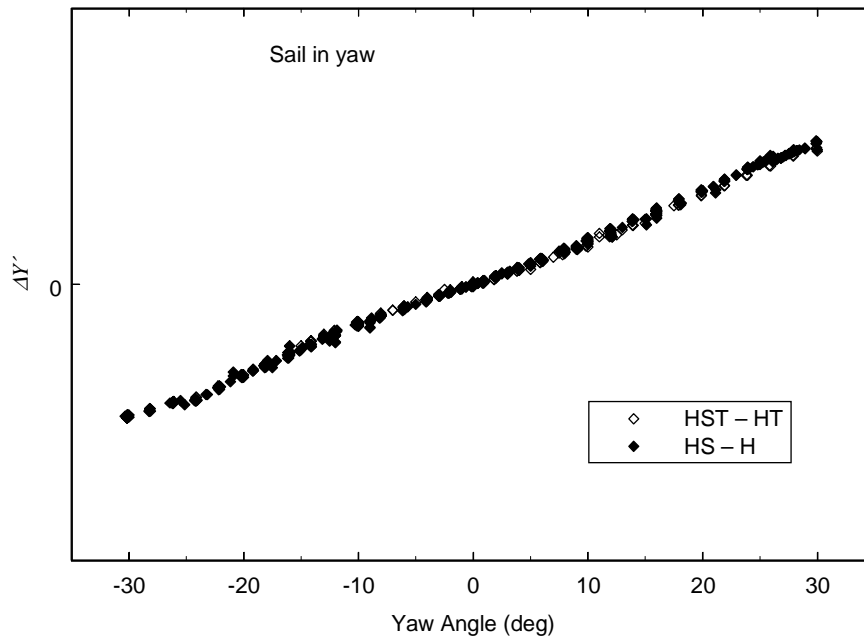


Figure 84. Sail incremental sideforce; (HST-HT) and (HS-H).

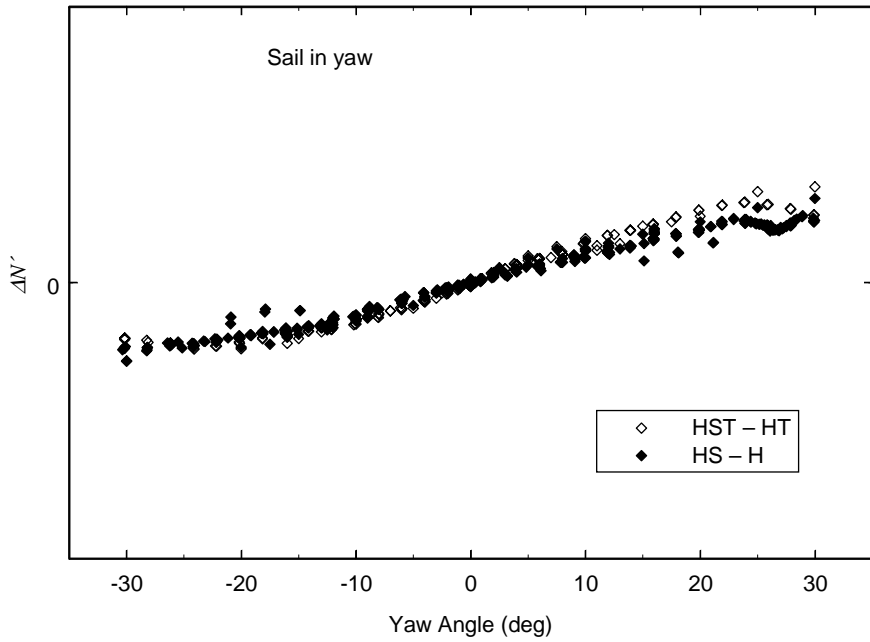


Figure 85. Sail incremental yawing moment; (HST-HT) and (HS-H).

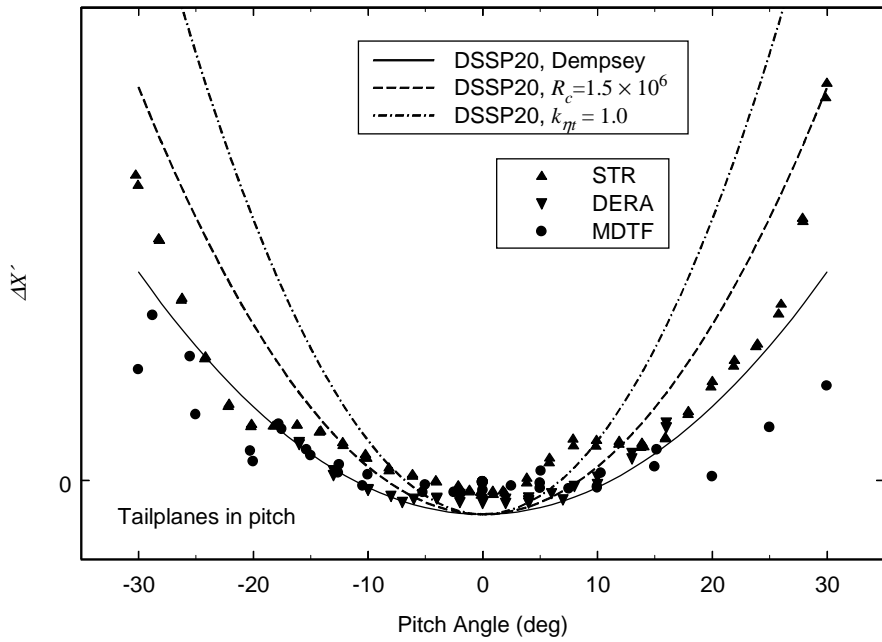


Figure 86. Tail incremental axial force (HT-H).

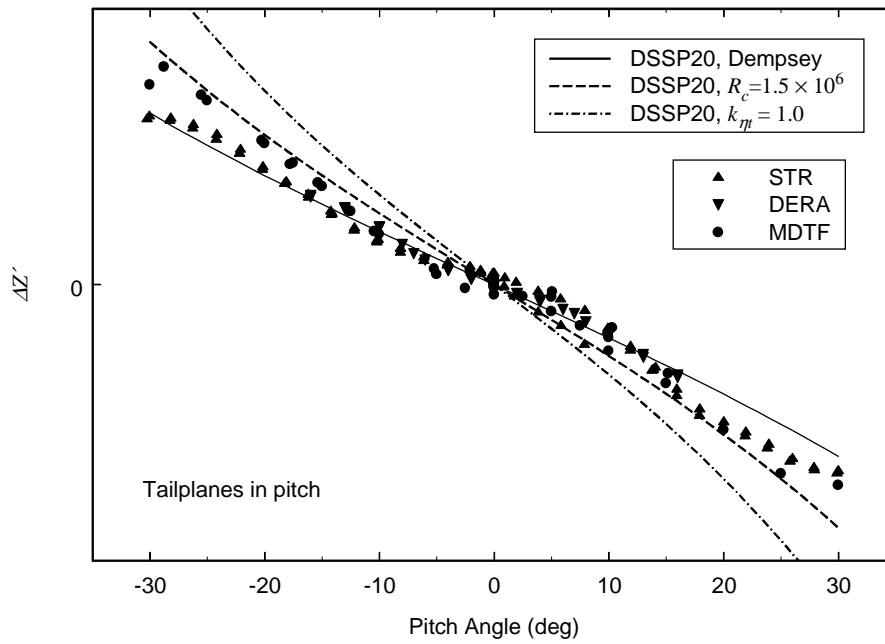


Figure 87. Tail incremental normal force (tail lift, HT-H); zero offsets removed.

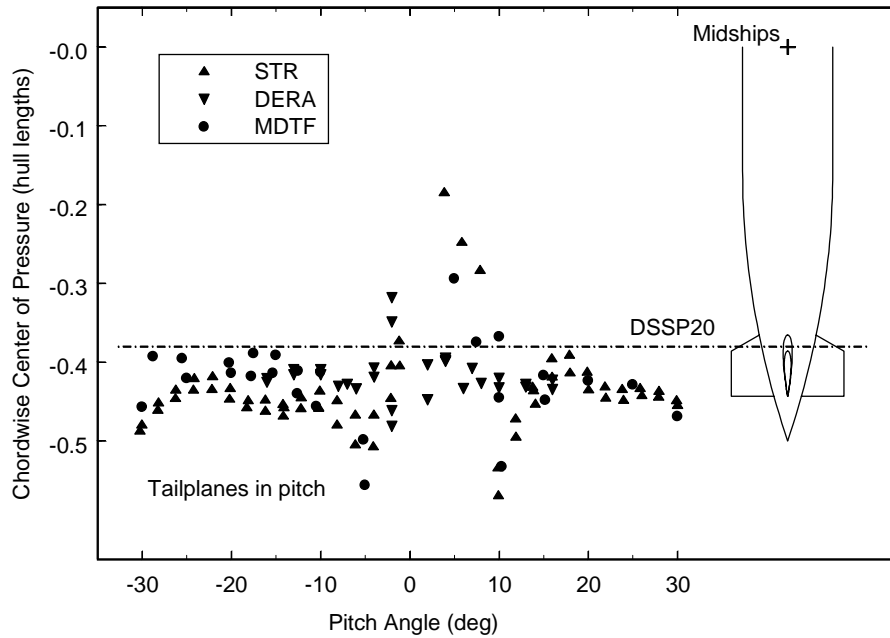


Figure 88. Pitching moment arm of tail incremental normal force (HT-H); zero offsets removed.

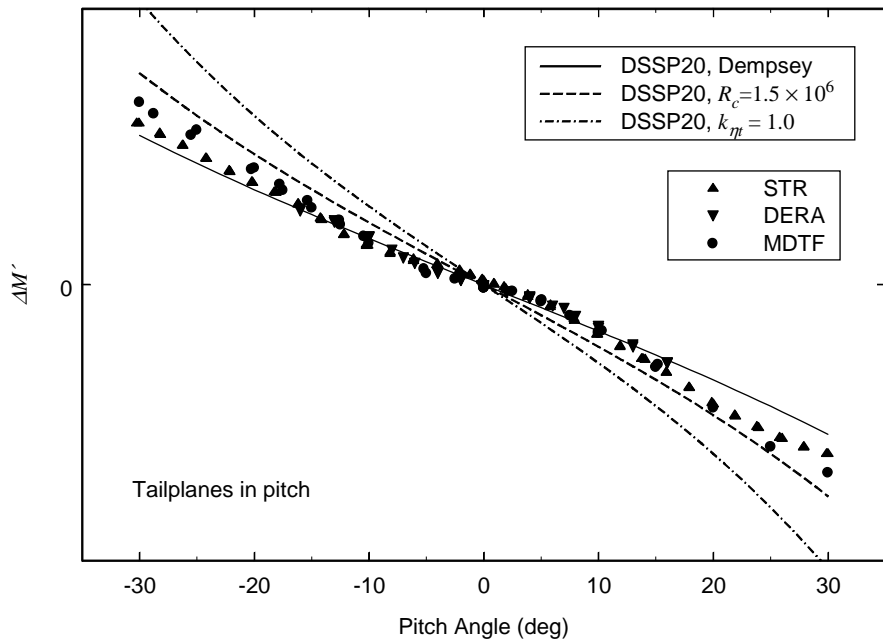


Figure 89. Tail incremental pitching moment (HT-H); zero offsets removed.

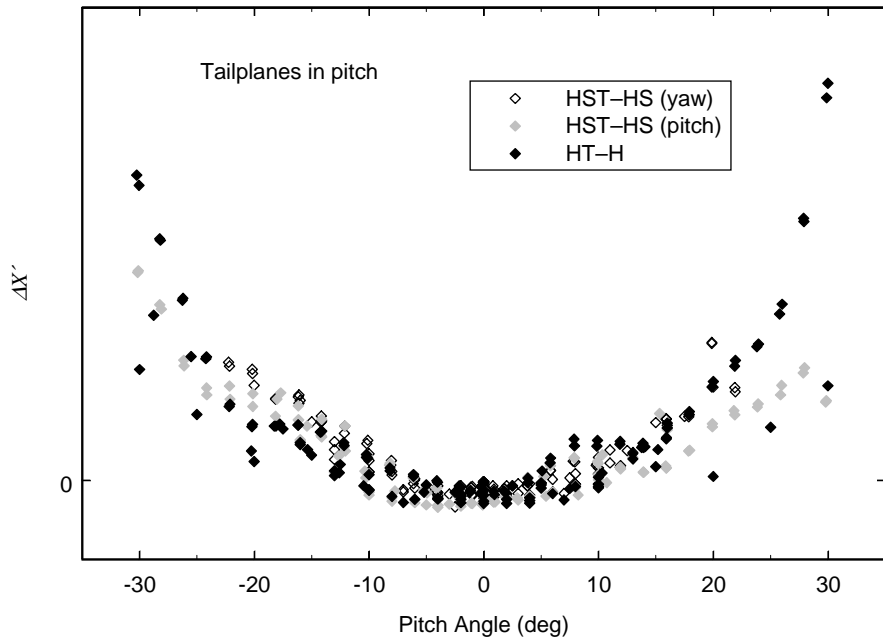


Figure 90. Tail incremental axial force; (HST-HS (yaw and pitch)) and (HT-H).

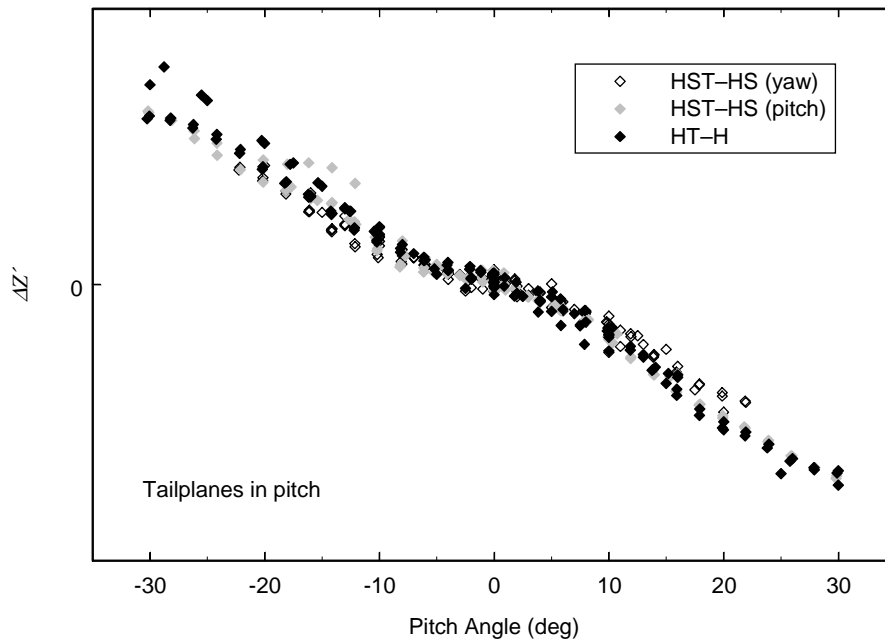


Figure 91. Tail incremental normal force; (HST-HS (yaw and pitch)) and (HT-H).

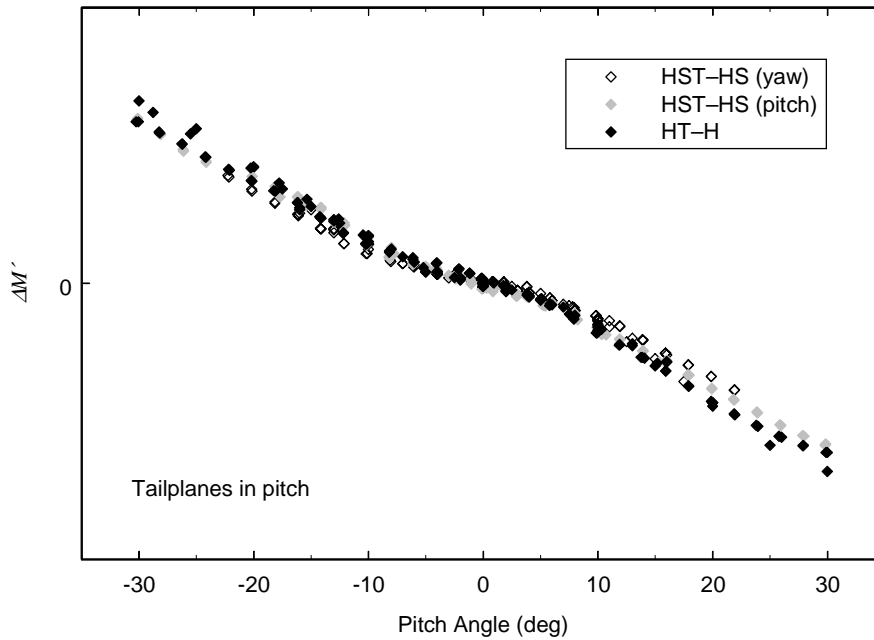


Figure 92. Tail incremental pitching moment; (HST-HS (yaw and pitch)) and (HT-H).

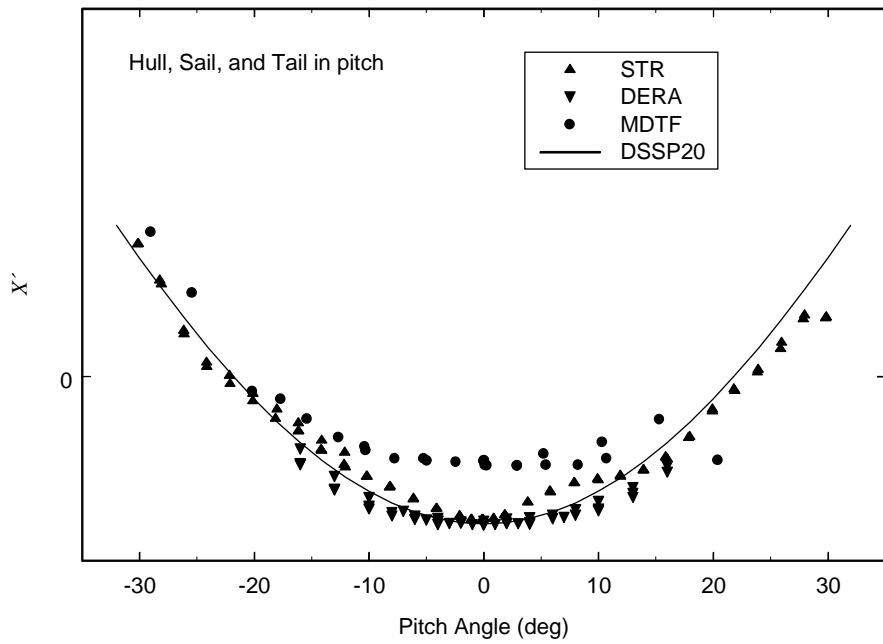


Figure 93. HST load comparison: X' (pitch)

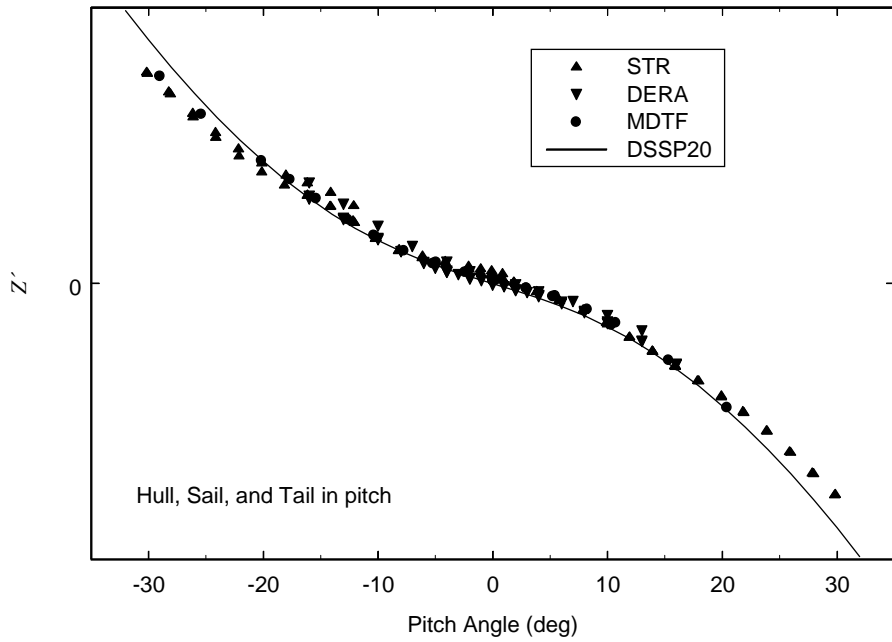


Figure 94. HST load comparison: Z' (pitch)

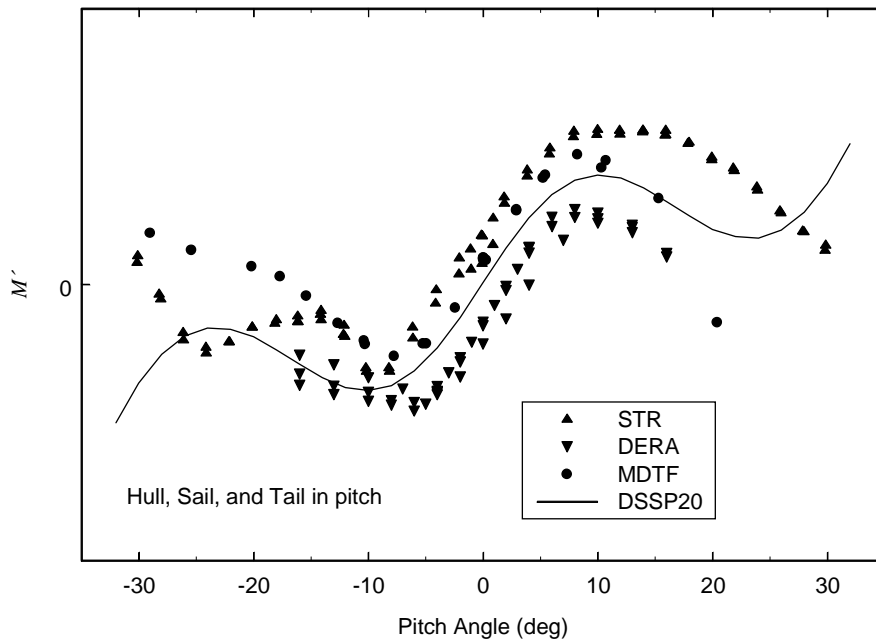


Figure 95. HST load comparison: M' (pitch)

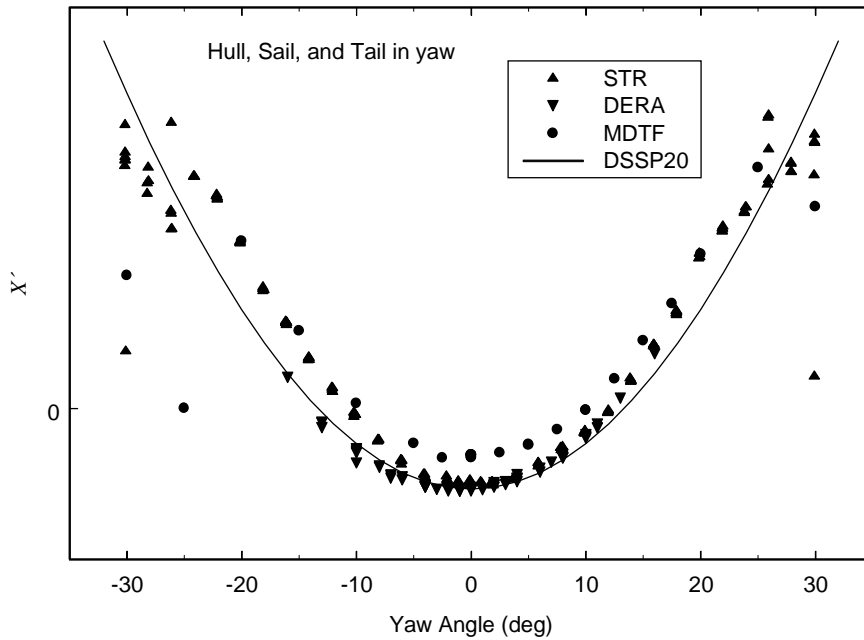


Figure 96. HST load comparison: X' (yaw)

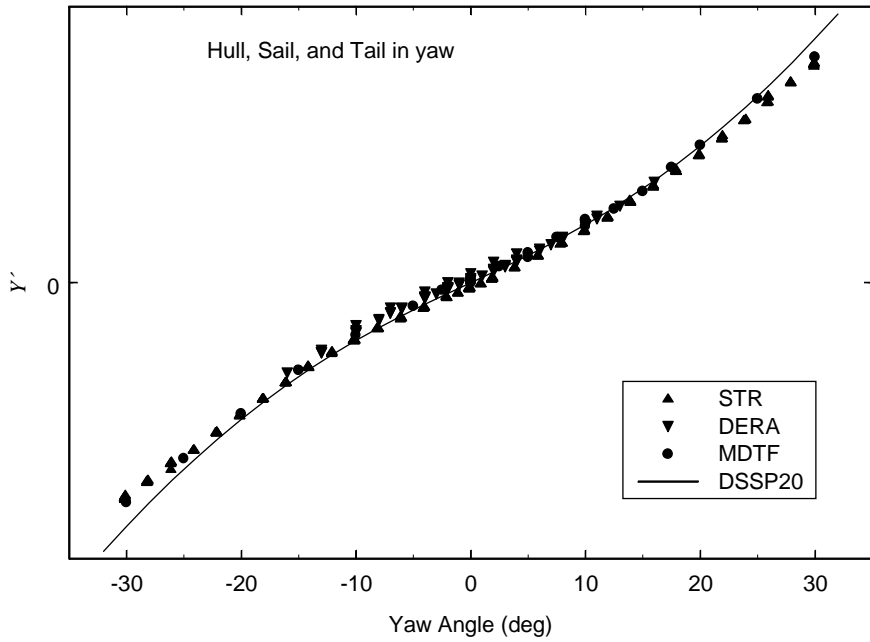


Figure 97. HST load comparison: Y' (yaw)

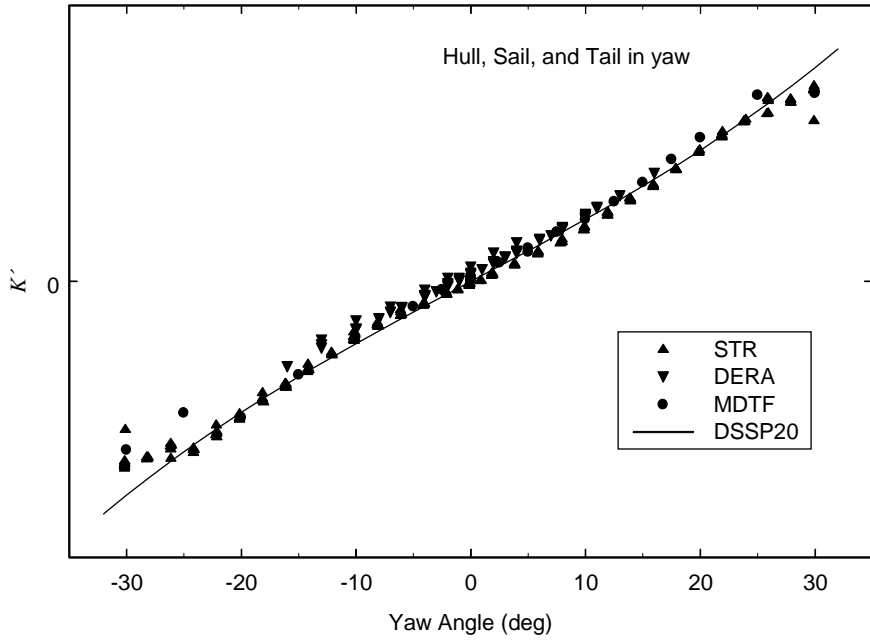


Figure 98. HST load comparison: K' (yaw)

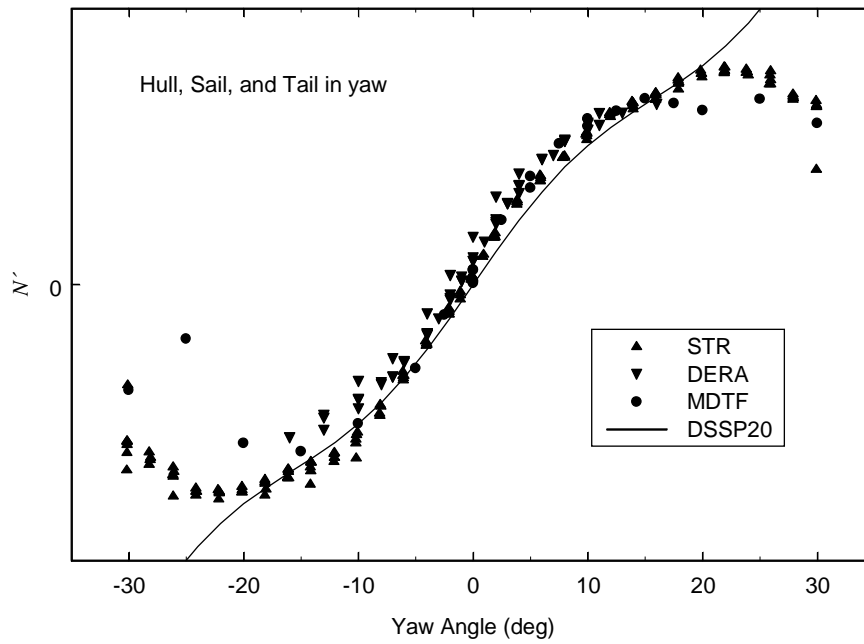


Figure 99. HST load comparison: N' (yaw)

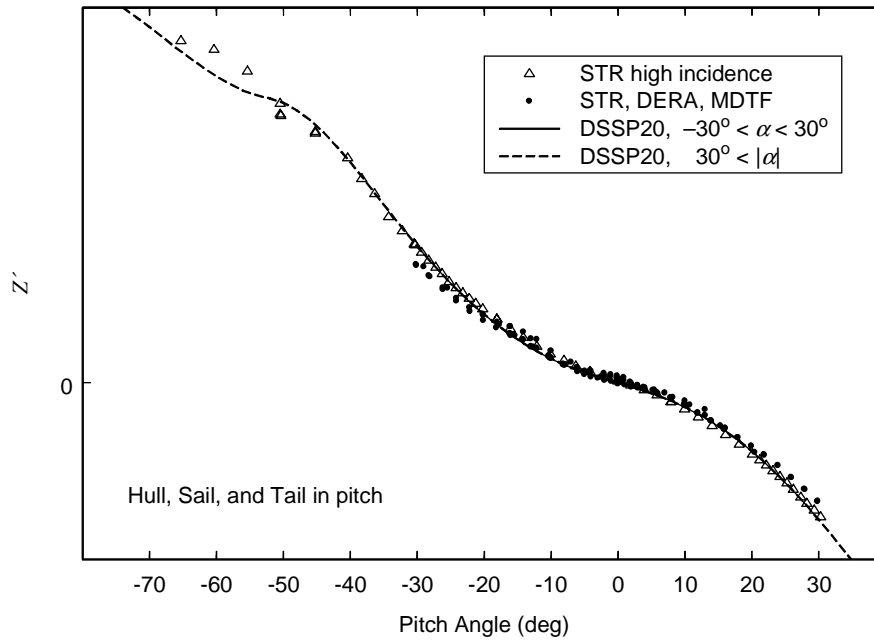


Figure 100. HST high incidence load comparison: Z' (pitch)

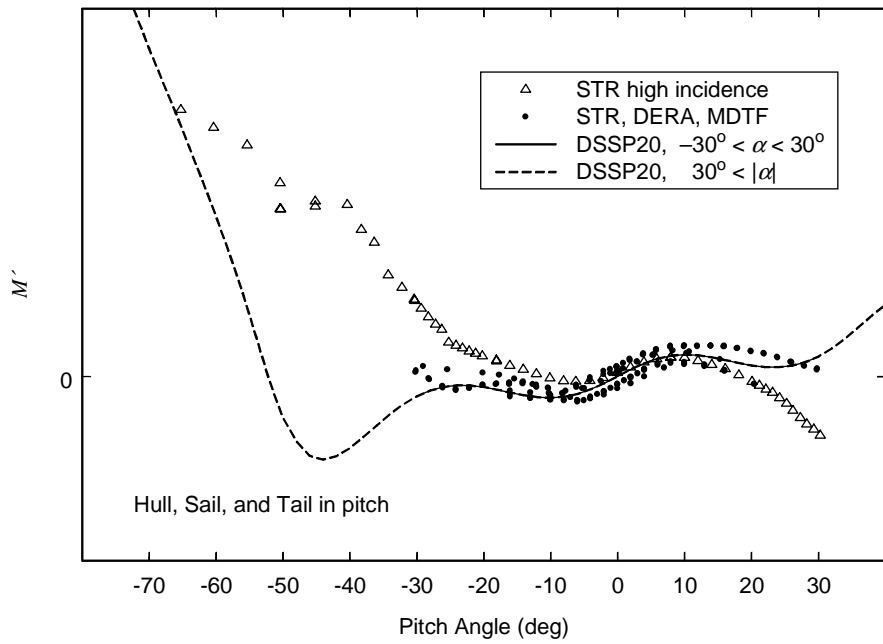


Figure 101. HST high incidence load comparison: M' (pitch)

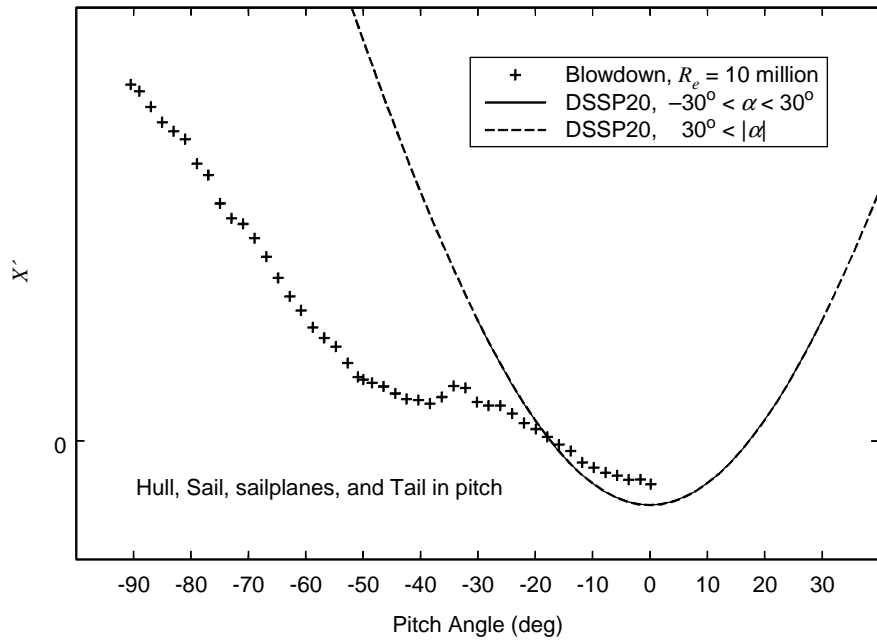


Figure 102. HSsT high incidence load comparison: X' (pitch); the blowdown tunnel model was sting-mounted

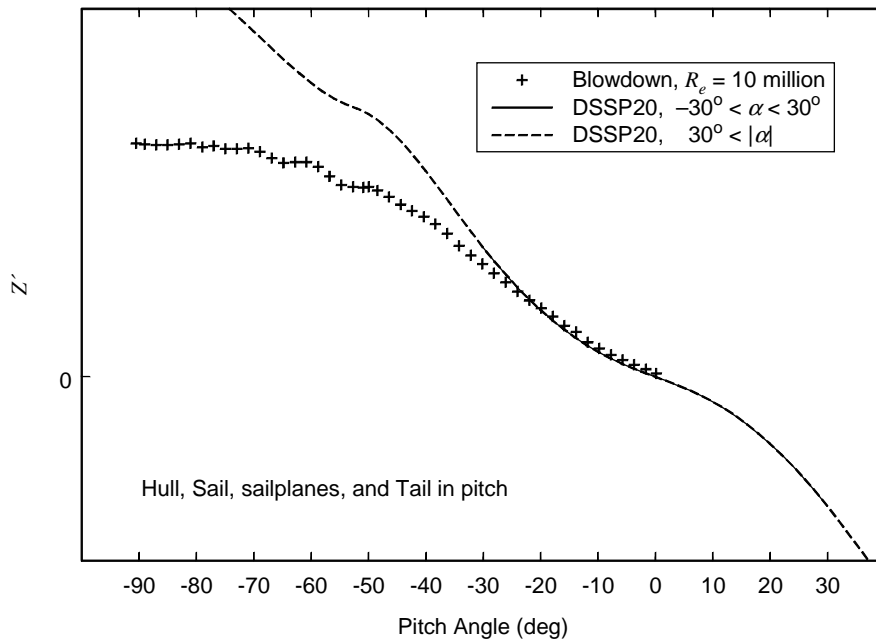


Figure 103. HSsT high incidence load comparison: Z' (pitch)

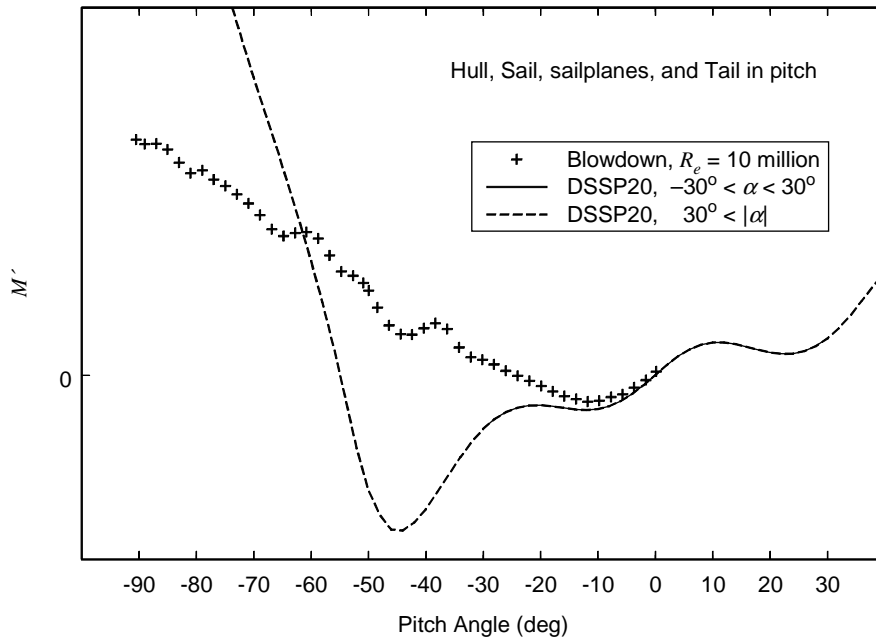


Figure 104. HSsT high incidence load comparison: M' (pitch)

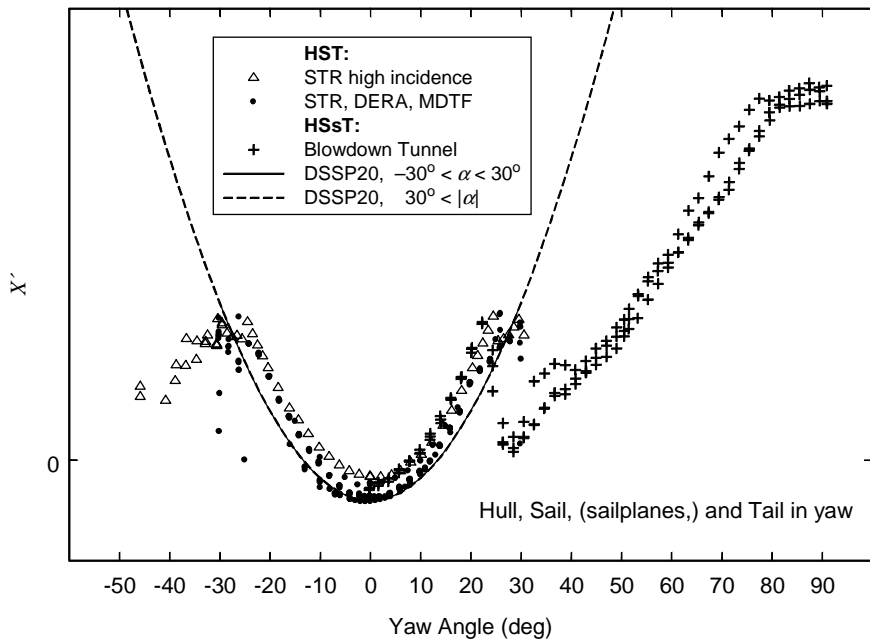


Figure 105. HST/HSsT high incidence load comparison: X' (yaw)

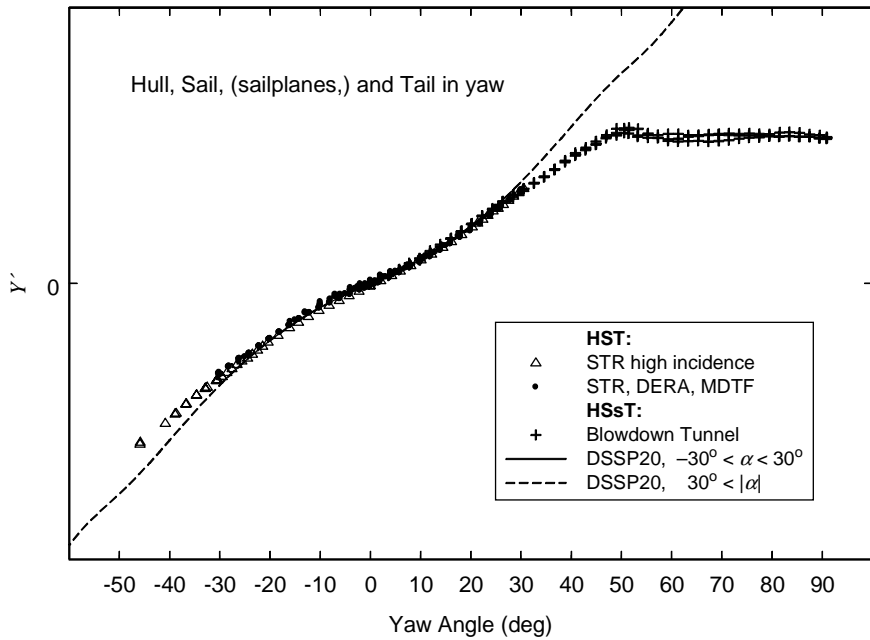


Figure 106. HST/HSsT high incidence load comparison: Y' (yaw)

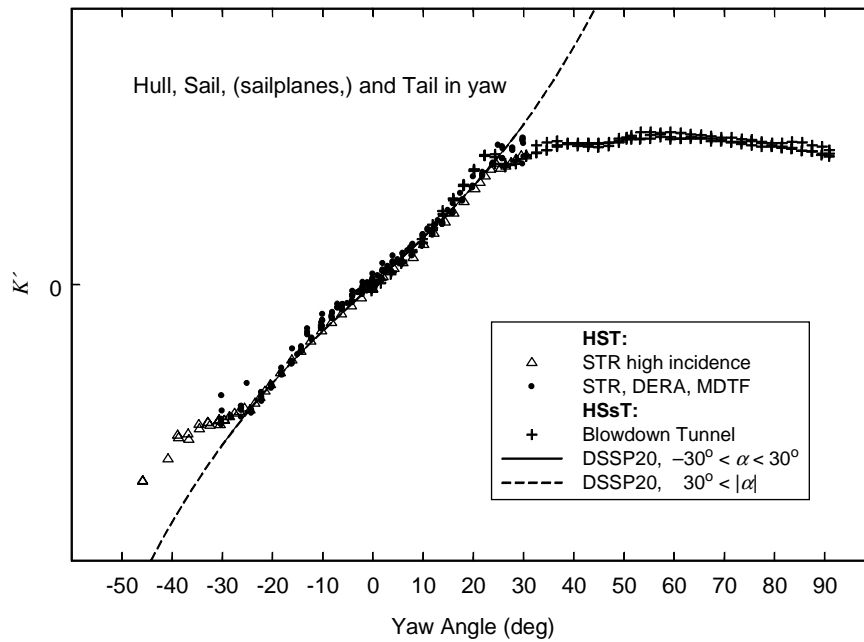


Figure 107. HST/HSsT high incidence load comparison: K' (yaw)

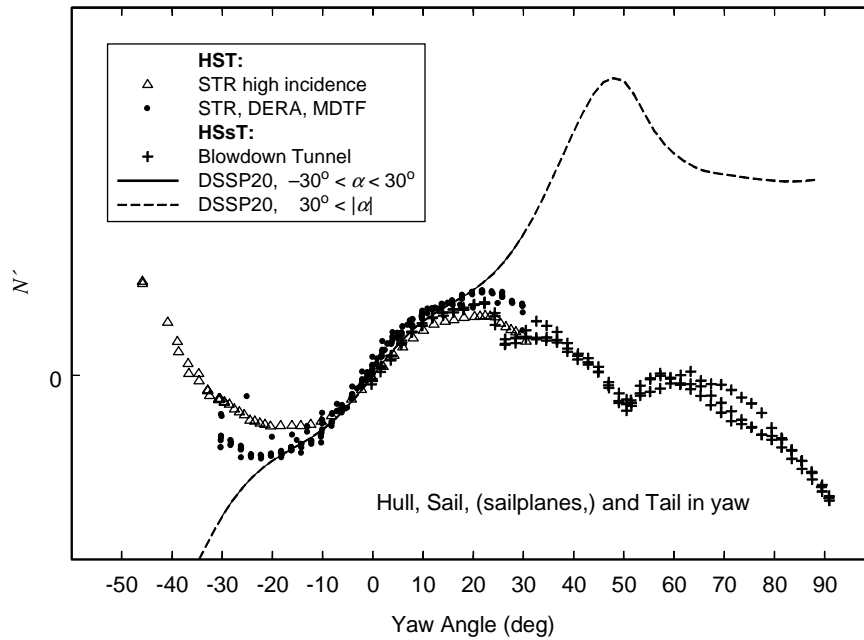


Figure 108. HST/HSsT high incidence load comparison: N' (yaw)

Annex A. Standard Submarine Series Experiments

Test programs are listed below by facility in the order that it was first used. Sponsors are indicated in cases where the experiment was not entirely funded by DRDC. The summaries indicate principal test configurations and conditions.

- IAR 0.35×0.35 m Water Tunnel, 0.389 m model.
 - 1984 exploratory flow visualization [1]
 - hull, sail, forward planes
 - R_e to 10^5 ; incidence to 20 deg.

- IAR 2×3 m Wind Tunnel, 1.8 m model.
 - 1985 flow visualization [2]
 - hull, sail variations
 - R_e to 9.5×10^6 ; incidence to 16 deg.
 - 1988–89 total forces and moments – external balance; force distribution [3]
 - included deck variations for out-of-plane study

- MARIN $220 \times 4 \times 4$ m high speed and $240 \times 18 \times 8$ m depressurized towing tanks, 5.3025 m model.
 - 1985–91 (DRDC/RNLN) total, sail, and rudder forces and moments [4–18]
 - resistance, static (incidence to 16 deg.), and PMM dynamic tests
 - strip tests and geometric variations (e.g., X-rudders, sailplanes, bowplanes. . .)
 - R_e to 13.5×10^6
 - depth from $1.5D$ to ∞ ; F_r various

- IAR 9×9 m Wind Tunnel, Static Test Rig, 6.0 m model.
 - 1988 total forces and moments – external balance, wake surveys, and flow visualization [19–22]
 - hull, sail, tail, strip tests
 - R_e to 23×10^6 ; incidence to 30 deg.
 - 1991 support interference subset [23,24]
 - two-strut, one-strut, sting support
 - 1992 propulsion tests – total + internal propulsor balance [25–27]
 - n' from -1 to $+1$; n to 10,000 rpm
 - 1993 high incidence for rising stability study [28]
 - sting support
 - incidence to 90 deg.

- MUN $21 \times 8 \times 4$ Flume Tank, 2.778 m model.
 - 1990 exploratory flow visualization [29]
 - bare hull
 - dye, bubbles, tufts, paint
 - R_e to 2.5×10^6 ; incidence to 20 deg.

- IAR 0.9×0.9 m Wind Tunnel, 0.6 m model.
 - 1990–91 exploratory support interference tests [30]
 - one-strut support
 - incidence to 30 deg.

- DERA(H) $120 \times 60 \times 5.5$ m Manoeuvring Tank, 4.606 m model.
 - 1991 (DRDC/DERA) rotating arm tests [31]
 - hull and sail; total forces and moments, and aft hull pressure distribution for OOP study
 - R_e , 8.5×10^6
 - drift, -5 to 25 deg., r' , 0.2 to 0.5
 - 1993 rotating arm tests
 - repeat for hull, sail, and tail

- MARIN $100 \times 25 \times 2.5$ m Seakeeping Basin, 3.1063 m model
 - 1992 (DRDC/RNLN) wave excitation forces – external (total) and sail balances [32–35]
 - bare hull and fully appended
 - depth, $1.5D$ and $1.75D$; F_r , 0 and 0.19
 - regular and irregular waves at up to 5 headings

- IAR 1.5×1.5 m Blowdown Wind Tunnel, 0.375 m model
 - 1992 total forces and moments for preliminary rising stability study [36]
 - fully appended; sting mounted
 - R_e to 12×10^6 ; incidence to 90 deg.

- MARIN $252 \times 10 \times 5.5$ m Towing Tank, 5.3025 m model
 - 1992–93 (DRDC/RNLN) propeller loading experiments [37,38]
 - LDV nominal and total wake surveys, unsteady shaft thrust and torque
 - drift to 10 deg.; rudders to 25 deg.

- IMD $200 \times 12 \times 7$ m Towing Tank, prototype MDTF
 - 1993 1.8 m model, total forces and moments
 - system evaluation tests
 - bare hull, R_e to 8×10^6
 - 1995 2.8 m model, total forces and moments [39,40]
 - harmonic oscillation strip tests for added mass study
 - fully appended model, turning circles
 - R_e to 7.5×10^6

- DERA(H) $270 \times 12 \times 5.5$ m Ship Tank, 4.606 m model
 - 1996 (DERA) total forces and moments, aft hull pressures [41]
 - strip tests, static incidence
 - R_e between 7.6 and 15.2×10^6

- IMD $200 \times 12 \times 7$ m Towing Tank, production 5DOF MDTF
 - 1998–99 (DRDC/IMD) total forces and moments, 4.445 m model
 - acceptance/commissioning tests
 - strip tests; static incidence, chirps, turning circles
 - R_e between 6 and 12×10^6

This page intentionally left blank.

Annex B. Symmetry Error Estimate

It is standard practice in model experiments to eliminate systematic errors due to support interference, blockage, tares, and so on, as much as possible in the data correction and reduction procedures. Nevertheless, some of these errors remain, some cannot be adequately measured or estimated, and others go undetected. Residual systematic errors result from a wide range of sources, including model misalignment, model and support deflections under load, instrumentation bias, and temperature drift. A large proportion of these errors are manifested as deviations from ideal symmetry in the results. This annex outlines the method suggested here to characterize these symmetry errors in order to compare different sets of data.

In what follows, x is a force or moment measurement and β is yaw or pitch angle; it is implicit that errors are associated with x and not β . (In practice, determination of incidence angle is invariably accompanied by systematic error but, since it is systematic, an equivalent error can be assigned to the dependent variable in the analysis.)

It is initially assumed that $x(\beta)$ is a purely even or odd function of β . Simple regression is used to fit a polynomial in β with coefficients a_0, a_1, a_2 , etc. If $x(\beta)$ is even, the odd terms in the polynomial represent residual systematic errors, and vice versa. Discarding these terms gives the idealized function $\tilde{x}(\beta)$,

$$\begin{aligned}\tilde{x}(\beta) &= a_0 + a_2\beta^2 + a_4\beta^4 + \dots && \text{for } x(\beta) \text{ even} \\ &= a_1\beta + a_3\beta^3 + a_5\beta^5 + \dots && \text{for } x(\beta) \text{ odd}\end{aligned}$$

The symmetry error S_x is the average difference between the idealized function and the measurements,

$$\begin{aligned}S_x &= \frac{1}{M} \left| \sum_{j=1}^M ((x_j - \tilde{x}_j) \cdot \text{Sign}(\beta_j)) \right| && \text{for } x(\beta) \text{ even} \\ &= \frac{1}{M} \left| \sum_{j=1}^M (x_j - \tilde{x}_j) \right| && \text{for } x(\beta) \text{ odd}\end{aligned}$$

where $x_j = x(\beta_j)$ are the measurements and $\tilde{x}_j = \tilde{x}(\beta_j)$.

For comparative purposes S_x is nondimensionalized by a selected value of \tilde{x} , in this instance $\tilde{x}(\beta_\bullet)$, where $\beta_\bullet = 0$ for axial force and 10° for the other forces and moments.

$$S'_x = \frac{S_x}{|\tilde{x}(\beta_\bullet)|}$$

If $x(\beta)$ is not purely even or odd, the idealized function must be modified to retain additional appropriate terms. For example, pitching moment is primarily an odd

function of pitch but requires an offset (a_0) to account for sail drag and other contributions arising from upper/lower asymmetry.

Although S'_x captures many of the residual systematic errors, it will miss those that are even for an even function, and odd for an odd function. For example, an error in the pitching moment offset arising from instrumentation bias would not be captured. For this reason, the estimate S'_x represents a lower bound on residual systematic errors.

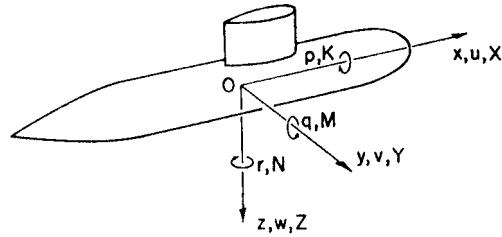
Nomenclature

Symbols

a_e	effective aspect ratio
$A(x)$	hull cross-sectional area
A_B	base area of the hull
A_{BM}	$A(x_{BM})$
A_P	planform area of the hull
b	semispan
C_{dc}	hull net crossflow drag based on A_P
C_{Pb}	spanwise center of pressure
C_{Pc}	chordwise center of pressure
C_X	appendage axial force coefficient
$C_{X0}, C_{X\alpha\alpha}, C_{XJ}$	terms in C_X ; see equations (6) and (9)
C_Z	appendage normal force coefficient
$C_{Z\alpha}, C_{Z\alpha\alpha\alpha}$	terms in C_Z ; see equations (6) and (9)
D	drag force; i.e., in flow axes
D'_0	hull zero-lift drag
k_s	sail factor
K, M, N	model rolling, pitching, and yawing moments
K', M', N'	nondimensional model moments, $K' = K/\frac{1}{2}\rho U^2 L^3$, etc.
$K'_{v'}$	rolling moment derivative dK'/dv'
K_{WB}	tailplane efficiency
L	length (typically hull length); also, lift force
L', D'	nondimensional lift and drag, $L' = L/\frac{1}{2}\rho U^2 L^2$, etc.
$M'_{w'}$	pitching moment derivative dM'/dw'
$N'_{v'}$	yawing moment derivative dN'/dv'
p, q, r	roll, pitch, and yaw rate
r	hull radius
R_c	Reynolds number based on chordlength
R_e	Reynolds number based on hull length
S_x, S'_x	symmetry error, nondimensionallized; see annex B

u, v, w	axial, lateral, and normal components of velocity
U	total velocity, $U = \sqrt{u^2 + v^2 + w^2}$
v'	nondimensional lateral velocity, $v' = -\sin \beta$
w'	nondimensional normal velocity, $w' = \sin \alpha$
x, y, z	model coordinate axes
x_{BM}	HULFOR “stalling point” [44]; where there is a maximum in $dA(x)/dx$
x_{cp}	planform area centroid in vehicle geometry coordinates
x_h	hydrodynamic center for axial or bi-planar symmetry, $x_h = x_{hh} = x_{vh}$
x_{hh}	horizontal plane hydrodynamic center, $x_{hh} = N'/Y'$
x_{hn}	horizontal plane neutral point, $x_{hn} = N'_{v'}/Y'_{v'}$
x_n	neutral point for axial or bi-planar symmetry, $x_n = x_{hn} = x_{vn}$
x_o	reference point (model axis origin) in vehicle geometry coordinates
x_t	hull tail, or base, location in vehicle geometry coordinates
x_{vh}	vertical plane hydrodynamic center, $x_{vh} = -M'/Z'$
x_{vn}	vertical plane neutral point, $x_{vn} = -M'_{w'}/Z'_{w'}$
X, Y, Z	model axial, side, and normal forces
X', Y', Z'	nondimensional model forces, $X' = X/\frac{1}{2}\rho U^2 L^2$, etc.
$Y'_{v'}$	side force derivative dY'/dv'
$Z'_{w'}$	normal force derivative dZ'/dw'
$Z_a, Z_{a(h)}, Z_h, Z_{h(a)}$	terms in Z for an appendage; see equation (5)
α	pitch angle, laboratory axes
β	yaw angle, laboratory axes
ρ	density
∇	hull volume

Coordinate System



Acronyms

CB	Center of Buoyancy
DERA	Defence Evaluation and Research Agency
DRDC	Defence Research & Development Canada
DSSP20	DRDC Submarine Simulation Program, version 2.0
IAR	(NRC) Institute for Aerospace Research
IMD	(NRC) Institute for Marine Dynamics
MARIN	Marine Institute Netherlands
MDTF	Marine Dynamic Test Facility
MUN	Memorial University of Newfoundland
NAE	National Aeronautical Establishment (now IAR)
NRC	National Research Council Canada
PMM	Planar Motion Mechanism
RNLN	Royal Netherlands Navy
STR	Static Test Rig

Standard Model Configurations:

H	Hull alone
HS	Hull and Sail
HSsT	Hull, Sail, sailplanes, and Tail
HST	Hull, Sail, and Tail
HT	Hull and Tail

This page intentionally left blank.

Unclassified

DOCUMENT CONTROL DATA		
1. ORIGINATOR Defence R&D Canada – Atlantic		2. SECURITY CLASSIFICATION Unclassified
3. TITLE The Standard Submarine Model: A Survey of Static Hydrodynamic Experiments and Semiempirical Predictions		
4. AUTHORS M. Mackay		
5. DATE OF PUBLICATION June 2003	6a. NO. OF PAGES 108	6b. NO. OF REFS 67
7. DESCRIPTIVE NOTES DRDC Atlantic Technical Report		
8. SPONSORING ACTIVITY		
9a. PROJECT OR GRANT NO. 11GL12		9b. CONTRACT NO.
10a. ORIGINATOR'S DOCUMENT NUMBER DRDC Atlantic Technical Report 2003–079		10b. OTHER DOCUMENT NOS.
11. DOCUMENT AVAILABILITY Unlimited		
12. DOCUMENT ANNOUNCEMENT (if different from 11) (As availability)		
13. ABSTRACT <p>This report describes comparison between measurements of static hydrodynamic loads on the Standard Submarine Model in a number of different test facilities, and comparison between selected experimental data and predictions from the DSSP20 manoeuvring simulation code. The experiments constitute a substantial database for code development and validation. Differences between data from various facilities are in general not very great. Agreement with the predictions is generally satisfactory within a modest range of incidence, i.e., angles below 20 to 30 degrees, although some significant deviations are observed outside this range.</p>		
14. KEYWORDS Standard Submarine Model Towing Tank Wind Tunnel DSSP20 Code		

This page intentionally left blank.

Defence R&D Canada

**Canada's leader in defence
and national security R&D**

R & D pour la défense Canada

**Chef de file au Canada en R & D
pour la défense et la sécurité nationale**



www.drdc-rddc.gc.ca